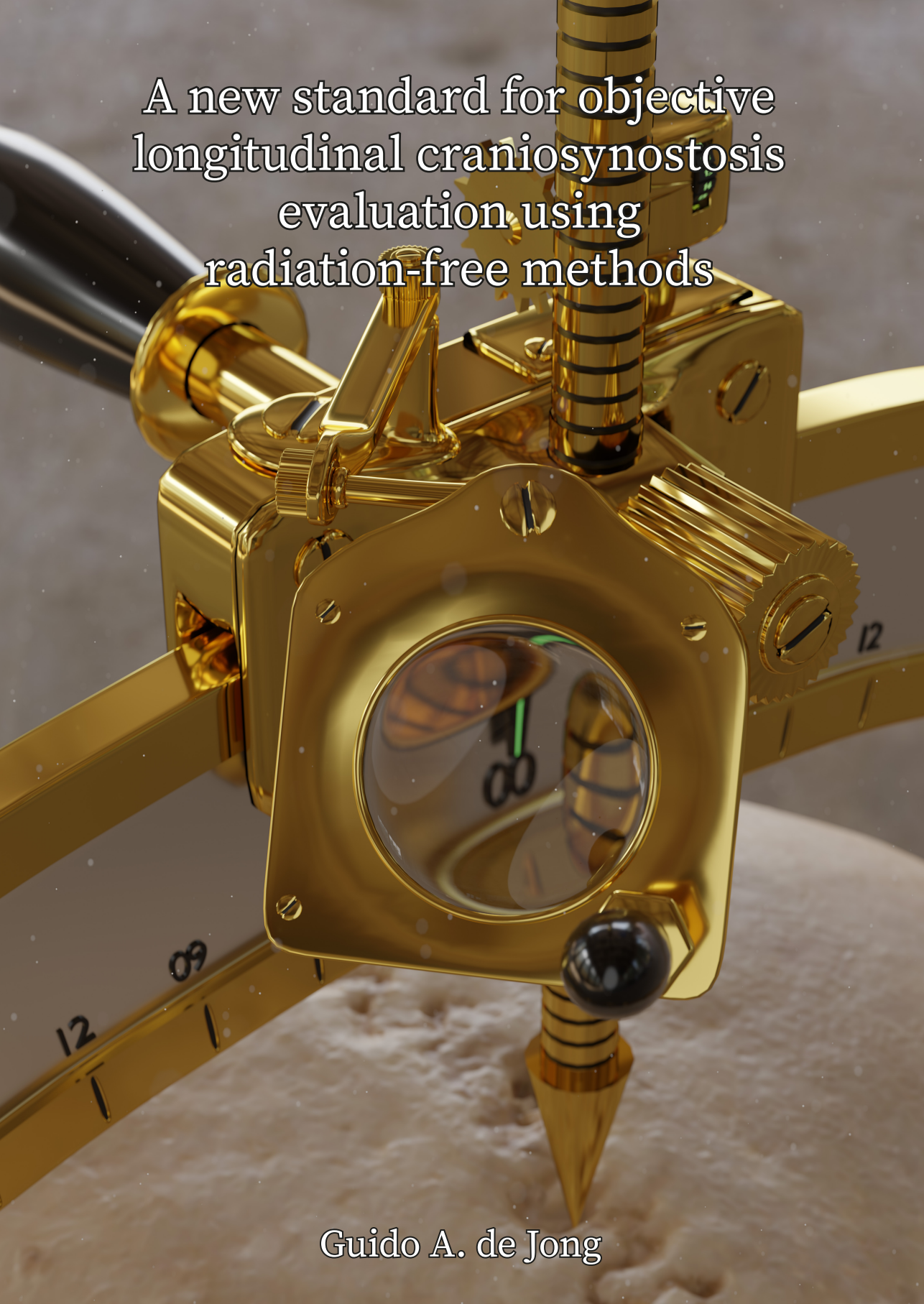

A new standard for objective longitudinal craniosynostosis evaluation using radiation-free methods

Guido A. de Jong

A new standard for objective longitudinal craniosynostosis evaluation using radiation-free methods

Guido A. de Jong

A new standard for objective longitudinal craniosynostosis evaluation using radiation-free methods

Proefschrift ter verkrijging van de graad van doctor
aan de Radboud Universiteit Nijmegen
op gezag van de rector magnificus prof. dr. J.H.J.M. van Krieken,
volgens besluit van het college voor promoties
in het openbaar te verdedigen op

maandag 22 november 2021
om 16:30 uur precies
door

Guido Adriaan de Jong

geboren op 29 april 1987
te Nijmegen

Promotoren:	Prof. dr. R.H.M.A. Bartels Prof. dr. T.J.J. Maal
Copromotor:	Dr. H.H.K. Delye
Manuscriptcomissie:	Prof. dr. D.J.O. Ulrich (voorzitter) Prof. dr. S.J. Bergé Prof. dr. ir. C.H. Slump *Universiteit Twente*

Scan QR-Code for the digital version

or visit: https://guidodejong.nl/PhD/

Cover:	Cover page image created by Adrian Magnussen and Guido de Jong
Lay-out:	Guido de Jong
Printed by:	Ipskamp printing
ISBN:	978-94-6421-521-2

Contents

Chapter 1

General Introduction

Guido A. de Jong

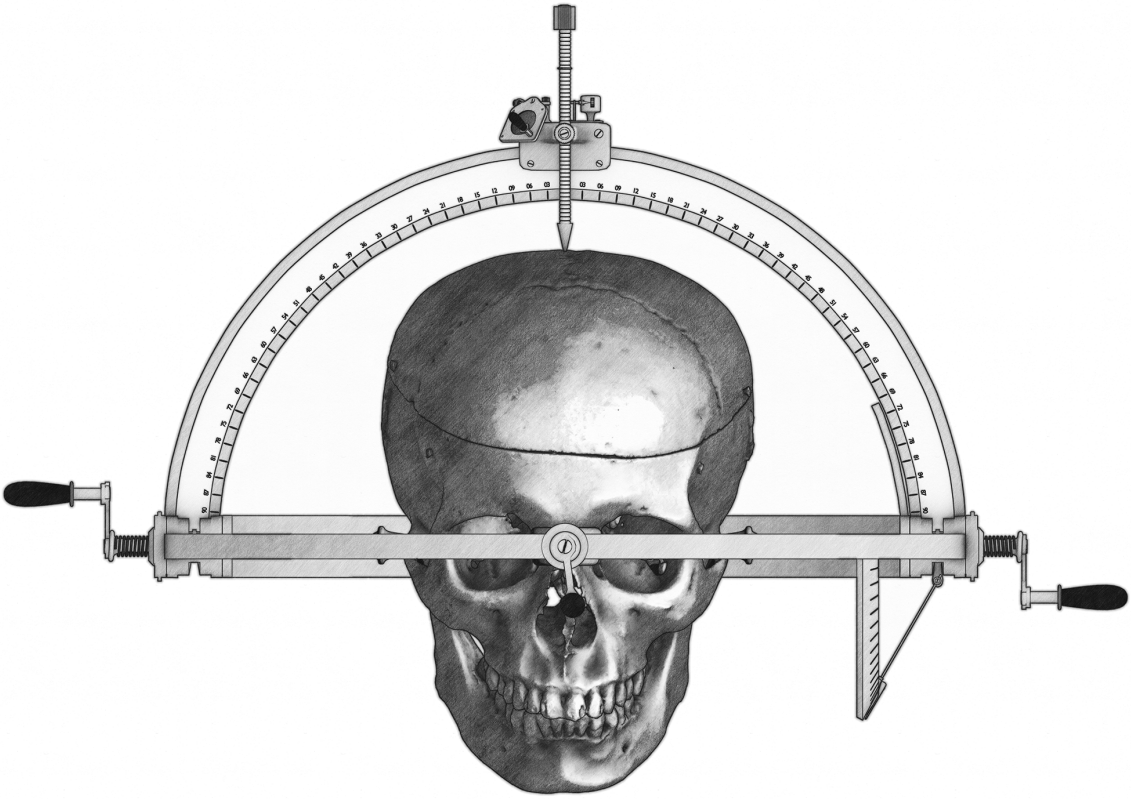

CRANIOSYNOSTOSIS

Craniosynostosis is the premature or pathological fusion of one or more cranial sutures with an incidence varying between 3.0 and 7.2 in 10,000 live births [1]–[3]. There are both syndromic and non-syndromic forms of craniosynostosis. The non-syndromic fusions leads to cranial malformations giving the distinguished shapes belonging to the various subtypes of craniosynostosis named after the affected suture(s) [4], [5]. The uni-suture craniosynostosis forms are the most common and called scaphocephaly, trigonocephaly and plagiocephaly. Within other literature these are also named after their respective closed suture in the form of sagittal synostosis, metopic synostosis or (uni)coronal synostosis. These distinguishing shapes are caused by the closed suture hampering growth in combination with compensatory growth of the other open suture [Figure 1]. Untreated craniosynostosis can lead to several issues over time including skull and facial asymmetry, increased intracranial pressure, cognitive deficits, and deafness depending on the form and severity of the condition [4], [6].

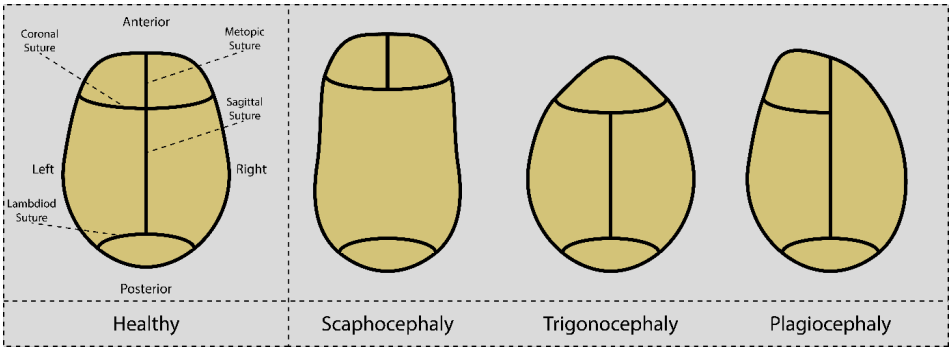

Figure 1: Schematic top view of a healthy skull and the three most common forms of uni-suture non-syndromic craniosynostosis.

Luckily there are several craniosynostosis treatment options. However, despite the various forms of diagnostics and follow-up methods there is still uncertainty regarding the best treatment option. It is key to understand the background on the diagnosis, treatment and follow-up (techniques) of craniosynostosis to comprehend the uncertainty that exists around the best treatment options. Within the next sections these subjects will be explained and used to formulate the aim of this thesis.

DIAGNOSIS AND TREATMENT

Diagnosis of craniosynostosis can occur by physical examination, cranial X-ray, ultrasound, computed tomography (CT), 3D stereophotogrammetry, and Magnetic Resonance Imaging (MRI) [5], [7], [8]. The preferred use of diagnosis depends on the availability of the technique and the experience with the given techniques. The most common forms still are the physical examination in combination with X-ray or CT scanning [8].

The standard care in craniosynostosis treatment is surgery with or without additional helmet therapy. Helmet therapy alone or preoperative helmet therapy is also considered but still remains controversial within craniosynostosis treatment due to the potential raise in intracranial pressure [4], [9]–[12]. Two primary surgical strategies exist: open cranial vault remodelling/ reconstruction (OCVR) or endoscopically assisted craniosynostosis surgery (EACS). Less frequently used forms of surgery include spring-assisted cranioplasty, distraction osteogenesis, and (fronto-orbital) advancement. The type of surgery often depends on the age, type of craniosynostosis, and institution. Although craniosynostosis interventions have been performed since 1890, the use of endoscopic techniques were not described till 1998 [13], [14]. The open surgery is primarily aimed at either reconstruction to a healthy age specific skull during surgery or distraction of the skull. EACS is primarily aimed at removing the affected suture to enable corrective growth [4]. After six months of age the EACS is no longer a viable option due to significant deformations caused by the compensatory growth during craniosynostosis and bone hardening [15], [16]. There are many variants of the OCVR technique, depending on the specific craniosynostosis form, patient-specific factors, and the preference and experience of the surgeons and craniofacial teams. After OCVR there is usually no need for a remodelling helmet, since the head is already shaped during surgery. In case of EACS it depends on the institution, if a remodelling helmet is required or recommended. The remodelling helmets applies pressure on the areas that already showed compensatory growth to prevent further expansion. On the other hand these helmets have areas without pressure zones to allow corrective growth where growth was previously hampered. These helmets usually are worn 23 hours a day over a 6-12 month period after surgery [17].

Early diagnosis of craniosynostosis is recommended due to having the option of early treatment (EACS) with improved surgical measures (e.g. blood loss, surgery time, and hospital stay) [17]–[27]. For both open and EACS the peri-operative and direct post-operative outcomes and complications other than cranial shape measures are well described [16]–[19], [23], [24], [26]–[30]. However, despite these outcomes, there is still no consensus on the best treatment options in either the endoscopic surgery or open surgery concerning long-term outcomes. Due to the growth of the skull over time it is unknown if a direct post-operative positive outcome leads to a long-term positive outcome. Long-term objective follow-up could therefore potentially help in determining the best treatment option.

LONG-TERM FOLLOW-UP

FOLLOW-UP MEASURES

After the primary surgery there will be a follow-up period aimed at monitoring the various cranial shape measures, volume, aesthetics, and absence of signs of increased intracranial pressure over time to determine the success and need for (re-) intervention. Commonly monitored cranial shape measures for scaphocephaly are the cranial index/cephalic index (CI) to determine head width to length ratio [14], [17], [20], [31]–[34], or asymmetry measures for mainly plagiocephaly [33], [35]–[37]. Other common measures in craniosynostosis for all forms are the evaluation of volumes. However, these volume measurements are often limited to pre-surgical cases [38]–[40]. Pre- to post-surgery volume evaluations help to some degree but lack the longitudinal evaluation [33], [41]. The final decision on what outcome measures to use can vary based on the craniosynostosis form, performed surgery, available techniques, and institution policy. Although these measures are valuable, they only provide a limited representation of the head shape and growth over time. Complete analysis of the 3D surface of the shape exists, but remain limited in the literature [42].

FOLLOW-UP TECHNIQUES

Each monitored cranial shape outcome measure requires a different measuring technique. The CI or head circumference can easily be monitored using callipers and a measuring lint while being consistent among techniques and observers [31], [34]. Other measurements like intracranial volume often

rely on CT-scans or MRI-scans. Nearly all common cranial shape measures being monitored can be calculated or determined using 3D CT-scans or 3D MRI-scans making these valuable in follow-up. Although these imaging techniques can result in accurate measurements, there are some major drawbacks in using these in young children. This can be for instance harmful radiation in CT scans and/or the need for sedation in MRI scans [43]–[45]. In the absence of CT-scans or MRI-scans some derivatives of intracranial/brain volume can be based upon other measurements. However, these only give an approximation of the volumes and differ for healthy and craniosynostosis affected heads [46], [47].

3D STEREOPHOTOGRAMMETRY

A new imaging modality in the diagnosis and follow-up of craniosynostosis and other craniofacial morphological pathologies is the use of 3D stereophotogrammetry. This fast and radiation-free technique enables to capture a 3D shape (or 3D mesh/object) of the face and/or cranium with colour information of the surface and stores this as a 3D Photo [Figure 2].

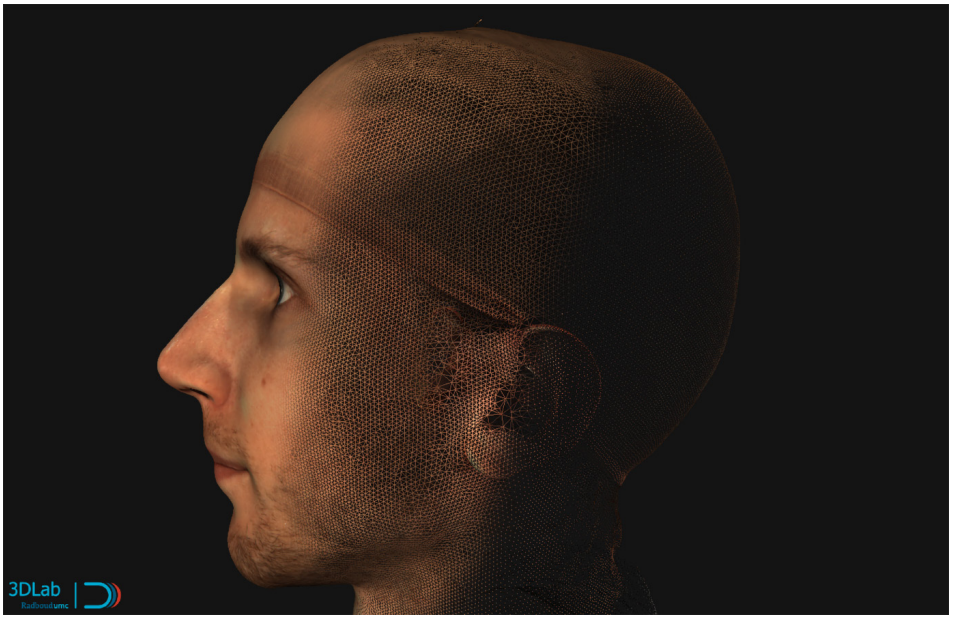

Figure 2: Example of a 3D Photo of a head with the respective building blocks. A fade is shown from left to right: the fully textured 3D Photo, the wireframe, and the point cloud.

This technique has the potential to perform many of the measurements that would normally be done during physical examination as well as other surface measurements that can be done on MRI or CT-scans. However, in contrast to MRI-scans or CT-scans there is only information of the surface of the head without capturing underlaying tissues like muscles, fat, brain, bones and others. At the moment, bony landmarks are often used in longitudinal follow-up measurements which are lacking in 3D Photos. This requires alternative landmarks or alternative methods in longitudinal follow-up with this technique. Also, regardless of the technique, landmarks can shift relatively towards each other which can hamper determining growth at areas which not directly hold these landmarks (e.g. the frontal cranial bone) [48]. Luckily there are still options which can be used with the lack of the (bony) landmarks in for instance in the CI or head circumference measurements [33].

REFERENCE FRAMES IN FOLLOW-UP

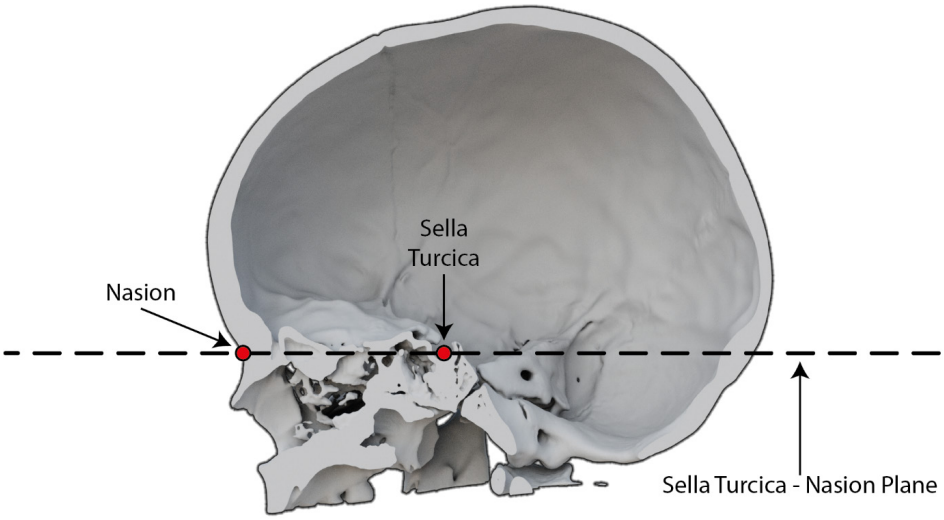

Figure 3: Example of a commonly used reference frame (Sella turcica-nasion) used in cranial CT-scans for determining cranial shape measures.

It is important to ensure consistency in 3D cranial longitudinal follow-up regardless of the technique. This is less straightforward than it seems when this follow-up. If, for instance, we want to measure the amount of posterior or anterior skull growth over time we must define a reference position (e.g. the external meatus). However, how can be sure that the external meatus has not (slightly) moved relatively towards the anterior or posterior portion of the

skull during growth? The difficulty in cranial growth is the uncertainty of the regional growth over time which in turn can influence the measurements by itself. To overcome these issues, so called references frames (or reference orientations) were introduced for X-rays, CT-scans or MRI-scans. A reference frames allow for standardized positions and orientations of heads for measurements or follow-up. These reference frames are often based on landmarks or sets of rules that are assumed to be not, or only partly, influenced over time. A common reference orientation/frame is the sella turcica – nasion orientation which has previously been used in X-ray and CT-scan studies [49]–[51] [Figure 3].

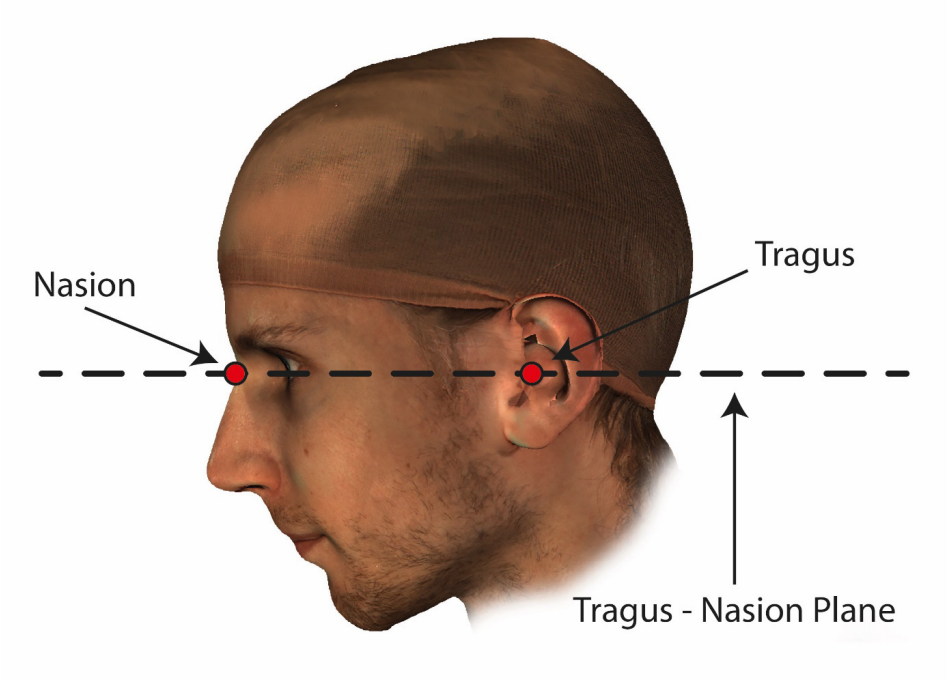

Figure 4: Example of a reference frame (Tragus-nasion) for used in cranial CT-scans and 3D Photos for determining cranial shape measures.

Within the 1950s this orientation was deemed relatively stable for evaluating cranial morphology and cephalometry [50], [52], [53]. Other forms of creating reference frames based on surface landmarks or the whole surface and are potentially usable for (or have been used for) 3D Photos [36], [37], [54]–[59]. Other reference frames for either CT-scans or 3D Photos mostly rely on the external meati/tragus to nasion/sellion plane, the Frankfurt plane or derived planes from these options [36], [37], [57]–[60] [Figure 4]. Nearly all these reference

frames have been used to some extend for both a single measurement as well as longitudinal follow-up. However, the question remains how the ground truth regarding the actual head growth can be determined as well as by which (if any) reference frame. Furthermore the mixed use of reference frames as well as the undetermined validity of these frames in specifically 3D photos makes longitudinal follow-up of craniosynostosis treatment difficult. This further hampers the evaluation of the optimum craniosynostosis treatments. There is therefore need for accurate follow-up techniques preferably aimed at 3D photos.

SUMMARY OF ISSUES IN LONGITUDINAL FOLLOW-UP

In the past couple of sections a background on the diagnosis, treatment and follow-up (techniques) of craniosynostosis is given. This background should explain the uncertainty that exists around determining the best craniosynostosis treatment options. Especially the limited knowledge on the longitudinal cranial shape measures after craniosynostosis surgery is key for this uncertainty. Moreover, full 3D shape analysis is often lacking and required to determine the best outcome and subsequently the best treatment option. These measures and outcomes could be obtained by the systematic follow-up of craniosynostosis using e.g. CT-scans or MRI-scans. However, as mentioned earlier these imaging techniques require sedation and, in case of the CT-scans, also involve a radiation dose. Therefore, these imaging modalities are not preferred for longitudinal follow-up. The option of using 3D Photos as a radiation-free, sedation-free, fast alternative remains limited due to the lack of a validated reference frame. Therefore, there is a need for a new standardized and validated method for objective longitudinal craniosynostosis evaluation using radiation-free methods.

AIM OF THE THESIS

The primary goal of this thesis is the creation of a new standardized method for objective longitudinal craniosynostosis evaluation using radiation-free methods. The new standardized method should provide tools in the objective evaluation of the different forms of craniosynostosis treatment. Additionally should this new method also function on CT-scans in the absence of 3D Photos or in combination with both 3D Photos and CT-scans.

OUTLINE OF THE THESIS

The creation and validation of a new standardized method for objective longitudinal craniosynostosis evaluation using radiation-free methods exists out of three main parts; the creation of the standardized method, the validation of the standardized method, and the evaluation of our institutes treatment data.

The most reliable methods of superposition in morphologically changing heads is considered based upon the sella turcica in combination with external landmarks. However, the sella turcica is not available within soft-tissue segmented CT-scans or 3D Photos. In order to overcome this issue, the Computed Cranial Focal Point (CCFP) is introduced in **Chapter 2**. The CCFP is a landmark with a robust position in relation towards the sella turcica that can be computed based upon 3D reconstructed the hard- or soft-tissue models of the head. The CCFP allows for correlation between these modalities as well as longitudinal radiation-free comparison of 3D Photos where this was previously not possible. Therefor this chapter is primarily focussed on the creation of the method.

It could be possible that the CCFP changes over time in the growing infants. In order to properly use superposition of single or multiple modalities over time using the CCFP it is important to define the characteristics of the changing CCFP in the growing infants. Looking at the main patient population of this thesis there might also be changes within the CCFP based upon the type of craniosynostosis present. In **Chapter 3** these characteristics and the scope of use of the CCFP is further explored. Within this chapter there is a further creation and validation of the use of the CCFP method.

The first evaluation of our institutes data concerning the follow-up of craniosynostosis is for the treatment of endoscopically assisted trigonocephaly using radiation-free methods. This is performed within **Chapter 4**.

In order to compare craniosynostosis treatment effects in regard to the normal population it is important to determine normal 3D head growth of healthy children of a similar age groups. This is the focus of **Chapter 5**. This chapter utilizes the methods from the previous chapters and provides the normative data as a reference for the later chapters.

In **Chapter 6** there will be a full evaluation of our institutions data of the children that have been treated for scaphocephaly and had follow-up using 3D photogrammetry. This includes both endoscopically assisted surgeries as well as open surgeries. This allows to critically look into both methods and the long-term effects they have on the head shape and form measures.

The methodologies developed in the earlier chapters used conventional evaluation methods and measures. However, parts of the methodology allow for evaluations using artificial intelligence. **Chapter 7** explores the potential of standardized 3D Photos in combination with artificial intelligence in the automated diagnosis of various craniosynostosis forms by using deep learning.

Finally, in **Chapter 8** the general discussion and future perspectives of this thesis are described. This chapter focuses on the creation and validation of a new standardized method for objective longitudinal craniosynostosis evaluation using radiation-free methods.

REFERENCES

[1] H. Q. Lee *et al.*, "Changing epidemiology of nonsyndromic craniosynostosis and revisiting the risk," *J. Craniofac. Surg.*, vol. 23, no. 5, pp. 1245–1251, 2012, doi: 10.1097/SCS.0b013e318252d893.

[2] M. . Cornelissen *et al.*, "Increase of prevalence of craniosynostosis," *J Craniomaxillofac Surg*, vol. 44, no. 9, pp. 1273–1279, 2016, doi: 10.1016/j.jcms.2016.07.007.

[3] C. F. Kweldam, J. J. Van Der Vlugt, and J. J. N. M. Van Der Meulen, "The incidence of craniosynostosis in the Netherlands, 1997-2007," *J. Plast. Reconstr. Aesthetic Surg.*, vol. 64, no. 5, pp. 583–588, 2011, doi: 10.1016/j.bjps.2010.08.026.

[4] D. Krakow, "Craniosynostosis," *Obstet. Imaging Fetal Diagnosis Care Second Ed.*, vol. 53, pp. 301-304.e1, 2017, doi: 10.1016/B978-0-323-44548-1.00062-0.

[5] M. L. Cunningham and C. L. Heike, "Evaluation of the infant with an abnormal skull shape.," *Curr. Opin. Pediatr.*, vol. 19, no. 6, pp. 645–51, Dec. 2007, doi: 10.1097/MOP.0b013e3282f1581a.

[6] R. E. Bristol, G. P. Lekovic, and H. L. Rekate, "The effects of craniosynostosis on the brain with respect to intracranial pressure," *Semin. Pediatr. Neurol.*, vol. 11, no. 4, pp. 262–267, 2004, doi: 10.1016/j.spen.2004.11.001.

[7] H. J. Kim, H. G. Roh, and I. W. Lee, "Craniosynostosis: Updates in radiologic diagnosis," *J. Korean Neurosurg. Soc.*, vol. 59, no. 3, pp. 219–226, 2016, doi: 10.3340/jkns.2016.59.3.219.

[8] F. Ursitti *et al.*, "Evaluation and management of nonsyndromic craniosynostosis," *Acta Paediatr. Int. J. Paediatr.*, vol. 100, no. 9, pp. 1185–1194, 2011, doi: 10.1111/j.1651-2227.2011.02299.x.

[9] S. Sood, A. Rozzelle, B. Shaqiri, N. Sood, and S. D. Ham, "Effect of molding helmet on head shape in nonsurgically treated sagittal craniosynostosis.," *J. Neurosurg. Pediatr.*, vol. 7, no. 6, pp. 627–32, Jun. 2011, doi: 10.3171/2011.4.PEDS116.

[10] N. Pediatr, "Neurosurgical forum Helmets and synostosis," *J Neurosurg Pediatr.*, vol. 9, no. June, pp. 680–682, 2012.

[11] N. I. Marupudi, S. Sood, A. Rozzelle, and S. D. Ham, "Effect of molding helmets on intracranial pressure and head shape in nonsurgically treated sagittal craniosynostosis patients," *J. Neurosurg. Pediatr.*, vol. 18, no. 2, pp. 207–212, 2016, doi: 10.3171/2016.1.peds15569.

[12] A. Hashmi, N. I. Marupudi, S. Sood, and A. Rozzelle, "Effect of Preoperative Molding Helmet in Patients with Sagittal Synostosis," *J. Craniofac. Surg.*, vol. 28, no. 4, pp. 898–903, 2017, doi: 10.1097/SCS.0000000000003512.

[13] M. A. Clayman, G. J. Murad, M. H. Steele, M. B. Seagle, and D. W. Pincus, "History of craniosynostosis surgery and the evolution of minimally invasive endoscopic techniques: The University of Florida experience," *Ann. Plast. Surg.*, vol. 58, no. 3, pp. 285–287, 2007, doi: 10.1097/01.sap.0000250846.12958.05.

[14] D. F. Jimenez and C. M. Barone, "Endoscopic craniectomy for early surgical correction of sagittal craniosynostosis.," *Journal of neurosurgery*, vol. 88, no. 1. pp. 77–81, 1998, doi: 10.3171/jns.1998.88.1.0077.

[15] M. R. Proctor, "Endoscopic craniosynostosis repair," *Transl. Pediatr.*, vol. 3, no. 3, pp. 247–258, 2014, doi: 10.3978/j.issn.2224-4336.2014.07.03.

[16] C. M. Barone and D. F. Jimenez, "Endoscopic craniectomy for early correction of craniosynostosis.," *Plast. Reconstr. Surg.*, vol. 104, no. 7, pp. 1965–73; discussion 1974-5, 1999, doi: 10.3171/jns.1998.88.1.0077.

[17] H. H. K. Delye *et al.*, "Endoscopically assisted craniosynostosis surgery (EACS): The craniofacial team Nijmegen experience," *J. Cranio-Maxillofacial Surg.*, vol. 44, no. 8, pp. 1029–1036, Aug. 2016, doi: 10.1016/j.jcms.2016.05.014.

[18] C. C. Cartwright, D. F. Jimenez, C. M. Barone, and L. Baker, *Endoscopic strip craniectomy: a minimally invasive treatment for early correction of craniosynostosis.*, vol. 35, no. 3. 2003, pp. 130–138.

[19] H. Yan *et al.*, "A systematic review of endoscopic versus open treatment of craniosynostosis. Part 2: The nonsagittal single sutures," *J. Neurosurg. Pediatr.*, vol. 22, no. 4, pp. 361–368, 2018, doi: 10.3171/2018.4.PEDS17730.

[20] M.-B. Le *et al.*, "Assessing long-term outcomes of open and endoscopic sagittal synostosis reconstruction using three-dimensional photography.," *J. Craniofac. Surg.*, vol. 25, no. 2, pp. 573–6, 2014, doi: 10.1097/SCS.0000000000000613.

[21] D. F. Jimenez, C. M. Barone, M. E. McGee, C. C. Cartwright, and C. L. Baker, "Endoscopy-assisted wide-vertex craniectomy, barrel stave osteotomies, and postoperative helmet molding therapy in the management of sagittal suture craniosynostosis," *J. Neurosurg. Pediatr.*, vol. 100, no. 5, pp. 407–417, May 2004, doi: 10.3171/ped.2004.100.5.0407.

[22] L. A. Dvoracek *et al.*, "Comparison of traditional versus normative cephalic index in patients with sagittal synostosis: Measure of scaphocephaly and postoperative outcome," *Plast. Reconstr. Surg.*, vol. 136, no. 3, pp. 541–548, Sep. 2015, doi: 10.1097/PRS.0000000000001505.

[23] M. N. N. Shah, A. A. A. Kane, J. D. D. Petersen, A. S. S. Woo, S. D. D. Naidoo, and M. D. D. Smyth, "Endoscopically assisted versus open repair of sagittal craniosynostosis: The St. Louis Children's Hospital experience - Clinical article," *J. Neurosurg. Pediatr.*, vol. 8, no. 2, pp. 165–170, 2011, doi: 10.3171/2011.5.PEDS1128.

[24] E. B. Ridgway, J. Berry-Candelario, R. T. Grondin, G. F. Rogers, and M. R. Proctor, "The management of sagittal synostosis using endoscopic suturectomy and postoperative helmet therapy," *J. Neurosurg. Pediatr.*, vol. 7, no. 6, pp. 620–626, 2011, doi: 10.3171/2011.3.peds10418.

[25] D. F. Jimenez, C. M. Barone, C. C. Cartwright, and L. Baker, "Early management of craniosynostosis using endoscopic-assisted strip craniectomies and cranial orthotic molding therapy.," *Pediatrics*, vol. 110, no. 1 Pt 1, pp. 97–104, 2002, doi: 10.1542/peds.110.1.97.

[26] C. P. P. Riordan *et al.*, "Minimally Invasive Endoscopic Surgery for Infantile Craniosynostosis: A Longitudinal Cohort Study," *J. Pediatr.*, vol. 216, pp. 142-149.e2, 2020, doi: 10.1016/j.jpeds.2019.09.037.

[27] A. Goyal, V. M. Lu, Y. U. Yolcu, M. Elminawy, and D. J. Daniels, "Endoscopic versus open approach in craniosynostosis repair: a systematic review and meta-analysis of perioperative outcomes," *Child's Nerv. Syst.*, vol. 34, no. 9, pp. 1627–1637, 2018, doi: 10.1007/s00381-018-3852-4.

[28] G. Tunçbilek, I. Vargel, A. Erdem, M. E. Mavili, K. Benli, and Y. Erk, "Blood loss and transfusion rates during repair of craniofacial deformities.," *J. Craniofac. Surg.*, vol. 16, no. 1, pp. 59–62, Jan. 2005, [Online]. Available: http://www.ncbi.nlm.nih.gov/pubmed/15699646.

[29] E. J. E. J. . Van Lindert *et al.*, "Intraoperative complications in pediatric neurosurgery: review of 1807 cases," *J. Neurosurg. Pediatr.*, vol. 18, no. 3, pp. 363–371, Sep. 2016, doi: 10.3171/2016.3.PEDS15679.

[30] J. Shillito and D. D. Matson, "Craniosynostosis: a review of 519 surgical patients.," *Pediatrics*, vol. 41, no. 4, pp. 829–53, Apr. 1968, [Online]. Available: http://www.ncbi.nlm.nih.gov/pubmed/5643989.

[31] E. J. van Lindert *et al.*, "Validation of cephalic index measurements in scaphocephaly," *Child's Nerv. Syst.*, vol. 29, no. 6, pp. 1007–1014, Jun. 2013, doi: 10.1007/s00381-013-2059-y.

[32] W. Likus, G. Bajor, J. Baron, J. Markowski, D. Milka, and T. Lepich, "Cephalic Index in the First Three Years of Life: Study of Children with Normal Brain Development Based on Computed Tomography," *Sci. World J.*, vol. 2014, pp. 1–6, 2014, doi: 10.1155/2014/502836.

[33] C. Linz *et al.*, "3D stereophotogrammetric analysis of operative effects after broad median craniectomy in premature sagittal craniosynostosis," *Child's Nerv. Syst.*, vol. 30, no. 2, pp. 313–318, 2014, doi: 10.1007/s00381-013-2253-y.

[34] J. F. Wilbrand *et al.*, "Value and reliability of anthropometric measurements of cranial deformity in early childhood," *J. Cranio-Maxillofacial Surg.*, vol. 39, no. 1, pp. 24–29, 2011, doi: 10.1016/j.jcms.2010.03.010.

[35] L. A. van Vlimmeren, T. Takken, L. N. A. van Adrichem, Y. van der Graaf, P. J. M. M. Helders, and R. H. H. H. Engelbert, "Plagiocephalometry: a non-invasive method to quantify asymmetry of the skull; a reliability study," *Eur. J. Pediatr.*, vol. 165, no. 3, pp. 149–157, Mar. 2006, doi: 10.1007/s00431-005-0011-1.

[36] P. Meyer-Marcotty *et al.*, "Head orthesis therapy in infants with unilateral positional plagiocephaly: an interdisciplinary approach to broadening the range of orthodontic treatment," *J. Orofac. Orthop. / Fortschritte der Kieferorthopädie*, vol. 73, no. 2, pp. 151–165, Apr. 2012, doi: 10.1007/s00056-011-0070-z.

[37] L. H. Plank, B. Giavedoni, J. R. Lombardo, M. D. Geil, and A. Reisner, "Comparison of infant head shape changes in deformational plagiocephaly following treatment with a cranial remolding orthosis using a noninvasive laser shape digitizer," *J. Craniofac. Surg.*, vol. 17, no. 6, pp. 1084–1091, 2006, doi: 10.1097/01.scs.0000244920.07383.85.

[38] C. A. Hill *et al.*, "Intracranial volume and whole brain volume in infants with unicoronal craniosynostosis," *Cleft Palate-Craniofacial J.*, vol. 48, no. 4, pp. 394–398, 2011, doi: 10.1597/10-051.

[39] D. T. Gault, D. Renier, D. Marchac, and B. M. Jones, "Intracranial pressure and intracranial volume in children with craniosynostosis.," *Plastic and reconstructive surgery*, vol. 90, no. 3. pp. 377–81, 1992, doi: 10.1097/00006534-199209000-00003.

[40] S. Sgouros, a D. Hockley, J. H. Goldin, M. J. Wake, and K. Natarajan, "Intracranial volume change in craniosynostosis.," *J. Neurosurg.*, vol. 91, pp. 617–625, 1999, doi: 10.3171/jns.1999.91.4.0617.

[41] D. Saiepour, P. Nilsson, J. Leikola, P. Enblad, and D. Nowinski, "Posterior cranial distraction in the treatment of craniosynostosis - Effects on intracranial volume," *Eur. J. Plast. Surg.*, vol. 36, no. 11, pp. 679–684, 2013, doi: 10.1007/s00238-013-0874-8.

[42] N. Rodriguez-Florez *et al.*, "Quantifying the effect of corrective surgery for trigonocephaly: A non-invasive, non-ionizing method using three-dimensional handheld scanning and statistical shape modelling," *J. Cranio-Maxillofacial Surg.*, vol. 45, no. 3, pp. 387–394, Mar. 2017, doi: 10.1016/j.jcms.2017.01.002.

[43] J. Pages, N. Buls, and M. Osteaux, "CT doses in children: A multicentre study," *Br. J. Radiol.*, vol. 76, no. 911, pp. 803–811, 2003, doi: 10.1259/bjr/92706933.

[44] Y. Arlachov and R. H. Ganatra, "Sedation/anaesthesia in paediatric radiology," *Br. J. Radiol.*, vol. 85, no. 1019, 2012, doi: 10.1259/bjr/28871143.

[45] K. P. Mason *et al.*, "Infant Sedation for MR Imaging and CT: Oral versus Intravenous Pentobarbital," *Radiology*, vol. 233, no. 3, pp. 723–728, 2007, doi: 10.1148/radiol.2333031872.

[46] A. A. Lindley, J. E. Benson, C. Grimes, T. M. Cole, and A. A. Herman, "The relationship in neonates between clinically measured head circumference and brain volume estimated from head CT-scans," *Early Hum. Dev.*, vol. 56, no. 1, pp. 17–29, Sep. 1999, doi: 10.1016/S0378-3782(99)00033-X.

[47] B. F. M. Rijken, B. K. den Ottelander, M.-L. C. van Veelen, M. H. Lequin, and I. M. J. Mathijssen, "The occipitofrontal circumference: reliable prediction of the intracranial volume in children with syndromic and complex craniosynostosis," *Neurosurg. Focus*, vol. 38, no. 5, p. E9, 2015, doi: 10.3171/2015.2.focus14846.

[48] S. Sgouros, "Skull vault growth in craniosynostosis," *Child's Nerv. Syst.*, vol. 21, no. 10, pp. 861–870, 2005, doi: 10.1007/s00381-004-1112-2.

[49] J. R. Marcus *et al.*, "Use of a three-dimensional, normative database of pediatric craniofacial morphology for modern anthropometric analysis.," *Plast. Reconstr. Surg.*, vol. 124, no. 6, pp. 2076–84, Dec. 2009, doi: 10.1097/PRS.0b013e3181bf7e1b.

[50] A. Björk, "Cranial base development: a follow-up x-ray study of the individual variation in growth occurring between the ages of 12 and 20 years and its relation to brain case," *Am. J. Orthod.*, 1955, doi: 10.1016/0002-9416(55)90005-1.

[51] B. Solow and A. Tallgren, "Head posture and craniofacial morphology," *Am. J. Phys. Anthropol.*, vol. 44, no. 3, pp. 417–435, 1976, doi: 10.1002/ajpa.1330440306.

[52] S. Pruzansky and E. F. Lis, "Cephalometric roentgenography of infants: Sedation, instrumentation, and research," *Am. J. Orthod.*, vol. 44, no. 3, pp. 159–186, Mar. 1958, doi: 10.1016/0002-9416(58)90012-5.

[53] W. M. Krogman, "Craniometry and cephalometry as research tools in growth of head and face," *Am. J. Orthod.*, vol. 37, no. 6, pp. 406–414, 1951, doi: 10.1016/0002-9416(51)90190-X.

[54] S. Dangi *et al.*, "Robust head CT image registration pipeline for craniosynostosis skull correction surgery," *Healthc. Technol. Lett.*, vol. 4, no. 5, pp. 174–178, 2017, doi: 10.1049/htl.2017.0067.

[55] N. R. Saber *et al.*, "Generation of normative pediatric skull models for use in cranial vault remodeling procedures.," *Childs. Nerv. Syst.*, vol. 28, no. 3, pp. 405–10, Mar. 2012, doi: 10.1007/s00381-011-1630-7.

[56] J.-F. Wilbrand *et al.*, "Objectification of cranial vault correction for craniosynostosis by three-dimensional photography," *J. Cranio-Maxillofacial Surg.*, vol. 40, no. 8, pp. 726–730, Dec. 2012, doi: 10.1016/j.jcms.2012.01.007.

[57] D. R. McKay *et al.*, "Measuring cranial vault volume with three-dimensional photography: A method of measurement comparable to the gold standard," *J. Craniofac. Surg.*, vol. 21, no. 5, pp. 1419–1422, 2010, doi: 10.1097/SCS.0b013e3181ebe92a.

[58] R. Toma *et al.*, "Quantitative morphometric outcomes following the Melbourne method of total vault remodeling for scaphocephaly.," *J. Craniofac. Surg.*, vol. 21, no. 3, pp. 637–43, May 2010, doi: 10.1097/SCS.0b013e3181d841d9.

[59] P. Meyer-Marcotty, H. Bohm, C. Linz, J. Kochel, A. Stellzig-Eisenhauer, and T. Schweitzer, "Three-dimensional analysis of cranial growth from 6 to 12 months of age," *Eur. J. Orthod.*, vol. 36, no. 5, pp. 489–496, Oct. 2014, doi: 10.1093/ejo/cjt010.

[60] M.-L. C. van Veelen *et al.*, "Volume measurements on three-dimensional photogrammetry after extended strip versus total cranial remodeling for sagittal synostosis: A comparative cohort study," *J. Cranio-Maxillofacial Surg.*, vol. 44, no. 10, pp. 1713–1718, Oct. 2016, doi: 10.1016/j.jcms.2016.07.029.

Chapter 2

The Computed Cranial Focal Point

G. A. de Jong, T. J. J. Maal, and H. Delye

Adapted from: G. A. de Jong, T. J. J. Maal, and H. Delye, "The computed cranial focal point," J. Cranio-Maxillofacial Surg., vol. 43, no. 9, pp. 1737–1742, Nov. 2015, doi: 10.1016/j.jcms.2015.08.023.

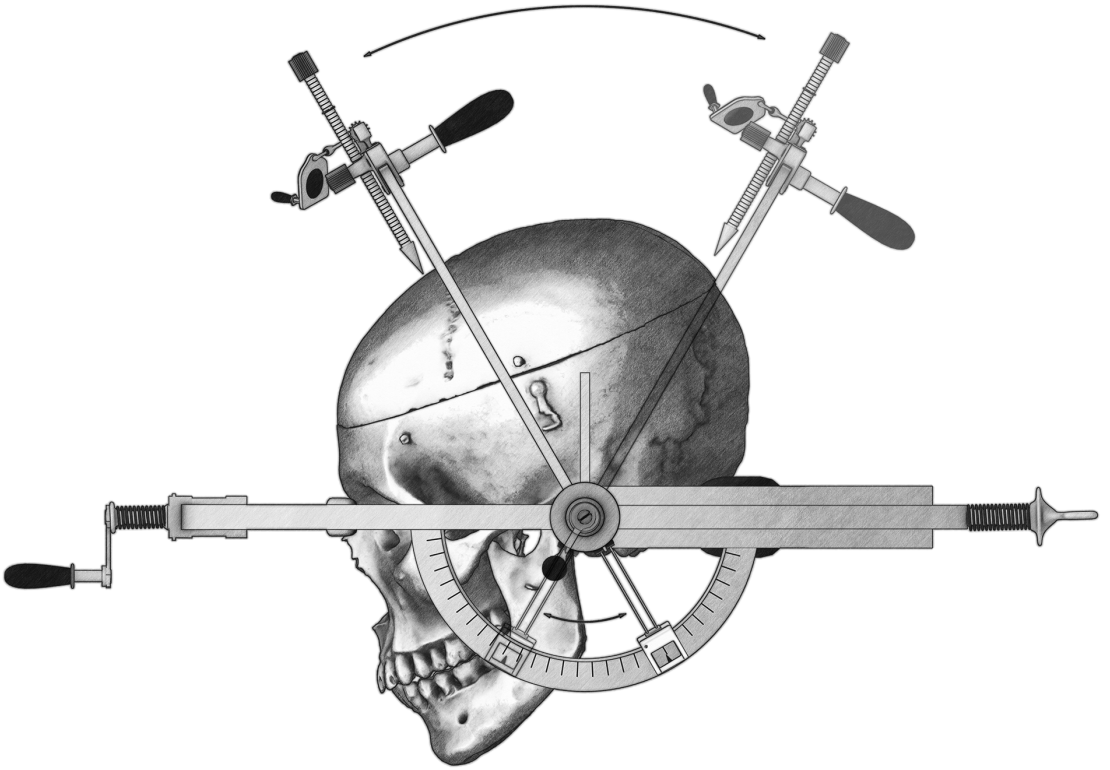

ABSTRACT

Introduction: Stereophotogrammetry is a radiation-free method for monitoring skull development after craniosynostosis repair. Lack of clear fixed reference points complicate longitudinal comparison of 3D photographs. Therefore we developed the 'computed cranial focal point' (CCFP).

Methods: The CCFP was calculated in segmented 3D CT-scans of 36 adult subjects using Matlab. The robustness of the CCFP calculation was evaluated in predefined hemi-ellipsoid shapes. Finally we used the CCFP in two clinical cases to correlate CT data with 3D-photographic data.

Results: The CCFP calculation was found to be hardly influenced by incomplete or deformed surface data which resulted in small deviations (<2.5 mm). The average position of the CCFP of the skin relative to the sella turcica was at (0.0, 27.1, 19.4) mm, with CCFPσ (0.6, 4.6, 3.9) mm. The mean difference between the CCFP for the skull and skin was (-0.1, 1.9, -1.4) mm, with CCFPσ (0.5, 1.4, 1.0) mm. Using the CCFP in two cases to correlate the skin from a 3D-photo and the segmented skin from a CT-scan resulted in absolute mean differences of 0.7 and 2.3 mm, with a standard deviation of 1.1 mm in both cases.

Conclusion: The CCFP calculation is a robust method to define a reference point relative to the sella turcica based on the skin or cranial bone surfaces. The CCFP can be used to correlate 3D photographs with CT-scan data or for longitudinal radiation-free comparison of 3D-photos.

INTRODUCTION

Craniosynostosis is defined by the premature fusion of cranial sutures with an incidence estimated at 1 in 2000 to 1 in 2500 live births [1]. Objective monitoring of the effects of craniosynostosis surgery relies heavily on the use of skull growth measurement. 3D skull measurements have become more widely used [2]–[5]. These newer methods primarily rely on defining 3D parameters of the skull using CT-scans, involving radiation techniques. Because this introduces an increased radiation dose during longitudinal follow up, alternative techniques like 3D photogrammetry have been proposed to monitor 3D skull parameters [6]–[10]. These techniques are limited to capturing the soft tissue surfaces. It has yet to be validated how the captured soft tissue correlates to the bony skull. Validation is difficult primarily due to the lack of consistent markers to overlay and match sequential 3D photos for growth monitoring. The current golden standard for overlaying skulls uses the sella turcica, dorsum sella or a nearby structure as skull to skull overlay point due to the assumption that these structures remain immobile during skull growth [11]. However these structures cannot be captured on 3D photos.

We propose a new method using the ”Computed Cranial Focal Point” (CCFP). The CCFP is the point in the cranium where all the surface normals of the skin or skull tend to intersect. The CCFP can be calculated for any spherical body like the skull or soft tissue surface of the head. The relative position from the sella turcica to the CCFP can be determined for the skin (CCFP-skin) and the skull (CCFP-skull) using CT-scans. In this study, we investigate how these points can be used for sequential photogrammetry matching, by defining the relation between the CCFP –skin and the CCFP-skull and their relative position to the sella turcica.

With the use of the CCFP we aim for a radiation free method to assist in objective sequential measurements of skull growth, to be used in craniosynostosis follow-up. This to reduce the need for CT-scans and thus to reduce the radiation exposure to pediatric patients with craniosynostosis.

MATERIALS AND METHODS

We developed the calculation of the CCFP and tested the robustness of this calculation method. Secondly, we performed an explorative patient study to define the relation between the CCFP-skin and the CCFP-skull and their relative position to the sella turcica. Finally, we used the CCFP-skin to match a CT-scan and 3D photo in two separate cases to evaluate the potential of the CCFP for matching a CT-scan and 3D photo.

COMPUTED CRANIAL FOCAL POINT CALCULATION

The CCFP can be calculated by determining the mean virtual intersection point of all the surface normals. All these intersection points combined create a point cloud in the cranium with a center point and spread (CCFPσ). In depth calculation of the CCFP can be found in Appendix A.

METHOD ROBUSTNESS TEST

SHAPE SELECTION

The method robustness test was done using a set of predefined shapes as meshes (triangulated objects). Since this is a new method no predefined set of shapes to benchmark the method exists. The shapes were chosen to distinguish the effect on the CCFP and CCFPσ caused by the conditions that could appear in real world cases. All the shapes are spherically centered around the origin (0,0,0). The x-direction is from medial to lateral as seen from the left side, the y-direction from caudal to cranial and the z-direction from anterior to posterior. We used approximately 50.000 triangles per shape for optimum computation time versus accuracy.

The CCFP and CCFPσ of these shapes were calculated and compared with known values to determine the calculation accuracy. The CCFP coordinates are defined relative to the origin (0, 0, 0) in *mm* as *xyz*. The CCFPσ is also defined in *mm* as *xyz*.

One shape is a sphere with a radius of 9.6 *cm*. There also were 4 hemi-ellipsoid shapes originating from a hemi-ellipsoid with a height and length radius of 9.6 *cm* and a width radius of 7.7 *cm* [Figure 1(a)]. These measures were chosen to approximate the average human head size. The other 3 hemi-ellipsoid shapes were either asymmetrical cut to remove approximately 20% of the total

surface at 15 degrees pitch and 5 degrees roll [Figure 1(b,d)] and/or irregular deformed up to 2.0 *cm* of the original [Figure 1(c,d)]. This is to mimic irregular skull shapes and partial missing data as could occur on a CT-scan. There were also two other shapes based on the hemi-ellipsoid resembling respectively trigonocephaly [Figure 1(e)] and scaphocephaly [Figure 1(f)].

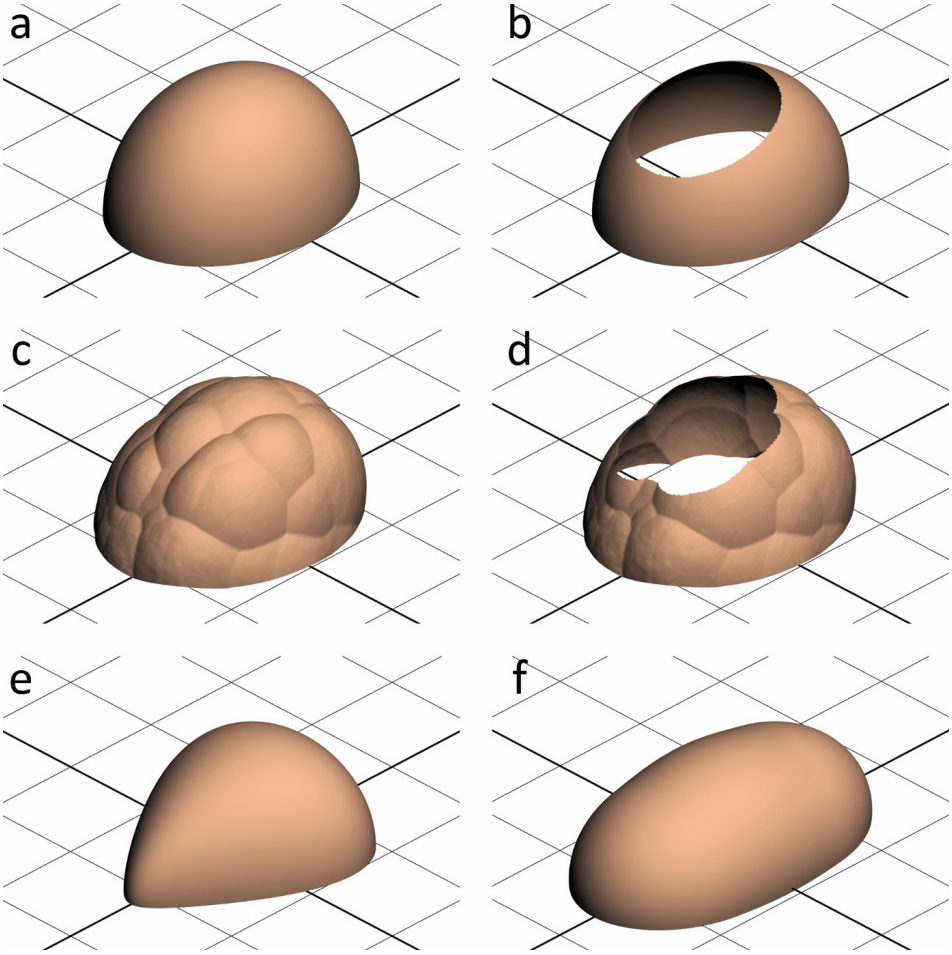

Figure 1: A selection of the meshes that have been used in the Method Robustness Test: a) hemi-ellipsoid; b) hemi-ellipsoid cut; c) hemi-ellipsoid deformed; d) hemi-ellipsoid deformed and cut; e) hemi-ellipsoid trigonocephaly; f) hemi-ellipsoid scaphocephaly.

CCFP OUTCOME COMPARISON

The sphere, full hemi-ellipsoid and the cut hemi-ellipsoid shapes have a known geometric focal point at the origin. The deformed hemi-ellipsoids shapes and the trigonocephaly- and scaphocephaly- shapes are constructed around the

origin but do not necessarily have a geometric focal point at the origin. The position of the CCFP relative to the origin and the CCFPσ to (0,0,0) for the sphere is caused by polygon inaccuracy and the calculation itself. A similar comparison for the cut and full shapes give the difference caused by removing a part of the shape. Comparing the CCFP and CCFPσ between the deformed and normal shapes gives the difference caused by deformation.

The trigonocephaly- and scaphocephaly- shaped hemi-ellipsoid shapes originated from the hemi-ellipsoid with a known focal point at the origin and have been freeform scaled. The difference of the CCFP and the relative CCFP difference compared to the normal hemi-ellipsoid give the error caused by variation.

PATIENT STUDY

PATIENT STUDY SCAN SELECTION

For the explorative study, we used scans from patients that underwent a cranial CT-scan in the ER in Radboudumc between June 2013 and June 2014. Scans showing cranial trauma or structural pathologies were excluded resulting in a group of 36 patients aged 18-65 y.o. (mean 42,6 y.o.) of which 19 were female. The scans were made with a Toshiba Aquilion ONE using a pixel spacing of 0.43 *mm* and a slice thickness of 0.5 *mm* with a slice resolution of 512x512 by 302 to 376 slices. The scans were anonymized in accordance to local rules from the institutional board of the academic hospital.

SEGMENTATION

All the CT-scans were segmented prior to the calculation of the CCFP to obtain the outer surface of the skull and the skin of the head as a mesh. A threshold of -150 HU for the skin and 500 HU for the bone was used and tweaked per scan for the optimum segmentation. Filters were applied removing small artifacts outside the head and to fill any surrounded structures. The resulting volume data was resized to create voxels of approximately 1x1x1 *mm*. Segmentation was applied from above the supraorbital process to the lowest possible point on the parietal bone. The mesh was made by using Matlab's [12] built-in 'isosurface' function.

REGISTRATION

The meshes underwent a translation so that the position of the sella turcica was aligned to the origin (0, 0, 0). Scaling was applied so that 1 unit in the mesh-space equals 1 *mm*.

The meshes were aligned with the sella nasion plane crossed with the horizon of the sphenoid at the sella turcica as the horizontal plane. Axis were directed so that sella to cranial is the positive y-direction, the sella to posterior is the positive z-direction, and the right to left is the positive x-direction. All triangles of the mesh $y < -5mm$ of the sella turcica were omitted in further calculations.

PATIENT STUDY OUTCOME COMPARISON

The main goal of the patient study is to investigate the relation between the CCFP-skull and CCFP-skin. The secondary goal is to determine the relation between the CCFP-skull/CCFP-skin and the sella turcica.

CASE STUDIES: MATCHING OF A CT-SCAN AND A 3D PHOTO

The first case was a 9 month old female suspected of craniosynostosis of which a 3D photo was made. A CT-scan followed 3 weeks after the photo disproving craniosynostosis. The second case was a 3 month old female patient with suspected craniosynostosis of which a CT-scan was made proving trigonocephaly. For further evaluation a 3D photo of this patient was made 6 weeks after the CT-scan. Both cases were individually used for matching the CT-scan and 3D photo using the CCFP.

Since the relative position between sella turcica, CCFP-skin and CCFP-skull is predictable both CCFPs can be used in matching. Hence the CCFP-skin of a 3D photo and CT-scan was used.

Per case the CCFP-skin was calculated for both the CT-scan and 3D photo. We aligned and rotated the CT-scan similar to that of the patient study. We transformed the 3D photo with the CCFP-skin to the CCFP-skin of the CT-scan. The 3D photo was then manually rotated to match the CT-scan using the CCFP as a pivot.

We calculated the difference between the two meshes using raycasting [13]. A raycast will be performed from the 3D photo with the origin in each vertex and the direction equal to the normal of each vertex. For each raycast the absolute

difference between the hitpoints of the CT-scan skin and 3D photo is expressed as the matching difference per triangle. The raycasting was accelerated using OpenCL [14], [15]. We determined the absolute mean difference, standard deviation and the maximum difference and the location of the maximum difference for the raycasting.

RESULTS

METHOD ROBUSTNESS TEST

The method robustness test focused on the accuracy of the CCFP for a known focal point and the spread of the CCFPσ for various meshes. All given CCFP coordinates and CCFPσ standard deviations are presented in [Table 1].

Table 1: The distance in for x, y and z from 0, 0, 0 to the computed cranial focal point (CCFP), and the standard deviation of x, y and z for the test models in mm.

Structure	CCFP (*mm*)			CCFPσ (*mm*)		
	X	Y	Z	σ(X)	σ(Y)	σ(Z)
Sphere	0.0	0.0	0.0	0.01	0.01	0.01
Hemi-ellipsoid	0.0	7.7	0.0	8.3	2.7	5.6
Hemi-ellipsoid cut	0.8	7.0	1.1	9.2	2.5	6.0
Hemi-ellipsoid deformed	-0.7	9.8	0.8	9.9	8.4	9.9
Hemi-ellipsoid deformed and cut	-1.6	10.0	0.9	9.6	7.8	11.7
Hemi-ellipsoid trigonocephaly	0.0	-5.6	10.7	9.5	5.7	9.7
Hemi-ellipsoid scaphocephaly	0.0	-6.2	-0.1	12.1	24.5	7.2

In the sphere there was no measurable deviation for the CCFP and a (0.01, 0.01, 0.01) *mm* spread for the CCFPσ. This can be considered negligible in CT-scans with a voxel spacing size of 0.5 .

The full, cut, and deformed hemi-ellipsoid shapes have a predominant y-component for the CCFP around 8 *mm* and small x- and z-components (ranging from -0.7 to 1.1 *mm*). Do note that the CCFP does not have to represent the geometrical focus. The distance between the full and the cut hemi-ellipsoid is 1.5 *mm* and between the full and deformed hemi-ellipsoid is 2.4 *mm*. The distance between the deformed hemi-ellipsoid and the deformed and cut hemi-ellipsoid is 0.9 *mm*. Removing approximately 20% of the surface results in a smaller difference of the CCFP than applying up to 2 *cm* deformations to the surface. In case of deformations the difference caused by the cut is almost similar to the cut alone.

The spread for the full, cut and deformed hemi-ellipsoid shapes ranges from 2.5 to 11.7 *mm*. The full and cut versions have a predominant spread in the x- and z-direction. The y-direction has the smallest spread in these cases. The deformations primarily add to the spread in the y- and z-direction and are even more present in the z-direction when cut.

The trigonocephaly hemi-ellipsoid has a CCFP of (0.0, -5.6, 10.7). This deviates 17.1 *mm* from the full hemi-ellipsoid and is most present in the y- and z-direction. The scaphocephaly hemi-ellipsoid in contrast has a CCFP of (0.0, -6.2, -0.1) which only significantly deviates in the y-direction from the full hemi-ellipsoid (13.9 *mm*).

The spread for the trigonocephaly primarily deviates from the full hemi-ellipsoid in the y- and z-direction. The spread for the scaphocephaly deviates in all directions with the highest deviation in the z-direction up to 24.5 *mm*.

PATIENT STUDY

The results of the CT-scans can be found in [Table 2]. The CCFP (*mm*) is expressed as relative to the sella turcica (0, 0, 0) in the sella-nasion orientation. The average CCFP-skull is at (-0.4, 28.9, 18.0) with a σ (0.5, 4.5, 4.4) while the CCFP-skin is at (0.0, 27.1, 19.4) with a σ (0.6, 4.6, 3.9). Using a Shapiro-Wilk test resulted in proven normal distributions in the x- and y-direction with CCFP-skull p-values of (0.226, 0.452, 0.000) and CCFP-skin p-values of (0.388, 0.526, 0.001).

The difference between the σ of the CCFPs is in sub-millimeter scale. The mean CCFP differs (-0.1, 1.9, -1.4) from skull to skin with a maximum σ of 1.4 *mm* and a maximum 95% CI of ± 0.6 *mm*.

Table 2: The mean CCFP, standard deviation and 95% CI for the population of 36 patients for the skull, skin and difference between the skull and skin (Δ) in mm.

CCFP	Mean (*mm*)	σ (*mm*)	95% CI (*mm*)
$Skull_x$	-0.1	0.5	-0.2 – 0.1
$Skull_y$	28.9	4.5	27.4 – 30.4
$Skull_z$	18.0	4.4	16.5 – 19.5
$Skin_x$	0.0	0.6	-0.1 – 0.2
$Skin_y$	27.1	4.6	25.5 – 28.6
$Skin_z$	19.4	3.9	18.1 – 20.8
Δ_x	-0.1	0.5	-0.3 – 0.0
Δ_y	1.9	1.4	1.4 – 2.5
Δ_z	-1.4	1.0	-1.8 – -1.1

CASE STUDIES: MATCHING OF A CT-SCAN AND A 3D PHOTO

CASE 1

Visual representation of the registration in 3D shows a nicely matched overlay [Figure 2]. The colors represent the difference between the 3D photo and CT-scan. The overlay shows the origin at the sella turcica as obtained from the CT-scan. A blue circle at the top shows the position of the maximum difference as caused by the hairnet.

The absolute average raycast difference was 0.7 *mm* with a standard deviation of 1.1 *mm*. The biggest difference was 6.72 *mm* at the bulge of the hairnet but did not seem to significantly impact the average.

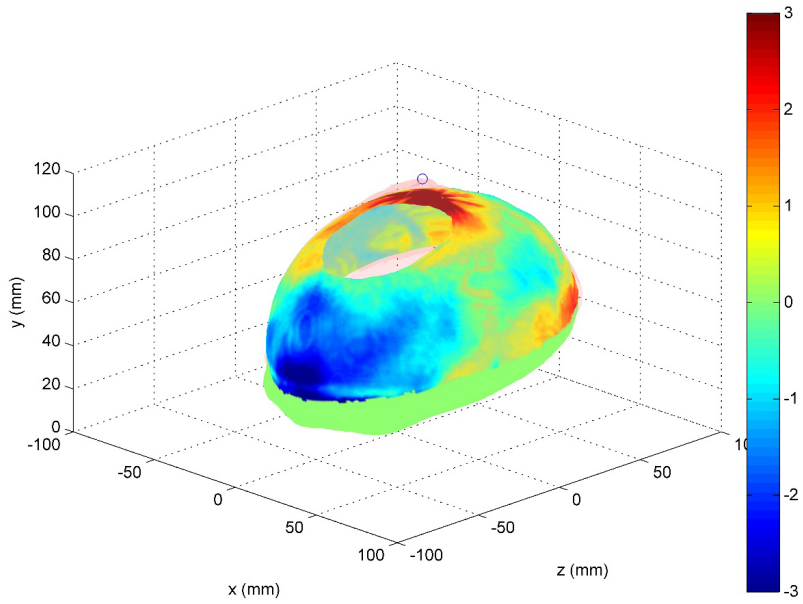

Figure 2: Overlaying and distance map of a 3D photo and CT-scan using CCFP-skin matching and manual rotation in a 9 month old female patient.

CASE 2

The visual representation of the registration in 3D shows a nicely matched overlay [Figure 3] with the origin at the sella turcica as obtained from the CT-scan. A blue circle at the top shows the position of the maximum difference as caused by the hairnet. Again the colors represent the difference between the 3D photo and CT-scan.

The absolute average raycast difference was 2.3 *mm* with a standard deviation of 1.1 *mm*. The biggest difference was 6.44 *mm* at the bulge of the hairnet at the back of the head.

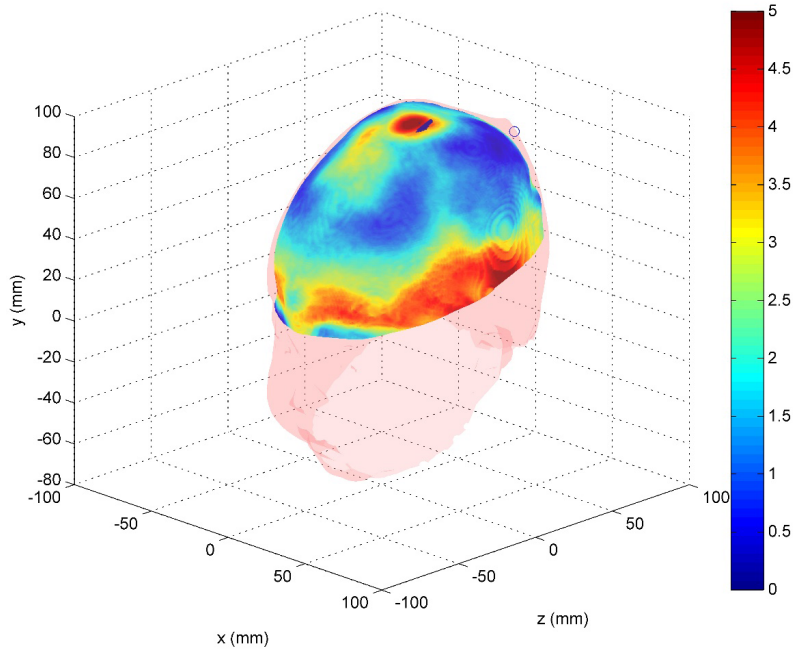

Figure 3: Overlaying and distance map of a 3D photo and CT-scan using CCFP-skin matching and manual rotation in a 3 month old female patient.

DISCUSSION

The method robustness test showed that the CCFP calculation is robust against missing data and deformation in hemi-ellipsoid shapes. The part of the head used for these calculations is roughly hemi-ellipsoid in healthy patients but shows different expressions in patients with craniosynostosis. The craniosynostosis shapes showed a deviant CCFP position as compared to the other cases. This makes it possibly useful for classifying these conditions but less useful for comparison between these and healthy heads without the use of additional reference points. Thus finding other reference points that can be related to the sella turcica or using only a partial CCFP calculation by excluding the affected part of the head might overcome this issue.

The segmentation process was done in Matlab [12] resulting in some limitations. Especially when CT scan was performed with considerable head flexion, segmentation and registration resulted in a smaller usable section for CCFP calculation. Missing data did not influence the CCFP calculation significantly in the robustness test, however accuracy improves utilizing all data. Changing the segmentation process in Matlab could resolve this issue. Another option is using software like ITK-snap to handle the segmentation [16].

The patient study consisted of 36 patients and was of an explorative nature. Hence the study only gives an indication of the distribution of the CCFP among the adult population. Using a larger sample results in even more accuracy, although this study showed a small 95% CI spread for CCFPs. Yet the few millimeter 95% CI spread for CCFPs suggest that the mean position for the CCFPs between individuals is at about the same position relative to the sella turcica. The 95% CI sub-millimetre spread for the mean difference between the CCFP-skin and CCFP-skull suggests that the position relative to each other is predictable.

The case studies of matching 3D photos with CT-scans using the CCFP showed a very high agreement. A follow-up study is needed to show pitfalls or problems during this process. Although the absolute average difference is bigger than in first case, the standard deviation of the difference is almost equal in both cases. This can be explained by the time between the CT-scan and 3D photo as well as the order in which these were taken. In the first case the 3D photo was made prior to the CT-scan which added the hairnet to the overall 3D photo volume but where growth added to the CT-scan volume and thus somewhat

compensating each other's additional volume. In the second case the CT-scan came prior to the 3D photo which allowed both the hairnet and the additional growth time (3 versus 6 weeks) to add to the volume of the 3D photo. Therefor it is to be expected that there was a bigger absolute average difference compared to the first case. Taking this in consideration as well as the near equal standard deviation and the visual inspection suggests that in both cases the overlay was performed with equal accuracy. Finally the trigonocephaly did not seem to impact the matching process. Further differences could be caused by inaccuracy of the 3D-photo system or the CT-scan and its segmentation or registration.

In a growing skull, the CCFP could change and might require parametric correction to be able to perform sequential overlay of 3D photo data. This should be the subject of a follow-up study with CT-scans in different pediatric age groups. The CCFPσ was only used for the method robustness test and was not further evaluated in the patient study. The CCFPσ might give insight in the shape of the head as well as the effect of possible abnormalities of the head as suggested in the robustness test for the trigonocephaly and scaphocephaly shapes. This should be looked into and can potentially be used in clinical practice.

A final limitation of this study was the manual rotation used during the registration process. This could result in small variation differences from patient to patient. An automated method to determine the rotations in these parts would be more objective and thus less vulnerable to these errors.

CONCLUSION

We have shown that the calculation of the CCFP is reliable and robust against deformations and missing data. Furthermore there is a considerable relative difference for the CCFP position in the synthetic shapes of the simulated trigonocephaly and scaphocephaly compared to the other shapes. This relative difference could potentially be used to quantify and/or qualify these conditions in CT-scans or 3D photo's. Future research should be directed to investigate these features.

In the adult population, the CCFP-Skin and CCFP-Skull only differ a few millimeter in mean, 95% CI and standard deviation. Thus obtaining either of these values can be used to accurately estimate the other value. Since the

difference of the CCFP-skin and CCFP-skull show few millimeter variations in individuals, the CCFP-skin can be used as an indication to where the sella turcica is located.

The CCFP-skull lies at average 1.9 *mm* more cranial and 1.4 *mm* more anterior than the CCFP-skin. The CCFP-skin is at (0.0, 27.1, 19.4) *mm* and the CCFP-skull at (-0.1, 28.9, 18.0) *mm* with a few-millimeter 95% CI, in relation to the sella turcica.

We have shown that the alignment of the skin surface of a 3D photo to a CT-scan while using the CCFP translation and manual rotation results in a near perfect match. We have shown a fit with an average sub millimeter difference in the first case and 2.3 *mm* difference in the second case which can be explained by growth and the use of a hairnet. In both cases there was a very small standard deviation for the difference (1.1 *mm*) suggesting that both cases were matched with equal accuracy. The hairnet in the 3D photo, and the missing data in the CT-scan had no observable impact on the CCFP calculation and matching. Hence the CCFP matching method is a viable option to match 3D photos with CT-scans. This could be done with sequential 3D photos as well, reducing the need for CT-scans and the radiation dose in the follow-up of cranial development.

In summary the CCFP method is a robust method for determining a position in the head by the skin surface or skull surface with a predictable position relative to the sella turcica. The CCFP of the skin and the skull have a known distance with a known variance relative to each other on which can be anticipated. Furthermore using the CCFP to overlay a 3D photo and CT-scan is a viable option that might also yield good results in sequential 3D photos. However more research is needed to fully explore the extent of the CCFP in cranial applications by itself and in relation to other cranial measurement methods. Distinguishing between age and sex can give insight in the CCFP in the developing cranium. But most important is the potential to reduce the need for CT-scans, along with the radiation exposure in the follow-up of cranial development by using the CCFP.

APPENDIX

CCFP CALCULATION

The CCFP is calculated by determining the average of so called center points in a triangulated spherical object. Each face/triangle/polygon in the triangulated object has a center and a normal. Each center and normal can be considered as a skew line with the origin in the face center and the direction as the face normal. A so called center point can be calculated for each combination of skew lines that can be made. A center point is a point between two skew lines that has the closest and equal distance to two skew lines. For this the positions s and t on lines $L_n(s)$ and $L_m(t)$ are used to calculate the center point as shown in *Ericson, Real-Time Collision Detection, 2005, (Chapter 5.1.8)* [17]. An example of two skew lines and their center point is given in [Figure 4].

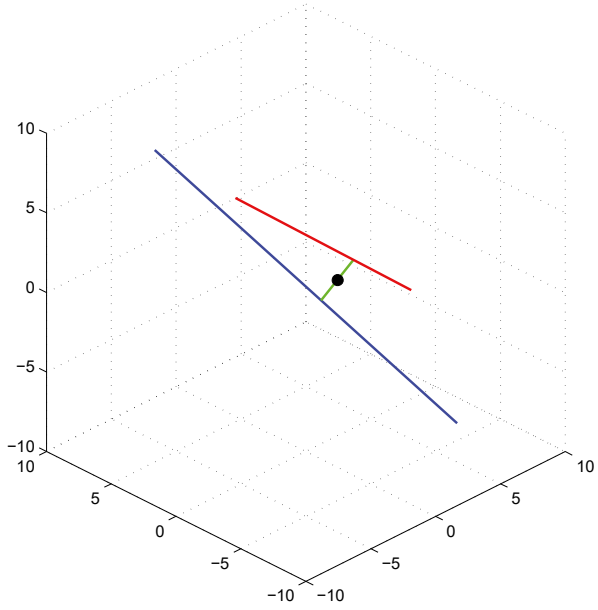

Figure 4: Example of two skew lines and the center point in 3D. A green line is drawn between two non-intersecting skew lines (red and blue) where the distance between these skew lines is shortest. The center of this green line is a center point. The distance from the center point to the each skew lines is equal.

Averaging all skew line combinations for one given face gives the center-point ($\boldsymbol{P}_{c,L_n}$) for that face as can be seen in [Equation (1)]. Only skew line combinations that have an absolute angle between each other larger than 30 degrees (and smaller than 330 degrees) will be used in the calculation. These cases will be add to the count of n_{f,L_n} as well. This is to exclude near-parrallel face calculations that would result in outliers.

$$\boldsymbol{P}_{c,L_n} = \frac{1}{n_{f,L_n}} \sum \frac{L_n(s) + L_m(t)}{2} \tag{1}$$

Finally all center points are averaged to get the CCFP as can be seen in [Equation (2)].

$$\boldsymbol{CCFP} = \frac{1}{n_{faces}} \sum_{n=1}^{n_{faces}} \boldsymbol{P}_{c,L_n} \tag{2}$$

CALCULATION SOFTWARE

Calculation of the CCFP is performed using Matlab 2014a (8.3) [12] with C++ and OpenCL 1.2 [14], [15]. Matlab is used to calculate the skew lines of each polygon. The skew lines are send to a C++ library that facilitates OpenCL to calculate the center points. OpenCL was used to accelerate the calculation of the CCFP. In Matlab the CCFPσ and CCFP are calculated using the standard deviation and average of these center points. The software used was as proof of concept and thus the CCFP calculation is not limited to Matlab or C++. Other software (e.g. the free alternative Octave (*Eaton*, online)) could be used to implement the CCFP calculation. Other acceleration techniques like CUDA [19] instead of OpenCL could also be used. Due to the simple math in the CCFP calculation completely stand-alone software could be written if desired.

REFERENCES

[1] B. J. Slater, K. a Lenton, M. D. Kwan, D. M. Gupta, D. C. Wan, and M. T. Longaker, "Cranial sutures: a brief review.," *Plast. Reconstr. Surg.*, vol. 121, no. 4, pp. 170e–8e, Apr. 2008, doi: 10.1097/01.prs.0000304441.99483.97.

[2] J. Marcus, L. Domeshek, and R. Das, "Objective three-dimensional analysis of cranial morphology.," *Eplasty*, vol. 8, pp. 175–187, 2007, Accessed: Jun. 10, 2014. [Online]. Available: http://europepmc.org/abstract/MED/18464892.

[3] J. R. Marcus *et al.*, "Use of a three-dimensional, normative database of pediatric craniofacial morphology for modern anthropometric analysis.," *Plast. Reconstr. Surg.*, vol. 124, no. 6, pp. 2076–84, Dec. 2009, doi: 10.1097/PRS.0b013e3181bf7e1b.

[4] N. R. Saber *et al.*, "Generation of normative pediatric skull models for use in cranial vault remodeling procedures.," *Childs. Nerv. Syst.*, vol. 28, no. 3, pp. 405–10, Mar. 2012, doi: 10.1007/s00381-011-1630-7.

[5] H. Delye, T. Clijmans, M. Y. Mommaerts, J. Vander Sloten, and J. Goffin, "Creating a normative database of age-specific 3D geometrical data, bone density, and bone thickness of the developing skull: a pilot study," *J. Neurosurg. Pediatr.*, vol. 16, no. 6, pp. 687–702, Dec. 2015, doi: 10.3171/2015.4.PEDS1493.

[6] J.-F. Wilbrand *et al.*, "Objectification of cranial vault correction for craniosynostosis by three-dimensional photography," *J. Cranio-Maxillofacial Surg.*, vol. 40, no. 8, pp. 726–730, Dec. 2012, doi: 10.1016/j.jcms.2012.01.007.

[7] D. R. McKay *et al.*, "Measuring cranial vault volume with three-dimensional photography: A method of measurement comparable to the gold standard," *J. Craniofac. Surg.*, vol. 21, no. 5, pp. 1419–1422, 2010, doi: 10.1097/SCS.0b013e3181ebe92a.

[8] R. Toma *et al.*, "Quantitative morphometric outcomes following the Melbourne method of total vault remodeling for scaphocephaly.," *J. Craniofac. Surg.*, vol. 21, no. 3, pp. 637–43, May 2010, doi: 10.1097/SCS.0b013e3181d841d9.

[9] P. Meyer-Marcotty, H. Bohm, C. Linz, J. Kochel, A. Stellzig-Eisenhauer, and T. Schweitzer, "Three-dimensional analysis of cranial growth from 6 to 12 months of age," *Eur. J. Orthod.*, vol. 36, no. 5, pp. 489–496, Oct. 2014, doi: 10.1093/ejo/cjt010.

[10] H. Schaaf, C. Y. Malik, P. Streckbein, J. Pons-Kuehnemann, H.-P. Howaldt, and J.-F. Wilbrand, "Three-dimensional photographic analysis of outcome after helmet treatment of a nonsynostotic cranial deformity.," *J. Craniofac. Surg.*, vol. 21, no. 6, pp. 1677–1682, 2010, doi: 10.1097/SCS.0b013e3181f3c630.

[11] A. Björk, "Cranial base development: a follow-up x-ray study of the individual variation in growth occurring between the ages of 12 and 20 years and its relation to brain case," *Am. J. Orthod.*, 1955, doi: 10.1016/0002-9416(55)90005-1.

[12] The MathWorks Inc., "MATLAB and Statistics Toolbox Release 2014a," *Natick, Massachusetts, United States*, 2014.

[13] T. Möller and B. Trumbore, "Fast, minimum storage ray/triangle intersection," in *ACM SIGGRAPH 2005 Courses on - SIGGRAPH '05*, 2005, vol. 2, no. 1, p. 7, doi: 10.1145/1198555.1198746.

[14] Khronos Group, "OpenCL: The open standard for parallel programming of heterogeneous systems." https://www.khronos.org/opencl/ (accessed Aug. 19, 2015).

[15] J. Stone, D. Gohara, and G. Shi, "OpenCL: A parallel programming standard for heterogeneous computing systems," *Comput. Sci. Eng.*, 2010, doi: 10.1109/MCSE.2010.69.

[16] L. Ibanez, W. Schroeder, L. Ng, and J. Cates, *The ITK Software Guide*, vol. Second, no. May. Kitware, Inc., 2005.

[17] C. Ericson, "Chapter 5 - Basic Primitive Tests," in *Real-Time Collision Detection*, C. Ericson, Ed. San Francisco: Morgan Kaufmann, 2005, pp. 125–233.

[18] J. W. Eaton, "GNU Octave." http://www.gnu.org/software/octave/ (accessed Aug. 19, 2015).

[19] J. Nickolls, I. Buck, M. Garland, and K. Skadron, "Scalable parallel programming with CUDA," *Queue*, vol. 6, no. 2, p. 40, 2008, doi: 10.1145/1365490.1365500.

Chapter 3

Technical Note: The Computed Cranial Focal Point in Trigonocephaly and Scaphocephaly

G.A. de Jong, J.W. Meulstee, T. J. J. Maal and H. Delye

Adapted from: the submitted manuscript to Journal of Cranio-Maxillofacial Surgery on September 2020.

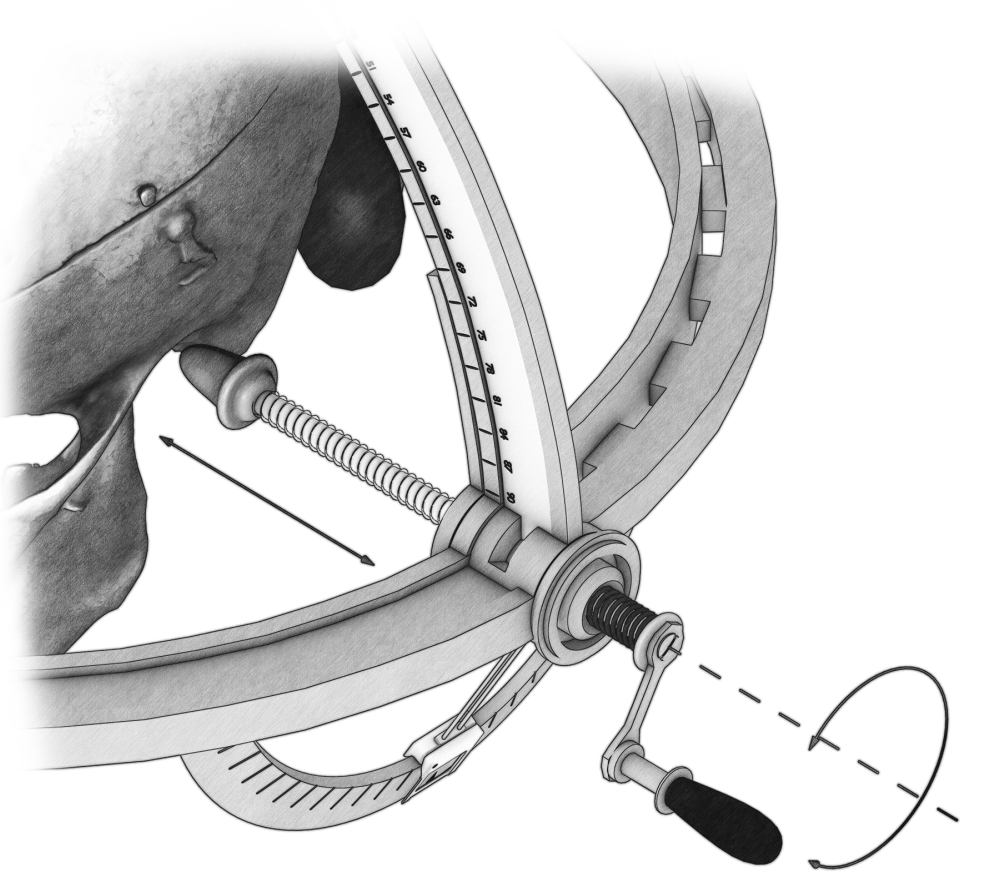

ABSTRACT

Introduction: The Computed Cranial Focal Point (CCFP) was introduced to standardize the alignment of cranial 3D photos and CT-scans in, for instance, soft-tissue matching. The effect of the presence of scaphocephaly or trigonocephaly on soft-tissue matching has not yet been investigated. Therefore, our goal was to investigate the soft-tissue matching error of the CCFP alignment method between CT-scans and 3D photos in scaphocephaly or trigonocephaly patients.

Methods: Time-matched cranial 3D photos and CT-scans of 20 scaphocephaly and 20 trigonocephaly patients were collected. The mean CCFP-offset was determined in the soft-tissue CT-scans for both patient groups. Two alignment strategies reflecting two different use cases were used for soft-tissue matching between the CT-scans and 3D photos using the CCFP alignment technique. The soft-tissue matching error was determined and visualized using distance maps for both strategies.

Results: Regardless of strategy, both patient groups showed a good surface matching fit. Both strategies had near identical distance map for either trigonocephaly or scaphocephaly.

Conclusion: Both alignment strategies showed a good fit with near identical surface matching performance in matching 3D Photos and CT-scans in either craniosynostosis form.

INTRODUCTION

Adequate cranial shape evaluation methods are important for the detection and follow-up of craniosynostosis [1]. Three-dimensional (3D) imaging techniques such as 3D stereophotogrammetry and 3D-CT are frequently used to perform 2D measurements, calculate ratios, or to generate distance maps of the cranial shape [2]–[4]. An important step in processing these 3D imaging forms is the alignment technique.

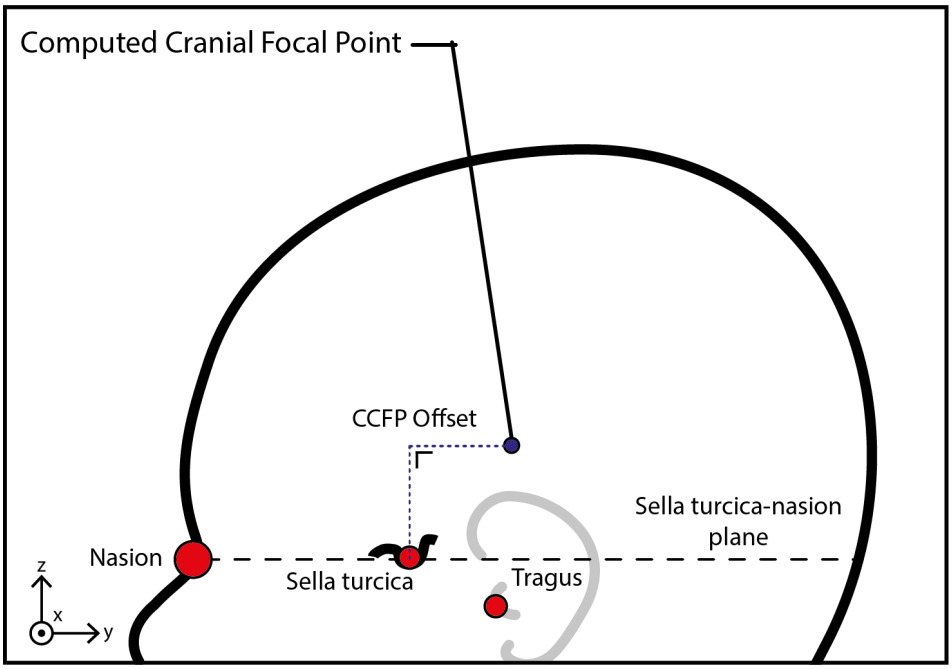

Figure 1: A 2D representation of the computed cranial focal point (CCFP) within the head. This uses the common type of expression in the form of the CCFP-offset value in the sella turcica-nasion orientation with the sella turcica as the origin (0,0,0).

In earlier studies, we presented the alignment technique using the Computed Cranial Focal Point (CCFP) [5], [6]. This technique is based on the CCFP-offset; the 3D position of the CCFP relative to the sella turcica in the sella-turcica nasion (StN) orientation [Figure 1]. The CCFP can be computed by determining the mean intersection of all the inwardly directed normal rays of the surface of the head starting 20 mm above the sella turcica–nasion plane [Figure 2]. This technique has been applied in several studies [6]–[8], however, it is still uncertain what the effects of deformations caused by craniosynostosis may have on the accuracy of alignment using the CCFP.

The goal of this study was to investigate the soft-tissue matching error of the CCFP alignment method between CT-scans and 3D photos in scaphocephaly or trigonocephaly patients.

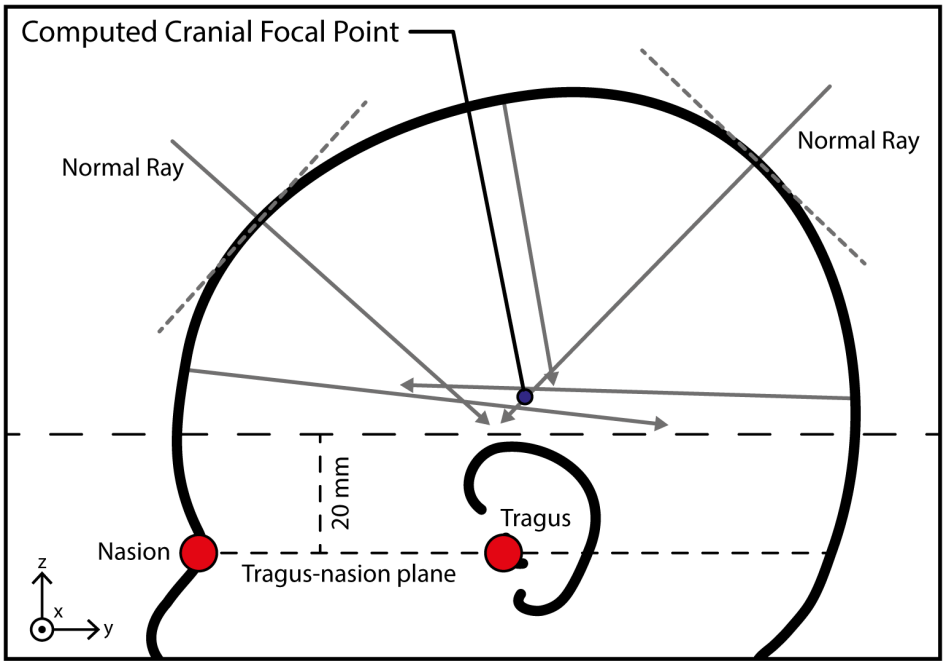

Figure 2: A 2D representation of the computation of the computed cranial focal point (CCFP). The CCFP is computed by determining the mean intersection of all normal rays of the 3D photo or CT-scan of the head 20 mm above the nasion-tragus plane.

MATERIALS AND METHODS

STRATEGY

The soft-tissue matching error of the CCFP alignment method between CT-scans and 3D photos in scaphocephaly or trigonocephaly patients is determined in two steps. First the CCFP-offset values for trigonocephaly and scaphocephaly patients are calculated and compared using CT-scans. These are then used in the second step. In the second step, the soft-tissue matching errors of CT-scans and 3D photos for scaphocephaly and trigonocephaly patients are determined after applying the CCFP alignment method.

ACQUISITION AND SUBJECTS

The first dataset consists of 20 time-matched pre-surgery CT-scans and 3D photos of scaphocephaly patients. The second dataset consists of 20 time-matched pre-surgery CT-scans and 3D photos of trigonocephaly patients. The time-matched CT-scans and 3D photos were acquired within 30 days of each other for each patient.

The 3D photos were obtained using a 3DMD Cranial System (3dMDCranial, 3dMD, Atlanta, USA). Scaphocephaly and trigonocephaly patients were randomly selected from the craniosynostosis registry of our institution. Patients scheduled for either endoscopic strip craniectomy as well as total vault remodeling were eligible. Patients who signed the opt-out for anonymous data use for scientific research were excluded. Patients with 3D photos or CT-scans that presented incomplete captured craniums or quality inconsistencies were excluded. If a patient was excluded, a random replacement was selected and checked for exclusion criteria until 20 scaphocephaly patients and 20 trigonocephaly patients were included. After data collection, patients were anonymized and labelled with either trigonocephaly or scaphocephaly.

Approval with an informed consent waiver from the regional institutional review board was obtained (CMO regio Arnhem – Nijmegen, 2020-6128). This study was conducted in compliance with the World Medical Association Declaration of Helsinki on medical research ethics.

DATA PRE-PROCESSING

The data pre-processing was mostly similar to that of Meulstee et al. [7]. All CT-scans were reconstructed to 3D surfaces using Maxilim software (Medicim NV, Mechelen, Belgium). All 3D surfaces of all the CT-scans were landmark annotated manually using custom software written in Unity v5.6.3 (Unity Technologies, San Francisco, CA, USA). Using a 3D photo version of the software [Figure 2], 3D photo landmarks were also annotated manually. The annotated landmarks for the CT-scans and 3D photos are listed in [Table 1].

Table 1: Landmarks on the 3D-photos and CT-scans.

3D photos	3D CT
• Pretragion/Tragus (left & right) • External cantion/exocanthion (left & right) • Internal cantion/endocantion (left & right) • Nasal bridge/Nasion • Nose tip • Subnasal landmark at the transition of the nose and upper lip/Subnasale	• Nasion • Sella turcica • Frontozygomatic suture • External acoustic meatus • Frontal intersection of the Pterion • Asterion • External occipital protuberance • Anterior fontanelle (center) • Posterior fontanelle (center)

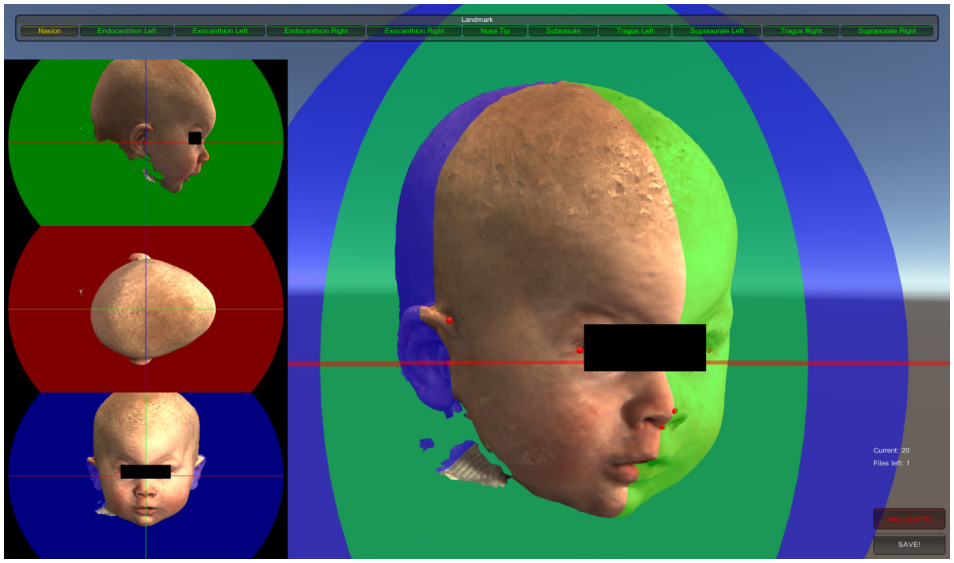

Figure 3: Example screenshot of the custom annotation tool to select 9 landmarks on 3D photos resulting in the preorientation (left).

CCFP-OFFSET COMPUTATION

The CCFP-offset in the sella turcica–nasion orientation was computed for all the CT-scans as reported in earlier studies [5]–[7]. The CCFP-offset values were reported per group for soft-tissue (CT-ST) and hard-tissue (CT-HT). The mean, standard deviation, and the 95% confidence interval (CI) were reported for every direction of the CCFP-offset (X, Y, Z) as represented in the sella turcica–nasion orientation [Figure 1]. The difference of means of the CCFP-offset was determined between the hard-tissue and soft-tissue for all datasets. Furthermore, the difference of means of the CCFP-offset was determined between the soft-tissue modalities for patient groups using a two-tailed

independent-samples T-test. All significance was assumed $p<0.05$. IBM SPSS Statistics version 25 (IBM Germany GmbH, Ehningen, Germany) was used for analysis.

SOFT-TISSUE MATCHING

Due to the math behind the CCFP computation method we are aware that the CCFP should be positioned at a similar location relative towards the surface of the head when using similar surfaces and landmarks. With multi-modality setup this leaves two variables in a sella turcica-nasion orientation in the: the CCFP-offset and the modality. Therefore, the matched CT-scans and 3D photos were oriented using two orientation strategies [Figure 4]. The first strategy (A) is the intended CCFP-based orientation workflow for matching CT-scans and 3D photos. In this workflow, the CT-ST is oriented in the sella turcica-nasion orientation using the bony landmarks. Each 3D photo is oriented in the sella turcica-nasion orientation using the mean population based CCFP-offset (either of trigonocephaly or scaphocephaly) [6], [7].

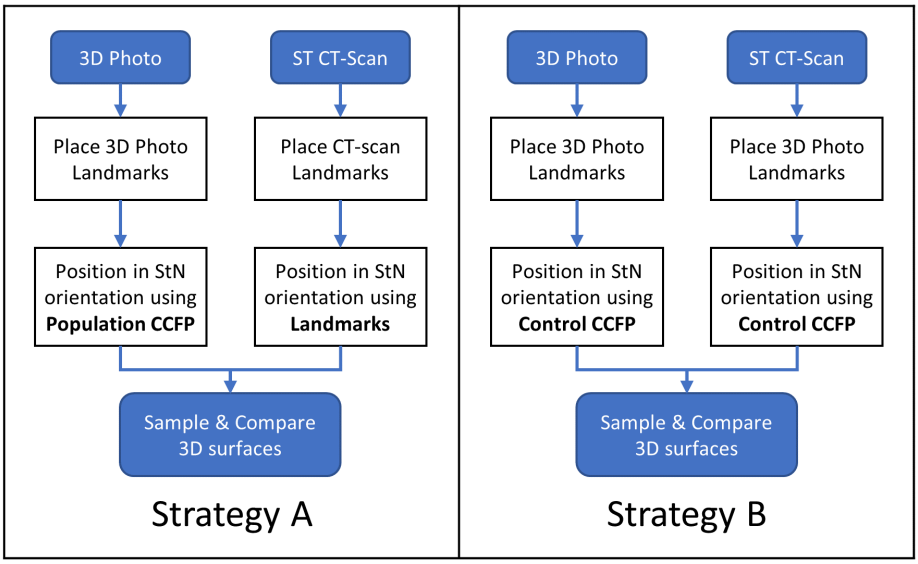

Figure 4: The orientation strategies for testing the soft-tissue matching between soft-tissue CT-scans and 3D photos using the CCFP. ST = Soft-tissue, StN = Sella turcica–nasion, CCFP = Computed cranial focal point.

The second strategy (B) tests the soft-tissue matching using an pseudo-arbitrary CCFP-offset value for both the CT-scan and 3D photo in cases where an exact CCFP-offset is not known. The arbitrary offset value chosen was the mean age-referenced healthy control CCFP-offset [Appendix Table 4]. This orientation strategy processes both the CT-ST and 3D photo identically by placing them in the sella turcica-nasion orientation using this CCFP-offset.

After applying the orientation strategy, sampling using a hemi-icosphere of both the CT-scan and 3D photo was performed as described in earlier studies [6], [7]. Distance maps between the CT-scans and 3D photos were created and averaged for both orientation strategies in each group. Furthermore, the Euclidian distance in mm per sampled point was used to determine the mean, absolute mean, standard deviation, minimum distance, and maximum distance in the distance maps. The mean distance maps and Euclidian distance metrics were used to determine the degree of soft-tissue matching.

RESULTS

POPULATION

The mean age of trigonocephaly patients was 3.6 months for the CT-scans and 3.7 months for the 3D photos (4.7-day difference). For the scaphocephaly group, the mean age during the CT-scan was 3.3 months and 3.6 months for the 3D photo (9.7-day difference).

CCFP-OFFSET VALUES

An overview of the CCFP-offset values from the craniosynostosis groups is presented in [Table 2]. There was no significant difference between the soft-tissue and hard-tissue for each patient or control group. The scaphocephaly and trigonocephaly groups differed in both CCFP-Y ($p<0.001$) and CCFP-Z ($p=0.001$) for the soft-tissue offsets.

Table 2: The mean, SD and 95% CI of the CCFP-offset values for the hard-tissue and soft-tissue CT-scans for each group in the X, Y, Z direction in the sella turcica-nasion orientation. P-values representing significant differences between these hard-tissue and soft-tissue values are also given.

	CCFP-offset Hard-tissue (mm)			CCFP-offset Soft-tissue (mm)			
	Mean	SD	95% CI	Mean	SD	95% CI	p-value
Scaphocephaly X	-0.1	0.7	-0.4 - 0.2	-0.2	0.8	-0.5 - 0.2	0.676
Scaphocephaly Y	8.5	4.1	6.6 - 10.4	9.0	4.0	7.1 - 10.9	0.698
Scaphocephaly Z	29.0	2.8	27.7 - 30.4	28.0	2.6	26.8 - 29.3	0.249
Trigonocephaly X	-0.1	1.1	-0.7 - 0.4	0.0	1.1	-0.5 - 0.5	0.997
Trigonocephaly Y	15.0	3.1	13.5 - 16.5	14.4	3.8	12.6 - 16.2	0.588
Trigonocephaly Z	32.7	3.6	31.0 - 34.4	32.2	3.6	30.5 - 34.0	0.663

SOFT-TISSUE MATCHING

The results of the mean soft-tissue matching are shown in [Table 3 and Figure 5]. Using strategy A with the population-specific CCFP-offset values, both trigonocephaly and scaphocephaly have a 0.1 mm difference between the mean and absolute mean. Furthermore, there is no apparent shift or rotation present in the distance maps. Using strategy B results in near identical soft-tissue matching maps and surface matching error values as strategy A for both trigonocephaly and scaphocephaly.

Table 3: The surface matching errors for different orientation strategies.

			Surface matching error (mm)				
Figure Id	Group	Strategy	Mean	Abs. Mean	Std.	Min	Max
5A	Trigonocephaly	A	1,8	1,9	1,2	-1,9	5,0
5B	Trigonocephaly	B	1,8	1,9	1,1	-1,7	4,6
5C	Scaphocephaly	A	1,1	1,2	0,8	-1,7	6,2
5D	Scaphocephaly	B	1,1	1,2	0,8	-1,8	6,0

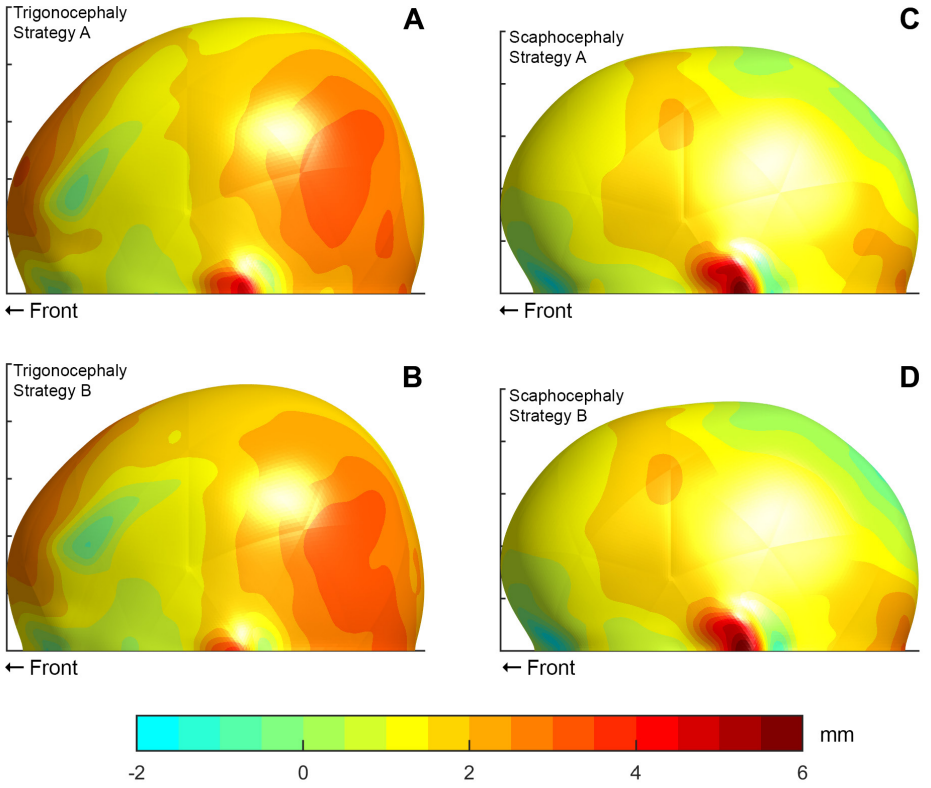

Figure 5: The mean matching distance map (in mm) between soft-tissue CT-scans and 3D photos for trigonocephaly (A, B) and scaphocephaly (C, D) cases using the two orientation strategies. Positive values represent additional volume in the 3D photos over the CT-scans.

DISCUSSION

CCFP-OFFSET VALUES

There was no significant difference between the soft-tissue and hard-tissue CCFP-offsets. The absolute differences varied per direction and were smaller than those in the earlier reported adult population which may be the results of additional skin thickness in adults [5]. Please note that the reporting on the axis of Y and Z are swapped between this and the adult study. This results in the caudal to cranial direction being defined by the Z-axis while the anterior to posterior direction being defined by the Y-axis. Only the CCFP-X-offset difference between the trigonocephaly and scaphocephaly group was not significant.

Comparing the reference CCFP-offset values of healthy controls aged 3-6 months [Appendix Table 4] [7] with the trigonocephaly and scaphocephaly group showed two significant differences. A significant difference ($p<0.001$) was found for the CCFP-Y in scaphocephaly and the CCFP-Y (anterior-posterior displacement) of the controls. This was similar for the control and trigonocephaly groups in CCFP-Z ($p=0.013$) (caudal-cranial displacement). These differences may indicate possible constraints of the interchangeability of the control CCFP-offset values with the patient groups. Although not specifically tested in this study, it is fair to assume that to achieve the best possible approximation of the sella turcica, a population-specific CCFP-offset is needed.

SOFT-TISSUE MATCHING

The first strategy (A) showed good results in both scaphocephaly and trigonocephaly. The 3D photos had additional volume over the CT-scans which can be explained by the hair and/or hairnet present in the 3D photos, age differences, and the aliasing/rounding errors of both modalities. On average, the 3D photos in the trigonocephaly cases were taken 4.7 days later than the CT-scans, resulting in 60 ml extra volume. For the scaphocephaly cases, this difference was 9.7 days on average, resulting in 40 ml extra volume. Although the additional volume effects are limited, the growth areas seem to be in line with the normal head growth and the closed sutures of the same age group [7]. There was no clear sign of a relative shift between the CT-ST and the 3D photos using this strategy.

The second strategy (B) showed a workflow of multi-modality matching using a control CCFP-offset for both the CT-scans and 3D photos. Interestingly, this method shows near identical matching compared to strategy A [Table 3, Figure 5]. The volume differences are close to those of the intended workflow; 60 ml versus 60 ml for trigonocephaly, and 39 ml versus 40 ml for scaphocephaly.

However, strategy B shows a slight shift in the surfaces when compared to strategy A. This is due to the differences in the CCFP-offset values used. Strategy A and B both compute an identical CCFP position, which is dependent on the surface of the skin or skull, but result in a different approximated sella turcica position which was based upon the CCFP position and the CCFP-offset.

As strategy A and strategy B yield near identical results regarding the surface matching error and distance maps, it is most likely that a control CCFP-offset (or any reasonable CCFP-offset) can be used to achieve proper matching between CT-scans and 3D photos. There is no need for knowing the (population) specific CCFP-offset in matching CT-scans and 3D photos as long as the approximated sella turcica position does not need to be accurate. However, since the CCFP-offset changes over time [5], [7], it is recommended to use both population and age-specific CCFP-offsets when using longitudinal follow-up after, for instance, craniosynostosis treatment.

LIMITATIONS

Follow-up CT-scans after craniosynostosis at our institution only occur in case of indications like complications or unexpected results, so there are no "normal" follow-up CT-scans. Furthermore, CT-scans of the head after craniosynostosis treatment due to a non-craniosynostosis indication are rare. This leaves a knowledge gap with respect to the evolution of CCFP-offset after surgery. Collecting the CT-scans required to determine the evolution of the CCFP-offset after craniosynostosis treatment prospectively will result in the use of either sedation or a radiation dose [9]–[12]. Despite the reduced radiation dose options in diagnosis of craniosynostosis [13], [14] it is still not standard clinical practice at our institute. A historic set of post-operative follow-up CT-scans in non-syndromic craniosynostosis similar to the syndromic variant may exist [15]; alternatively (ultra/super) low-dose CT-scans might be a feasible option in a prospective setup if the quality is sufficient for the CCFP computation [14].

Other cranial shape orientation strategies may allow for even better results. So far the CCFP strategy seems to result in the best soft-tissue orientation. We have tested the suitability for population-based orientations rather than individual orientations. The use of longitudinal orientation of individuals was not feasible with the current data, and therefore was not part of this study. However, considering the stable nature of the CCFP-offset we consider the CCFP a good candidate in longitudinal setups when using e.g. interpolation over time.

Other forms of craniosynostosis like anterior plagiocephaly were also not included in this study due to the number of available patients and their respective 3D photos and CT-scans at our institution. Due to the asymmetric

nature of these patients, it is uncertain if the CCFP alignment method will work. However, it is assumed that, based on this study, the asymmetry could be overcome by e.g. mirroring and averaging of the 3D photos and CT-scans.

CONCLUSION

The goal of this study was to investigate the soft-tissue matching error of the CCFP alignment method between CT-scans and 3D photos in scaphocephaly or trigonocephaly patients. Two alignment strategies for matching CT-scans and 3D photos were tested using either a population-specific CCFP-offset or a control CCFP-offset. Both alignment strategies showed a good fit with near identical results, and could be applicable depending on availability of a known CCFP-offset and the need for approximating the sella turcica position in 3D photos.

APPENDIX

Reference CCFP-offset values of healthy controls aging 3-6 months of age (n=13) as obtained (but not explicitly reported) in a different study are shown in [Appendix Table 4] [7].

Table 4: The mean, SD and 95% CI of the CCFP-offset values for the hard-tissue and soft-tissue CT-scans for the 3 & 6 month old controls in the X, Y, Z direction in the sella turcica-nasion orientation. P-values representing significant differences between these hard-tissue and soft-tissue values are also given.

	CCFP-offset Hard-tissue (mm)					**CCFP-offset Soft-tissue (mm)**					
	Mean	**SD**	**95% CI**			**Mean**	**SD**	**95% CI**			**p-value**
X	0.4	1.0	-0.2	-	1.0	0.4	1.0	-0.2	-	1.0	1.000
Y	13.9	3.2	11.9	-	15.8	14.0	3.1	12.2	-	15.9	0.936
Z	29.2	4.0	26.7	-	31.6	28.8	3.9	26.5	-	31.1	0.799

REFERENCES

[1] H. Delye, T. Clijmans, M. Y. Mommaerts, J. Vander Sloten, and J. Goffin, "Creating a normative database of age-specific 3D geometrical data, bone density, and bone thickness of the developing skull: a pilot study," *J. Neurosurg. Pediatr.*, vol. 16, no. 6, pp. 687–702, Dec. 2015, doi: 10.3171/2015.4.PEDS1493.

[2] W. Likus, G. Bajor, J. Baron, J. Markowski, D. Milka, and T. Lepich, "Cephalic Index in the First Three Years of Life: Study of Children with Normal Brain Development Based on Computed Tomography," *Sci. World J.*, vol. 2014, pp. 1–6, 2014, doi: 10.1155/2014/502836.

[3] A. Mcgarry, M. T. Dixon, R. J. Greig, D. R. L. Hamilton, S. Sexton, and H. Smart, "Head shape measurement standards and cranial orthoses in the treatment of infants with deformational plagiocephaly," *Developmental Medicine and Child Neurology*, vol. 50, no. 8. pp. 568–576, Aug. 2008, doi: 10.1111/j.1469-8749.2008.03017.x.

[4] L. A. van Vlimmeren, T. Takken, L. N. A. van Adrichem, Y. van der Graaf, P. J. M. M. Helders, and R. H. H. H. Engelbert, "Plagiocephalometry: a non-invasive method to quantify asymmetry of the skull; a reliability study," *Eur. J. Pediatr.*, vol. 165, no. 3, pp. 149–157, Mar. 2006, doi: 10.1007/s00431-005-0011-1.

[5] G. A. de Jong, T. J. J. Maal, and H. Delye, "The computed cranial focal point," *J. Cranio-Maxillofacial Surg.*, vol. 43, no. 9, pp. 1737–1742, Nov. 2015, doi: 10.1016/j.jcms.2015.08.023.

[6] G. de Jong *et al.*, "Radiation-free 3D head shape and volume evaluation after endoscopically assisted strip craniectomy followed by helmet therapy for trigonocephaly," *J. Cranio-Maxillofacial Surg.*, vol. 45, no. 5, pp. 661–671, May 2017, doi: 10.1016/j.jcms.2017.02.007.

[7] J. W. Meulstee, G. A. de Jong, W. A. Borstlap, G. Koerts, T. J. J. Maal, and H. Delye, "The normal evolution of the cranium in three dimensions," *Int. J. Oral Maxillofac. Surg.*, Nov. 2019, doi: 10.1016/j.ijom.2019.10.012.

[8] J. W. Meulstee *et al.*, "A new method for three-dimensional evaluation of the cranial shape and the automatic identification of craniosynostosis using 3D stereophotogrammetry," *Int. J. Oral Maxillofac. Surg.*, vol. 46, no. 7, pp. 819–826, Jul. 2017, doi: 10.1016/j.ijom.2017.03.017.

[9] Y. Arlachov and R. H. Ganatra, "Sedation/anaesthesia in paediatric radiology," *Br. J. Radiol.*, vol. 85, no. 1019, 2012, doi: 10.1259/bjr/28871143.

[10] K. P. Mason *et al.*, "Infant Sedation for MR Imaging and CT: Oral versus Intravenous Pentobarbital," *Radiology*, vol. 233, no. 3, pp. 723–728, 2007, doi: 10.1148/radiol.2333031872.

[11] J. Pages, N. Buls, and M. Osteaux, "CT doses in children: A multicentre study," *Br. J. Radiol.*, vol. 76, no. 911, pp. 803–811, 2003, doi: 10.1259/bjr/92706933.

[12] J. C. Montoya *et al.*, "Low-dose CT for craniosynostosis: Preserving diagnostic benefit with substantial radiation dose reduction," *Am. J. Neuroradiol.*, vol. 38, no. 4, pp. 672–677, 2017, doi: 10.3174/ajnr.A5063.

[13] T. Schweitzer, H. Böhm, P. Meyer-Marcotty, H. Collmann, R. I. Ernestus, and J. Krauß, "Avoiding CT scans in children with single-suture craniosynostosis," *Child's Nerv. Syst.*, vol. 28, no. 7, pp. 1077–1082, 2012, doi: 10.1007/s00381-012-1721-0.

[14] T. Kaasalainen *et al.*, "Limiting CT radiation dose in children with craniosynostosis: phantom study using model-based iterative reconstruction," *Pediatr. Radiol.*, vol. 45, no. 10, pp. 1544–1553, 2015, doi: 10.1007/s00247-015-3348-2.

[15] M. C. Meazzini *et al.*, "Long-term follow-up of syndromic craniosynostosis after le Fort III halo distraction: A cephalometric and CT evaluation," *J. Plast. Reconstr. Aesthetic Surg.*, vol. 65, no. 4, pp. 464–472, 2012, doi: 10.1016/j.bjps.2011.09.048.

Chapter 4

Radiation-free 3D head shape and volume evaluation after endoscopically assisted strip craniectomy followed by helmet therapy for trigonocephaly

G. de Jong, M. Tolhuisen, J. Meulstee, F. van der Heijden, E. van Lindert, W. Borstlap, T. Maal, H. Delye

Adapted from: G. de Jong et al., "Radiation-free 3D head shape and volume evaluation after endoscopically assisted strip craniectomy followed by helmet therapy for trigonocephaly," J. Cranio-Maxillofacial Surg., vol. 45, no. 5, pp. 661–671, May 2017, doi: 10.1016/j.jcms.2017.02.007.

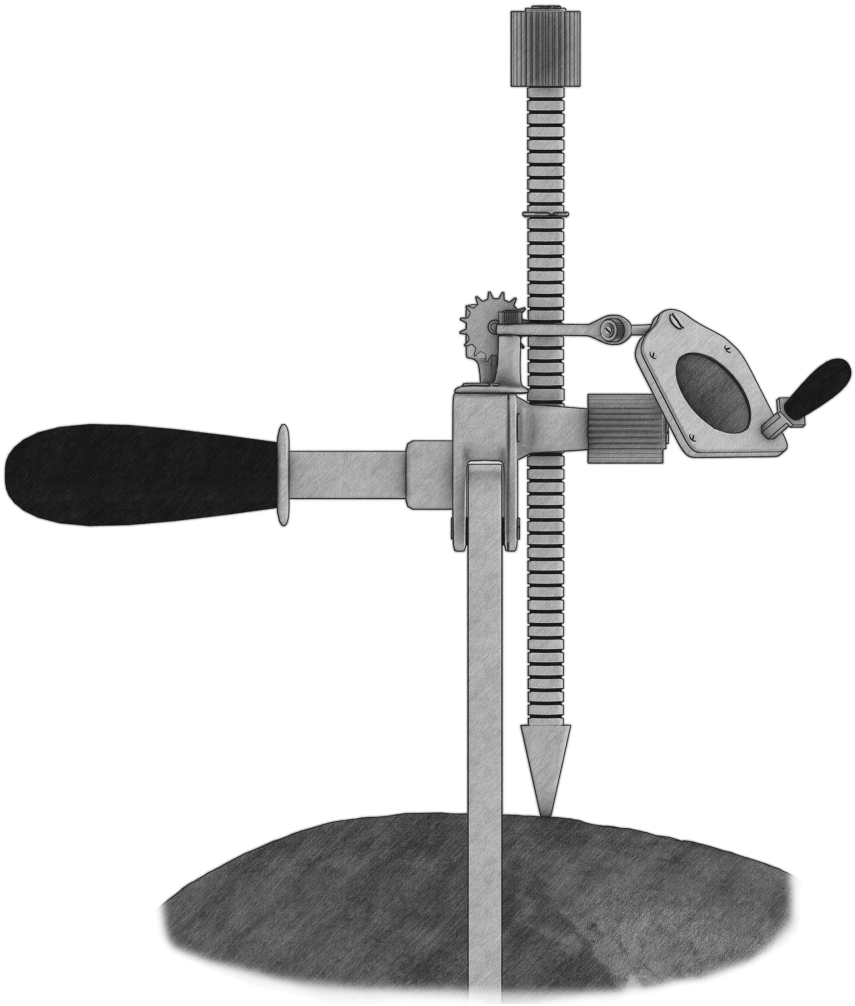

ABSTRACT

Introduction: Radiation-free 3D post-operative sequential follow-up in craniosynostosis is hindered by the lack of consistent markers restricting evaluation to subjective comparison. However, using the computed cranial focal point (CCFP), it is possible to perform correct sequential image superposition and objective evaluation. We used this technique for mean volume and shape change evaluation of the head utilizing 3D photos after endoscopically assisted trigonocephaly surgery.

Methods: We performed a mean head shape and volume evaluation on age grouped 3D photos (n = 86) of children who underwent endoscopically assisted strip craniectomy with helmet therapy. We used CT-scans of healthy children as reference. We performed a mean shape evolution analysis and calculated the anterior fossa to total volume ratio (A/T-ratio). The volume- and A/T-ratio pattern were compared with the reference group.

Results: The mean anterior fossa volume evolved from 336 ml (33.4% A/T-ratio) pre-surgery to 664 ml (36.0% A/T-ratio) at 37-48 months post-surgery. Both groups have a near similar volume- and A/T-ratio pattern over time. The first 18 months show a predominant growth around the resected metopic suture. Between 18 and 24 months we observed mostly anterior orbital rim growth. From 24 months till 36-48 months the head grows predominantly at the temporal area. The least outward growth was observed at the temporal bones.

Conclusion: Using a novel technique we were able to objectively evaluate head shape and volume using stereophotogrammetry after endoscopically assisted strip craniectomy. The A/T-ratio and volume growth pattern of endoscopically treated patients is near identical to that of the normal reference group.

INTRODUCTION

Craniosynostosis is the premature fusion of cranial sutures occurring at 1 in 2000 to 1 in 2500 live births [1]. Treatment for craniosynostosis comes with different approaches. Trigonocephaly has two main approaches; the open cranial vault reconstruction and (endoscopic) suturectomy with spring- or / helmet therapy [2]–[6]. Objective comparison, follow-up and evaluation of these approaches remain difficult. Modern clinical diagnosis of head shapes and follow-up after surgical craniosynostosis interventions usually relies on the use of CT-scans, cranial x-rays and in the past few years also three dimensional (3D) photogrammetry [7]–[13] . 3D Photogrammetry using 3D Photo systems were introduced as a radiation-free alternative but are limited to capturing soft tissue surfaces lacking the bony structures used in traditional follow-up. However it is possible to use 3D photos for objective follow-up. A common reference point for skull comparison is the sella turcica since its relative position is assumed to be more or less stable during skull growth [14]. A new method to determine a similar reference point, the computed cranial focal point (CCFFP), was proposed using a 3D surface from a 3D Photo [15]. The CCFP has a fixed location relative to the sella turcica. This allows orienting 3D photos of the head in the sella turcica-nasion plane anchored to the sella turcica for radiation-free longitudinal follow-up.

Since it is possible to perform radiation-free longitudinal follow-up using 3D photos and we want to initiate this practice by describing our methodology for this follow-up as well as the results for the endoscopically assisted craniosynostosis surgery. At our institute we have database of 3D photos of patients that underwent this surgery. Using the CCFP for registration of 3D photos we are able to perform longitudinal evaluations. We evaluate the head shape changes over time to determine the growth pattern in these patients that underwent this this surgery. Furthermore we look at the longitudinal volume change of the anterior fossa and the total head for this patient group. The anterior fossa volume is of interest due to being the volume in the affected region of the head. We compare these volumes changes in CT-scans with a reference group of children that did not undergo this surgery.

MATERIALS AND METHODS

Since December 2010 we used 3D photography in our craniosynostosis follow-up using a 3DMDhead System (3dMD Limited, London United Kingdom) in Radboudumc, Nijmegen, the Netherlands. In our follow-up database we selected all 3D photos of children that underwent endoscopically assisted metopic craniosynostosis surgery with helmet therapy that had a pre-surgery 3D photo and at least one post-surgery 3D photo. 26 Patients were identified that met these criteria of which we evaluated the head shape and volume changes over time up to October 2015. The 3D photos were grouped according to age between 2 and 48 months old [Table 1]. Each 3D photo underwent orientation in a reference frame and resampling. Volumes of anterior fossa and whole head were determined and analyzed. The volumes of the heads of the 3D photos were compared to volumes of healthy children, based on CT-scan calculations. We defined healthy if the CT-scan showed no pathological, traumatic, or morphological changes of the bony tissue of the head as well as the absence of hydrocephalus or tumors. The CT-scans were acquired of children that underwent a head CT-scan at the emergency room and were between 2 and 48 months old. CT-scans were used as a reference since we do not have a 3D photo set of healthy children yet. Average head shapes and normalized average head shapes per group were made for shape evaluation over time.

Table 1: Number of patients included in each age group for 3D Photos and CT-scans. * = Pre-surgery patients.

Group	**Age** (months)	**3D Photos**	**CT-scans**
1	2-4	22*	6
2	5-7	4*	3
3	8-10	17	4
4	11-14	14	11
5	15-18	8	8
6	19-24	8	8
7	25-36	8	5
8	37-48	5	8

ORIENTATION AND RESAMPLING

We compared the volume pattern differences between the CT-scans and 3D photos as well as the morphology of the head based on the 3D photos. In order to perform these measurements we had to orient the CT-scans and 3D photos in the same reference frame. These steps are displayed in the flowchart in [Figure 1]. In depth information on these steps can be found in the appendix. Orientating the 3D photos in the reference frame of the CT-scan was executed by determining an age-specific CCFP to sella turcica offset using the CT-scans. This offset is used to approximate the sella turcica in the 3D photos prior to positioning these in the sella turcica-nasion reference frame. Once the CT-scans and 3D photos were registered in the reference frames the age specific volumes could be determined as well as the mean shapes for the 3D photos. All calculations were performed using MATLAB 2015a (8.5) [16] with C++ and OpenCL 1.2 [17].

VOLUME ANALYSIS

For both the CT-scans and 3D Photos in each age group the mean volume, standard deviation and range of volumes were calculated above the sella turcica-nasion plane as well as for the anterior part of the head. We defined the anterior part of the head by the volume above the sella turcica-nasion plane and the volume in front of the plane crossing the center of the sella turcica perpendicular to both the sella turcica-nasion plane and the mid-sagittal plane. This approximates the anterior cranial fossa. Additionally the ratio between the anterior part and the entire head was calculated. The outer skin layer of the skull in the CT-scans was incomplete in the majority of the cases hence we used the outer bony surface for the CT-scan volume calculations.

Since we used two different surfaces on which we determine the volumes (skin for 3D and skull for CT), we only compared the patterns of the volumes and volume ratios between the surgery group and reference group.

STATISTICAL ANALYSIS

We compared the means of the volumes of the patients per age group for the total volume and anterior volume to determine if there was a significant difference. We started with a Shapiro-Wilks Test to test for normality in each group. Secondly we performed a Levene's Test to test if the variances of each age group are equal. These tests determine the choice of the statistical method for further analyzing the differences in means. Since there was normality in each group and there were no equal variances we used a Brown Forsythe and Welch Test to test if there was a difference in means between groups and a Games-Howell Post-hoc test to determine which groups were significantly different from other groups (α=0.05).

SHAPE ANALYSIS

Table 2: Number 3D Photos of trigonocephaly patients per group.

Group	# 3D Photos
Pre-surgery	26
6 Months post-surgery	21
12 Months post-surgery	19
18 Months post-surgery	8
24 Months post-surgery	8
36-48 Months post-surgery	4

Shape analysis between age groups was performed by comparing the average head shape per age group. Heatmaps were generated to show the absolute and normalized change between two sequential age groups. We were able to interpolate between two age groups for the vertex position and heatmap color. We used interpolation on the heatmaps to create animations of the average absolute shape change with the corresponding heatmap [see http://dx.doi.org/10.1016/j.jcms.2017.02.007].

For the shape analysis we grouped the 3D Photos to their respective follow-up time since we were interested in the effect of the surgery. The group distribution for the shape analysis can be seen in [Table 2].

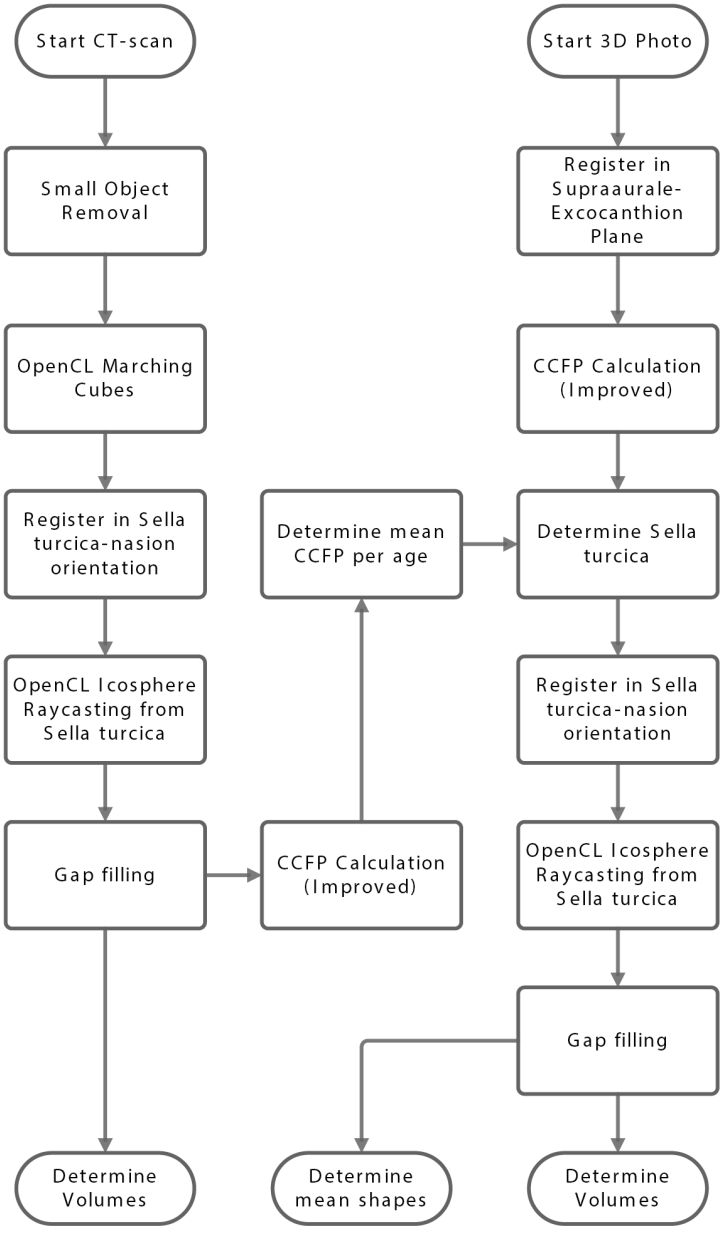

Figure 1: Flowchart depicting the steps used to determine the mean shape per age group for 3D photos and the mean volume per age group for CT-scans and 3D photos, as described in Appendix.

RESULTS

VOLUME ANALYSIS

The mean total and mean anterior head volumes above the sella turcica-nasion plane of the 3D photos can be seen in [Table 3] and [Figure 2]. The mean total volume starts at 942 ml and increases to 1846 ml (96.0% incline). The mean anterior volume starts at 308 ml and increases to 664 ml (116.0% incline). The volumes are based on the outer skin layer as observed by the 3D camera.

The mean total and mean anterior head volumes above the sella turcica-nasion plane of the CT-scans can be seen in [Table 4] and [Figure 2]. The mean total volume starts at 818 ml and increases to 1396 ml (73.5% incline). The mean anterior volume starts at 262 ml and increases to 454 ml (70.8% incline). The volumes are based on the outer bony skull layer of the CT-scan.

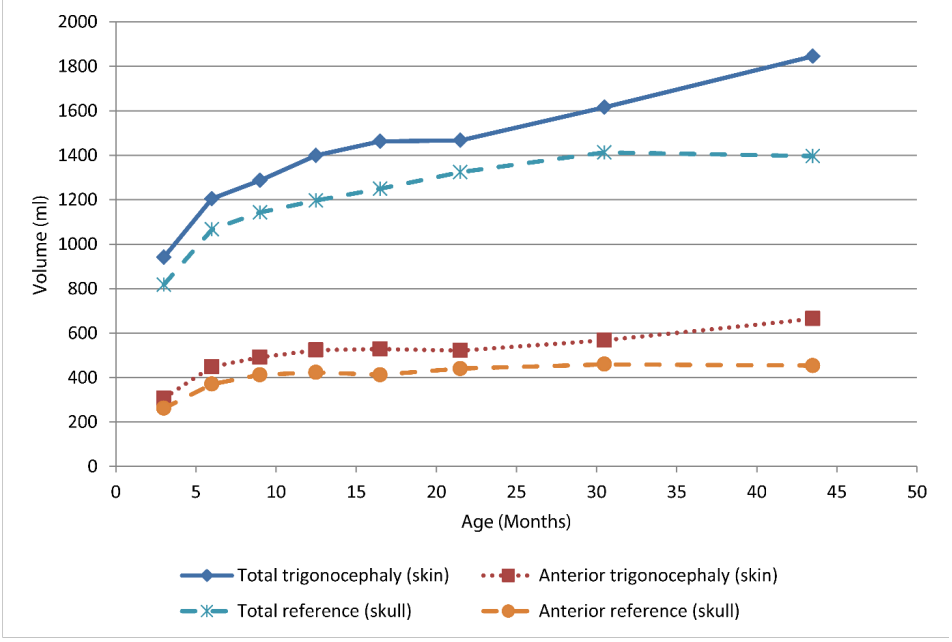

Figure 2: Average volumes of the full and anterior part of the head above the sella turcica-nasion plane for the trigonocephaly group (skin) and reference group (skull).

Table 3: Outer skin trigonocephaly 3D photo head volume measurement above sella turcica-nasion plane per group. * = Pre-surgery patients.

		Total head volume (ml)			**Anterior head volume**			**Ratio**
Group	**n**	**Mean**	**Range**	**Std**	**Mean**	**Range**	**Std**	**A/T** (%)
1 (2-4 months)*	22	942	[748–1110]	98	308	[233–380]	38	32.7
2 (5-7 months)*	4	1205	[1011–1378]	184	489	[311–586]	86	37.2
3 (8-10 months)	17	1287	[1055–1614]	131	491	[464–518]	52	38.1
4 (11-14 months)	14	1400	[1133–1670]	172	524	[480–567]	74	37.4
5 (15-18 months)	8	1463	[1318–1697]	133	528	[478–679]	60	36.1
6 (19-24 months)	8	1467	[1281–1627]	106	521	[485–579]	44	35.5
7 (25-36 months)	8	1616	[1361–1901]	165	568	[501–634]	79	35.1
8 (37-48 months)	5	1846	[1717–2007]	110	664	[590–739]	60	36.0

Table 4: Outer skull reference CT head volume measurement above sella turcica-nasion plane per group.

		Total head volume (ml)			**Anterior head volume**			**Ratio**
Group	**n**	**Mean**	**Range**	**Std**	**Mean**	**Range**	**Std**	**A/T** (%)
1(2-4months)	6	818	[687–1153]	174	262	[213–378]	69	32.0
2(5-7months)	3	1067	[1047–1105]	33	371	[367–374]	4	34.7
3(8-10months)	4	1143	[1081–1239]	68	412	[378–445]	30	33.1
4(11-14months)	11	1196	[995–1390]	116	423	[337–515]	63	35.3
5(15-18months)	8	1249	[1119–1400]	90	412	[348–508]	51	33.0
6(19-24months)	8	1324	[1208–1505]	91	440	[385–518]	40	33.3
7(25-36months)	5	1413	[1263–1577]	119	460	[394–509]	42	32.5
8(37-48months)	8	1396	[1269–1624]	113	454	[398–606]	67	32.5

Since we used two different surfaces (skin for 3D and skull for CT), we only compared the patterns of the volumes and anterior/total-ratios between the surgery group and reference group. Looking at the volumes over time [Figure 2] we can see that both the surgery group and reference group follow a similar growth pattern with some minor differences. One difference is that the surgery group still shows an increase in growth both total and anteriorly volume after 36 months (group 8) of age while the reference group does not. Another observation is that there is a plateau between 15 and 24 months old (group 5 & 6) for the mean total volume and mean anterior volume growth in the surgery

group. A similar plateau can be observed between 8 and 18 months old (groups 3-18) for the mean anterior volume growth of the reference group.

The anterior/total-ratio of both groups is shown in [Figure 3]. Again we see a similar ratio pattern. Both groups start at a lower ratio to increase in ratio until the age of 8-10 month. From here on there is a decline up to the 25-36 month group. A small incline could be observed in between for the reference group at 19-24 months old. The ratio stays near equal for the reference group until 37-48 months of age while the ratios of the surgery group still shows a slight increase from 35.1 to 36 %.

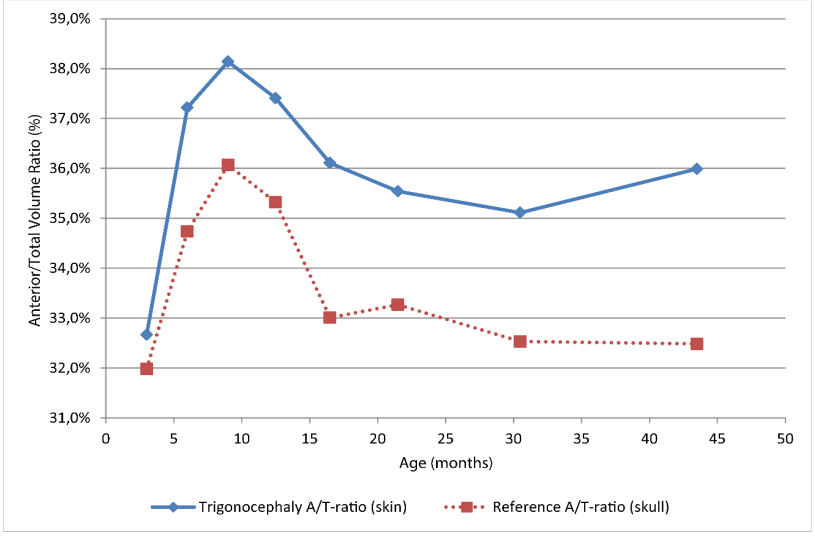

Figure 3: Average volume ratios between the full and anterior part of the head above the sella turcica-nasion plane for the trigonocephaly group (skin) and reference group (skull).

COMPARISON OF ANTERIOR GROWTH PERCENTAGES

The results of the anterior growth comparison between the surgery group and reference group can be seen in [Table 5]. We distinguish between two measures: the growth progress (percentage of total volume achieved starting at group 1 with 0%) and the relative growth (percentage of difference in

volume compared to the previous group). The surgery group starts with 39.5% of the growth progress completed at 5-7 months old whereas the reference group already completed 56.8 %. The reference group progress goes up to 78.4 % at 8-10 months old while the surgery group only achieves 51.4 %. A small plateau is present for the reference group up till 15-18 months old at around 80%. The surgery group growth progress will go to 60.5 % at 11-14 months to stay at a plateau up to 19-24 months old (59.9%). The reference group achieved full growth for our observation window at 25-36 months old. The surgery group has a steady increase from 19-24 months old to 37-48 months old achieving full growth for our observation windows without the plateau as observed at the reference group.

Table 5: Anterior growth progress and relative growth for the trigonocephaly and reference groups. The growth progress shows the percentage of growth achieved. The relative growth shows the percentage of difference in volume compared to the previous group.

	Growth Progress (%)		**Relative Growth** (%)	
Group	**Trigonocephaly**	**Reference**	**Trigonocephaly**	**Reference**
2 (5-7 months)	39.5	56.8	45.8	41.7
3 (8-10 months)	51.4	78.4	9.5	11.2
4 (11-14 months)	60.5	83.8	6.6	2.5
5 (15-18 months)	61.9	78.5	0.9	-2.5
6 (19-24 months)	59.9	93.1	-1.3	6.8
7 (25-36 months)	72.8	103.1	8.8	4.4
8 (37-48 months)	100.0	100.0	17.1	-1.3

STATISTICAL ANALYSIS

The total and anterior volumes for the 3D Photos were distributed normally as seen by the Shapiro-Wilks Test ($p >= 0.255$ in all groups). The Levene's Test indicated equal variances for the total volumes ($F = 1.556$, $p = 0.161$) and unequal variances for the anterior volumes ($F = 2.273$, $p = 0.037$). However, the ratio between the minimum and maximum variances are 3.5 for the total volumes and 4.9 for the anterior volumes. Thus equal variances cannot be assumed. The Welch Test showed a significant difference in means for both the total volumes ($F = 56.164$, $p < 0.001$) and anterior volumes ($F = 40.758$, $p < 0.001$). The Brown-Forsythe shows a similar result for the total volumes ($F = 50.203$, $p < 0.001$) and anterior volumes ($F = 32.225$, $p < 0.001$).

Finally we did a Games-Howell Post-hoc test to determine which means were significantly different from the other groups (α=0.05). The total volume means of the 2-4 month group were significantly different from all other groups except for the 5-7 month group. The 37-48 month group was significantly different for the mean total volumes from all groups except the 25-36 month group. The 8-10 month group was significantly different from the 19-24 month, 25-36 month, and 37-48 month group for the mean total volumes.

For the mean anterior volumes the 2-4 month group was significantly different from all other groups except for the 5-7 month group. The 37-48 month group was significantly different for the mean total volumes from all groups except the 25-36 month and 5-7 month group.

SHAPE ANALYSIS

ABSOLUTE SHAPE

The average growth and shape change over time in mm can be seen in [Figure 4]. In the first 6 months post-surgery there is a predominant growth around the frontal and occipital area of the head up to 8 mm along with growth of the orbital rims. The strip site shows the least growth in the frontal region [Figure 4 top left]. Between the period of 6 to 12 months post-surgery most growth on and around the site where the strip was removed, peaking up to 5 mm along with more frontal growth of the orbital rim area [Figure 4 top right]. Between 12 and 18 months old there is an overall growth in the frontal area peaking 3 mm [Figure 4 middle left]. No notable growth above 1 mm can be found between 18 to 24 months old except for growth of the orbital rims and the occipital area [Figure 4 middle right]. Between 24 and 36-48 months old the growth is focused at the temporal area of the head [Figure 4 bottom left]. The total growth from Pre-surgery to 36-48 months post-surgery indicates the strongest growth along the orbital rims and below the anterior fontanel [Figure 4 bottom right]. Furthermore a considerable amount of growth can be found near the centers of the parietal bones. The sphenoid wing, and temporal bone show the smallest amount of growth. No predominant orbital widening seems to occur over time. A video of the absolute shape change from pre-surgery to 36-48 months is provided for online media [see http://dx.doi.org/10.1016/j.jcms.2017.02.007].

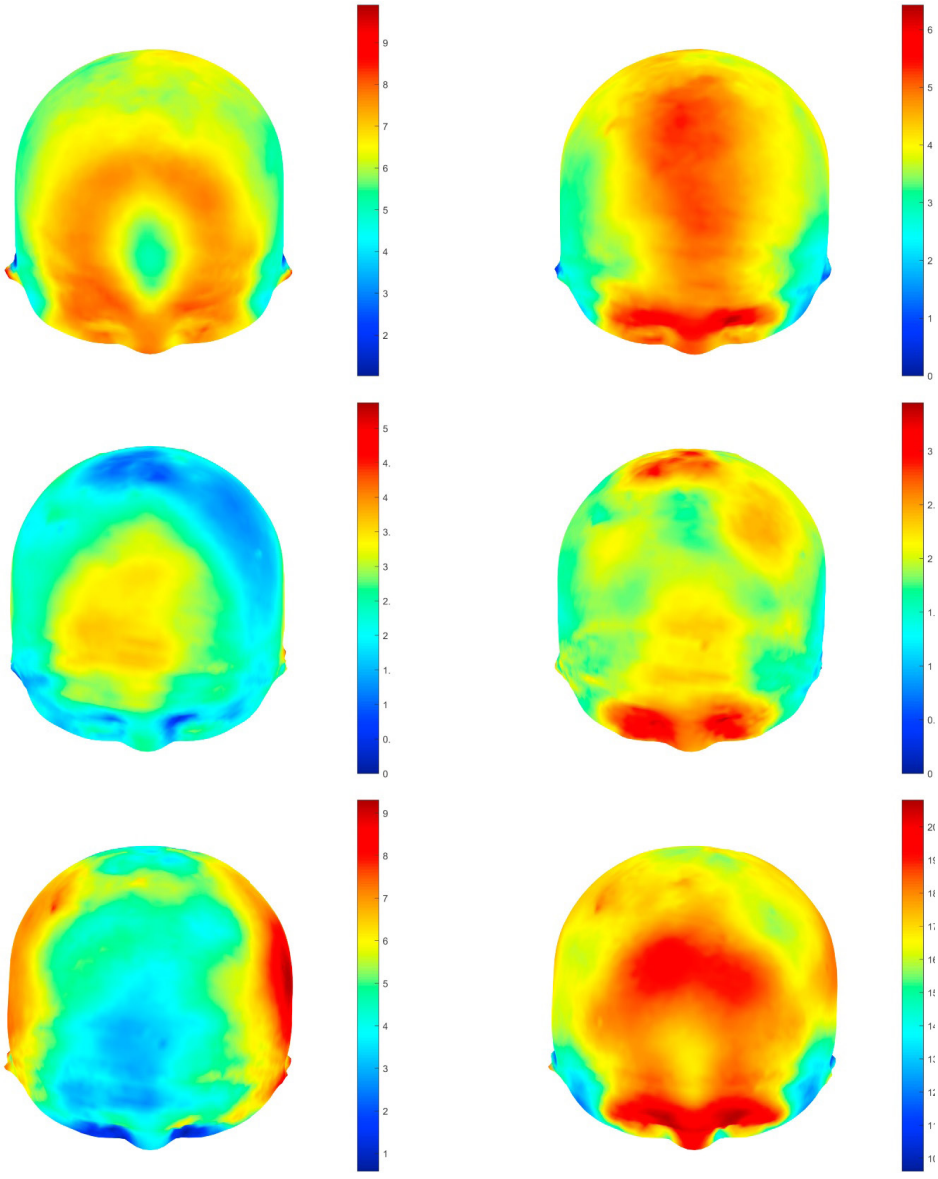

Figure 4: Mean head shapes with heatmaps of the absolute head growth in mm for the trigonocephaly group (Please note the different color scales). Top-left: Pre-surgery to 6 months post-surgery. Top-right: 6 to 12 months post-surgery. Middle-left: 12 to 18 months post-surgery. Middle-right: 18 to 24 months post-surgery. Bottom-left: 24 months post-surgery to 36-48 months post-surgery. Bottom-right: pre-surgery to 36-48 months post-surgery.

NORMALIZED SHAPE

The normalized growth and shape changes per time in percentage can be seen in [Figure 5]. Normalized growth ensures that the volume over time stays equal, showing relative growth. This means that if there is relative growth at one site, relative shrinkage must occur at the rest of the head. Between pre-surgery and 5 months post-surgery we see a relative growth around the surgery site, orbital rims, temporal bone and occipital area [Figure 5 top left]. In the center of the frontal bone is an area with relative shrinkage. Between 6 months and 12 months there is a similar growth to the absolute shape change [Figure 5 top right]. Between 12 to 18 months old there is relative growth in the overall frontal area and the left occipital area [Figure 5 middle left]. The latter is most likely an artifact due to naturally occurring asymmetry and sample size. Between 18 and 24 months old there is a relative growth of the orbital rims and the occipital area [Figure 5 middle right]. In the group from 24 to 36-48 months old there is a predominant growth in the temporal area of the head [Figure 5 bottom left]. When looking from pre-surgery to 36-48 months post-surgery we see a growth in the orbital rims, below the frontal fontanel and the temporal to occipital area of the head [Figure 5 bottom right]. In the frontal center of the frontal bone there is a relative shrinkage equal to that of the cranial part of the parietal bones. A video of the normalized shape change from pre-surgery to 36-48 months is provided for online media [see http://dx.doi.org/10.1016/j.jcms.2017.02.007].

DISCUSSION

With the use of the CCFP and 3D Photos it is possible to perform a longitudinal radiation free follow-up of head shape and volume. The current population on which this was performed consisted of patients that underwent endoscopically assisted metopic suture craniosynostosis surgery. We have started in December 2010 to create full head 3D Photos of children with craniosynostosis pre- and post-surgery over time. So far only 27 patients could be used in the follow-up with in total 86 usable 3D Photos on which we based our analysis. This analysis already shows the initial results whereas we keep expanding our database with more 3D Photos to further improve this analysis.

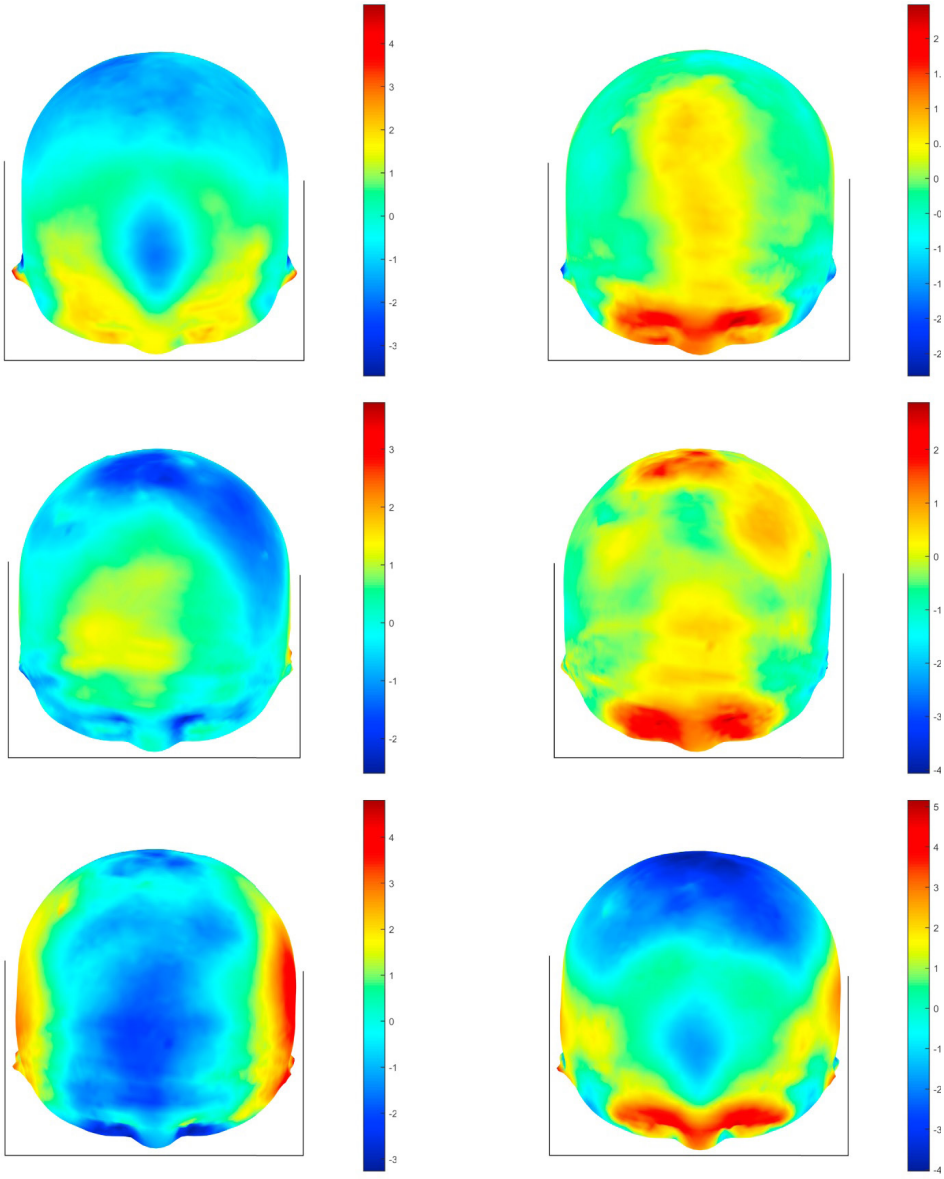

Figure 5: Normalized mean head shapes with heatmaps of the normalized head growth in mm for the trigonocephaly group (Please note the different color scales). Top-left: Pre-surgery to 6 months post-surgery. Top-right: 6 to 12 months post-surgery. Middle-left: 12 to 18 months post-surgery. Middle-right: 18 to 24 months post-surgery. Bottom-left: 24 months post-surgery to 36-48 months post-surgery. Bottom-right: pre-surgery to 36-48 months post-surgery.

We compared the growth patterns between patients that underwent endoscopically assisted metopic suture craniosynostosis surgery and a reference group of healthy children using two different modalities. The different modalities were chosen based on the availability in our clinic. Because of the difference between these two modalities we also have a difference in the segmented/observed surface and thus volume. The bony outer surface will always result in a smaller volume compared to the skin outer surface. Unfortunately, CT-scans of healthy children that include the complete skin surface are very scarce and we had to use the outer bony surface in order to obtain enough CT-scan data for the reference group. However, this limited our study by only comparing the growth patterns between our reference group and surgery group and not the absolute volumes. Using a correction value as determined by *Mckay et al.* for volumes above the lateral canthus and tragus could be an option to correct for the sella turcica-nasion plane if determined [12]. In our case these correction values of the total mean CT-scan outer bony surface volumes to the total mean trigonocephaly skin surface volume values would be between 1.11 and 1.17 depending on the age (nonlinear). However since these correction values are between the skull of normal reference groups and the skin of surgery groups we did not use these correction values.

For the growth and shape analysis we used different grouping as compared to the volume analysis. This was done to monitor the growth and shape effects caused by the surgery in detail. However we did not have reference 3D photos of healthy children. If we do, we can distinguish shape changes caused by natural growth and those that are caused by the surgery. We are currently building a database with 3D Photos of healthy children for future research.

The absolute and relative shape analysis showed growth around the surgical site with a relative shrinkage at the center of the frontal bone. Skull widening occurs in the later phase after surgery. Although there is a considerable amount of growth at the orbital rims, we did not see orbital widening in this time frame. Absolute growth at the sphenoid wing and temporal bone show an overall smallest growth of the entire analyzed area.

Other studies that evaluated shape changes either in pre- to post-surgery or long-term are often limited to a selection of parameters and not the whole head growth analysis [7], [11]. Analysis of using the whole head shape in sagittal craniosynostosis have been done before, however still using CT-scans [8].

Longitudinal whole head shape analysis of metopic suture craniosynostosis was not performed in earlier research to our best knowledge.

The mean anterior volume, mean total volume and A/T-ratio showed a near similar pattern over time. Although some differences were observed. When looking at the volume pattern it can be seen that there is a small plateau in the surgery group for both the mean total and mean anterior volume at 15 to 24 months. This could potentially point towards slowing down of the growth although this could also be due to our limited sample size. The mayor difference can be observed at 37-48 months old. The patient group still shows some additional volume growth (+ 0.9%) while the reference group does not. Statistically there was no difference between the means of the volumes at 24-36 months and 37-48 months. So it could be that this effect is caused by our sample size.

Intracranial volume measurement in craniosynostosis has been done before [18]–[21]. However these are limited to pre-surgery [18]–[20], or only compare pre- to post-surgery [21]. The pre- to post-surgery comparison did include the anterior fossa to total volume analysis, but was limited to brachycephalic craniosynostosis. To our knowledge no longitudinal follow-up of the volumes after metopic suture craniosynostosis surgery exist to date.

Using an objective measure significantly helps in the evaluation and quantification of the effects of craniosynostosis interventions. This is not only the case for our institution, but also for others around the world performing craniosynostosis interventions. The current 3D camera systems are getting cheaper and more accessible for both the mainstream and professional clients. Using these 3D cameras and new analysis techniques as shown in this study can help with reducing the amount of preventable ionizing radiation that is used in craniosynostosis follow-up. We hope that by the method shown in this study more institutes performing craniosynostosis surgery will use 3D photos or retrospective CT-scans to further quantify the effects of the surgery. We further hope to provide a method to objectively compare and further improve craniosynostosis surgery.

CONCLUSION

We performed a retrospective study to evaluate the head shape and volume changes over time after endoscopically assisted metopic craniosynostosis surgery. We have been able to analyze the volume changes over time above the sella nasion plane thanks to the use of the CCFP[15]. The mean total and anterior head volume growth pattern was almost equal to the reference group. A total mean volume increase of 96.0% and an anterior mean increase of 116.0% was observed in the surgery group.

The A/T-ratio pattern is also nearly similar in both groups. Again a deviation occurs at the later age from the 24-36 months to 37-48 months. The A/T-ratio for the surgery group increases while the reference group stays equal.

When looking at the overall growth progress of the mean anterior volume of both groups, we observed that the reference group was at the final anterior volume earlier than the surgery group and had a stronger incline at the start.

The shape analysis showed the growth pattern over time both absolute and relative. The surgical site and orbital rims show the most prominent growth along with the center of the parietal bones. The site of the removed strip showed the least local growth of the anterior portion of the head. The shape analysis shows the smallest growth in the orbital widening, sphenoid wing, and temporal bone over the evaluated period.

Our method for head shape and volume analysis gives insight in the growth pattern after endoscopically assisted metopic craniosynostosis intervention. This method can be used for healthy patients as well as other forms of craniosynostosis evaluation in the future. We hope that other institutes adapt and possibly improve this methodology to objectively compare the longitudinal effects of craniosynostosis surgery as well to further improve this surgery.

APPENDIX

ORIENTATION PROCEDURE

CT-SCANS

For the orientation of the CT-scans we start by removing small objects in the scan with a167 HU intensity or above. We created the surface data by using an OpenCL accelerated marching cubes algorithm also at 167 HU [22]. The CT-scans were manually placed in the sella turcica-nasion orientation.

After orientation resampling was performed using raycasting for the sampling [23] on the vertices (3D points) of a hemi-icosphere as reference shape. Resampling reduces the amount of 3D points used to describe an object while maintaining the overall shape [Figure 6]. Using a reference shape enables simple mathematical and statistical analysis. The number of vertices was chosen as low as possible for less computation time while ensuring that the inaccuracy of the CCFP position caused by sampling would be less than 1 mm.

Gaps in the resampled surface can occur naturally or by the CT-scan scanning procedure. The gaps were filled by iteratively determining the 3D points based on the average position of the neighborhood of neighboring 3D points to the origin.

After filling the gaps the CCFP position and volumes were determined and averaged per age. The CCFP is later used to determine the sella turcica position in the 3D photos of the same age group. An improved CCFP calculation was used that weights triangle size differences that can occur in 3D Photos as described later in the appendix.

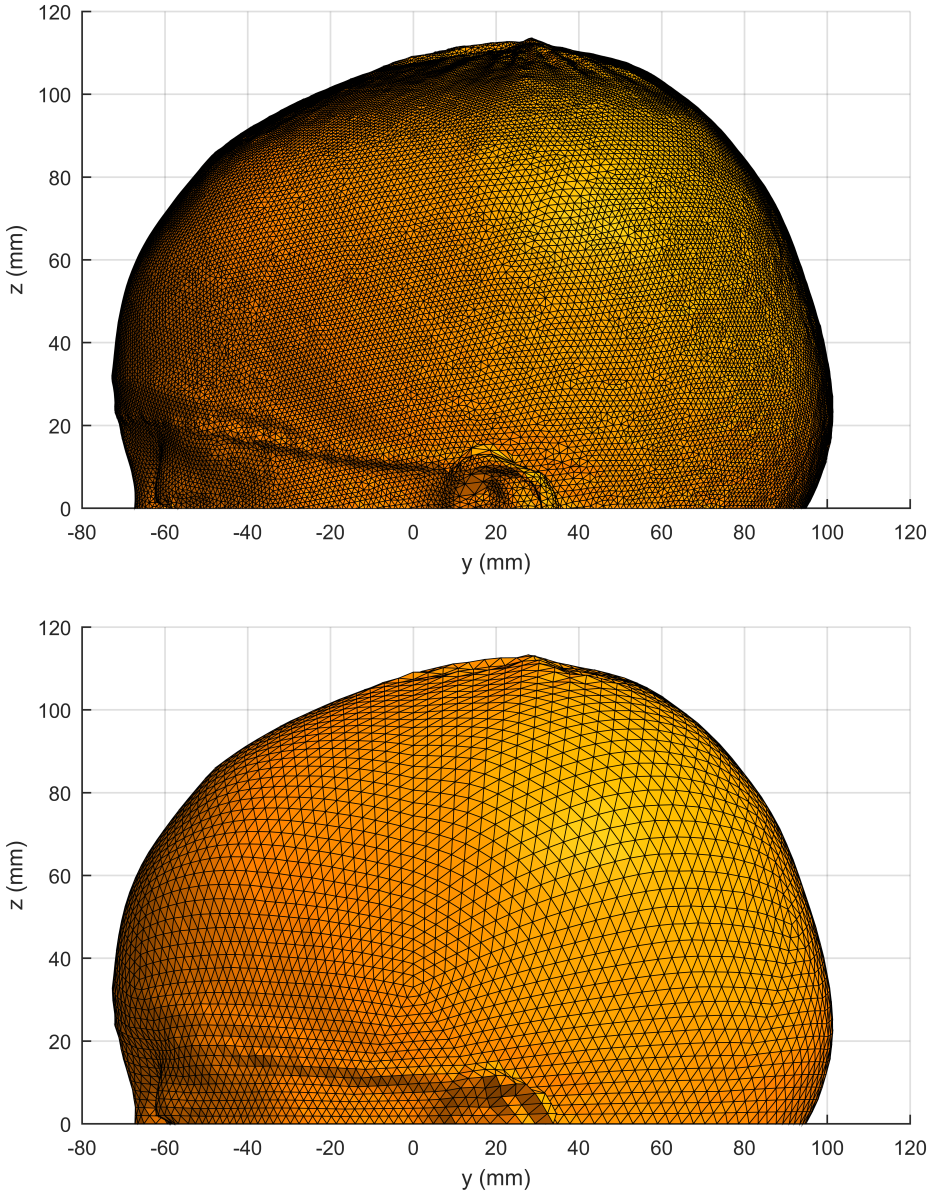

Figure 6: 3D Photo before (top) and after (bottom) resampling after orientation. The original version has 106268 triangles and the resampled version has 10240 triangles.

3D PHOTOS

The 3D photos were manually placed in a supraaurale-exocanthion orientation. The origin was placed at the midsaggital plane crossing the line between the

two exocanthions. We determined the CCFP position using the surface that was at 20 mm above the supraaurale-exocanthion plane after a 20 degree anterior rotation. [Figure 7].

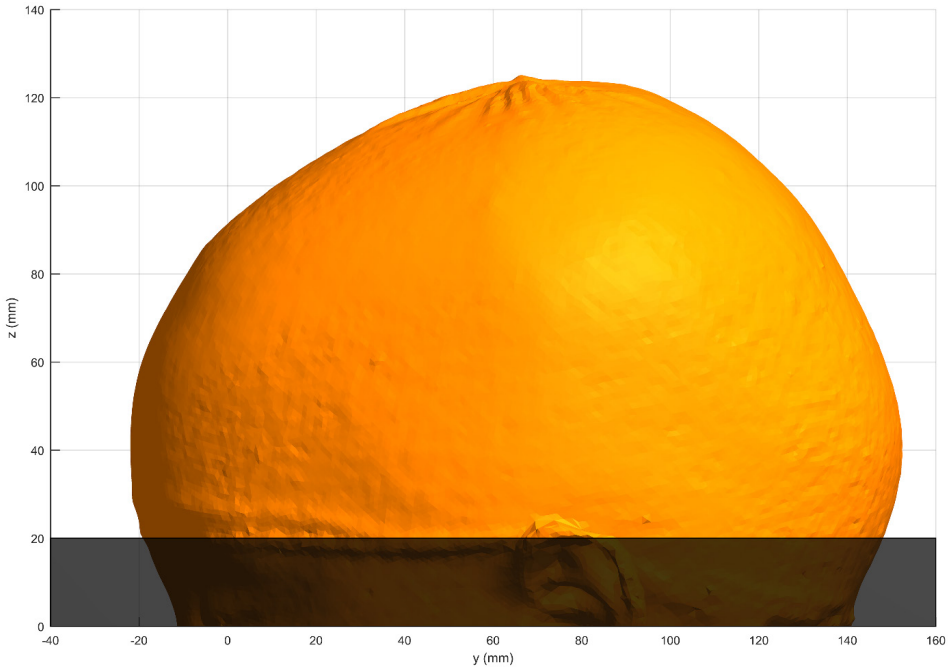

Figure 7: 3D Photo after pre-orientation in the supraaurale-exocanthion plane with 20 degrees anterior rotation. The highlighted area is used for the CCFP calculation.

We use the CCFP-sella turcica offset from the CT-scans of the same age group and the CCFP position in the 3D photo to calculate the center of the sella turcica in the 3D photo. We translate the 3D photo so that (0,0,0) position is the center of the calculated sella turcica. We rotate the 3D photo so that the head was positioned in the sella turcia-nasion plane.

Gap filling was performed similarly as in the surface of the CT-scans. Finally the mean volumes and the mean shapes per age group were determined for the 3D photos. The mean shapes consisted of the absolute shape as well as the normalized shape. The normalized shape is the absolute shape scaled by the inverse of the cubic root of the volume. These normalized shapes have an equal volume regardless of the age group and thus only shape is different.

IMPROVING THE CCFP CALCULATION

The improved CCFP calculation adds a correction for triangle size. Triangle sizes in a 3D photo can typically vary up to 50x larger to 20x smaller than the mean triangle size [Figure 8]. This can result in less accurate CCFP calculations since larger triangles have an equal influence as smaller triangles. This makes the accuracy prone to the sampling resolution and 3d reconstruction. In order to compensate for this effect there is a weight factor for the triangle size implemented in the CCFP calculation.

ORIGINAL CCFP CALCULATION

In the original CCFP is calculated by determining and averaging the center points in a triangulated spherical object [15]. In the original article two properties of a triangle are used: the normal and the center. A skew line is determined by using the normal and a center of a triangle. The original center point calculation for a given triangle is described in [Equation (1)].

The center point $\mathbf{P}_{C,Ln}$ is determined by the position of s and t on the skew lines $L_n(s)$ and $L_m(t)$ where the distance between these skew lines is minimal. The skew line $L_n(s)$ is the line of the triangle of which the center point is determined. The skew lines $L_m(t)$ are the lines that can form a pair with $L_n(s)$. A pair can be formed if there is absolute angle larger than 30 degrees and smaller than 330 degrees between the two skew lines. The total is divided by the amount of formed pairs $n_{f,Ln}$.

$$\boldsymbol{P}_{c,L_n} = \frac{1}{n_{f,L_n}} \sum \frac{L_{n(s)} + L_{m(t)}}{2} \tag{1}$$

As a final step all center points are averaged to determine the CCFP [Equation (2)].

$$\boldsymbol{CCFP} = \frac{1}{n_{faces}} \sum_{n=1}^{n_{faces}} \boldsymbol{P}_{c,L_n} \tag{2}$$

IMPROVED CCFP CALCULATION

The first step of the improvement calculation is in the center point calculation. In this calculation we consider the surface area of the paired triangles as a weighting factor for the center point. For this we use the surface area (A_m)

of each triangle of which skew line can be used as a pair. In this version we multiply the surface area per sub-center point and later on divide the sum of these sub-center points by the sum of the surface area of the triangles that can be used as a pair. This results in the new [Equation (3)] where the effect of the size of the paired triangles is taken in consideration.

$$\boldsymbol{P}_{c,L_n} = \frac{1}{\sum A_m} \sum A_m \frac{L_{n(s)} + L_{m(t)}}{2} \tag{3}$$

The second step of the improvement is in the averaging calculation. Here we take the effect of the size of the triangle of the center point on the CCFP itself. This is done by multiplying the surface area (A_n). per center point and dividing the total with the sum of the surface area as seen in [Equation (4)].

$$\boldsymbol{CCFP} = \frac{1}{\sum A_n} \sum_{n=1}^{n_{faces}} \boldsymbol{P}_{c,L_n} A_n \tag{4}$$

REFERENCES

[1] B. J. Slater, K. a Lenton, M. D. Kwan, D. M. Gupta, D. C. Wan, and M. T. Longaker, "Cranial sutures: a brief review.," *Plast. Reconstr. Surg.*, vol. 121, no. 4, pp. 170e–8e, Apr. 2008, doi: 10.1097/01.prs.0000304441.99483.97.

[2] S. Keshavarzi, M. G. Hayden, S. Ben-Haim, H. S. Meltzer, S. R. Cohen, and M. L. Levy, "Variations of Endoscopic and Open Repair of Metopic Craniosynostosis," *J. Craniofac. Surg.*, vol. 20, no. 5, pp. 1439–1444, 2009, doi: 10.1097/SCS.0b013e3181af1555.

[3] J. Hinojosa, "Endoscopic-assisted treatment of trigonocephaly," *Child's Nerv. Syst.*, vol. 28, no. 9, pp. 1381–1387, 2012, doi: 10.1007/s00381-012-1796-7.

[4] F. Ozlen *et al.*, "Surgical treatment of trigonocephaly: technique and long-term results in 48 cases.," *J. Neurosurg. Pediatr.*, vol. 7, no. 3, pp. 300–10, 2011, doi: 10.3171/2010.12.PEDS10359.

[5] D. F. Jimenez and C. M. Barone, "Endoscopic craniectomy for early surgical correction of sagittal craniosynostosis.," *Journal of neurosurgery*, vol. 88, no. 1. pp. 77–81, 1998, doi: 10.3171/jns.1998.88.1.0077.

[6] C. M. Barone and D. F. Jimenez, "Endoscopic craniectomy for early correction of craniosynostosis.," *Plast. Reconstr. Surg.*, vol. 104, no. 7, pp. 1965–73; discussion 1974-5, 1999, doi: 10.3171/jns.1998.88.1.0077.

[7] J. Marcus, L. Domeshek, and R. Das, "Objective three-dimensional analysis of cranial morphology.," *Eplasty*, vol. 8, pp. 175–187, 2007, Accessed: Jun. 10, 2014. [Online]. Available: http://europepmc.org/abstract/MED/18464892.

[8] J. R. Marcus *et al.*, "Use of a three-dimensional, normative database of pediatric craniofacial morphology for modern anthropometric analysis.," *Plast. Reconstr. Surg.*, vol. 124, no. 6, pp. 2076–84, Dec. 2009, doi: 10.1097/PRS.0b013e3181bf7e1b.

[9] N. R. Saber *et al.*, "Generation of normative pediatric skull models for use in cranial vault remodeling procedures.," *Childs. Nerv. Syst.*, vol. 28, no. 3, pp. 405–10, Mar. 2012, doi: 10.1007/s00381-011-1630-7.

[10] H. Delye, T. Clijmans, M. Y. Mommaerts, J. Vander Sloten, and J. Goffin, "Creating a normative database of age-specific 3D geometrical data, bone density, and bone thickness of the developing skull: a pilot study," *J. Neurosurg. Pediatr.*, vol. 16, no. 6, pp. 687–702, Dec. 2015, doi: 10.3171/2015.4.PEDS1493.

[11] M.-B. Le *et al.*, "Assessing long-term outcomes of open and endoscopic sagittal synostosis reconstruction using three-dimensional photography.," *J. Craniofac. Surg.*, vol. 25, no. 2, pp. 573–6, 2014, doi: 10.1097/SCS.0000000000000613.

[12] D. R. McKay *et al.*, "Measuring cranial vault volume with three-dimensional photography: A method of measurement comparable to the gold standard," *J. Craniofac. Surg.*, vol. 21, no. 5, pp. 1419–1422, 2010, doi: 10.1097/SCS.0b013e3181ebe92a.

[13] J.-F. Wilbrand *et al.*, "Objectification of cranial vault correction for craniosynostosis by three-dimensional photography," *J. Cranio-Maxillofacial Surg.*, vol. 40, no. 8, pp. 726–730, Dec. 2012, doi: 10.1016/j.jcms.2012.01.007.

[14] A. Björk, "Cranial base development: a follow-up x-ray study of the individual variation in growth occurring between the ages of 12 and 20 years and its relation to brain case," *Am. J. Orthod.*, 1955, doi: 10.1016/0002-9416(55)90005-1.

[15] G. A. de Jong, T. J. J. Maal, and H. Delye, "The computed cranial focal point," *J. Cranio-Maxillofacial Surg.*, vol. 43, no. 9, pp. 1737–1742, Nov. 2015, doi: 10.1016/j.jcms.2015.08.023.

[16] The MathWorks Inc. and U. S. Natick, Massachusetts, "Matlab 2015a." The MathWorks Inc., Massachusetts, United States, 2015.

[17] J. Stone, D. Gohara, and G. Shi, "OpenCL: A parallel programming standard for heterogeneous computing systems," *Comput. Sci. Eng.*, 2010, doi: 10.1109/MCSE.2010.69.

[18] C. A. Hill *et al.*, "Intracranial volume and whole brain volume in infants with unicoronal craniosynostosis," *Cleft Palate-Craniofacial J.*, vol. 48, no. 4, pp. 394–398, 2011, doi: 10.1597/10-051.

[19] D. T. Gault, D. Renier, D. Marchac, and B. M. Jones, "Intracranial pressure and intracranial volume in children with craniosynostosis.," *Plastic and reconstructive surgery*, vol. 90, no. 3. pp. 377–81, 1992, doi: 10.1097/00006534-199209000-00003.

[20] S. Sgouros, a D. Hockley, J. H. Goldin, M. J. Wake, and K. Natarajan, "Intracranial volume change in craniosynostosis.," *J. Neurosurg.*, vol. 91, pp. 617–625, 1999, doi: 10.3171/jns.1999.91.4.0617.

[21] D. Saiepour, P. Nilsson, J. Leikola, P. Enblad, and D. Nowinski, "Posterior cranial distraction in the treatment of craniosynostosis - Effects on intracranial volume," *Eur. J. Plast. Surg.*, vol. 36, no. 11, pp. 679–684, 2013, doi: 10.1007/s00238-013-0874-8.

[22] E. Smistad, A. C. Elster, and F. Lindseth, "Real-Time Surface Extraction and Visualization of Medical Images using OpenCL and GPUs," *Nik-2012*, no. november, pp. 141–152, 2012.

[23] T. Möller and B. Trumbore, "Fast, minimum storage ray/triangle intersection," in *ACM SIGGRAPH 2005 Courses on - SIGGRAPH '05*, 2005, vol. 2, no. 1, p. 7, doi: 10.1145/1198555.1198746

Chapter 5

The Normal Evolution Of The Cranium In Three Dimensions

J. W. Meulstee*, G. A. de Jong*, W. A. Borstlap, G. Koerts, T. J. J. Maal, and H. Delye

*J.W. Meulstee and G.A. de Jong contributed equally as co-first authors

Adapted from: J. W. Meulstee, G. A. de Jong, W. A. Borstlap, G. Koerts, T. J. J. Maal, and H. Delye, "The normal evolution of the cranium in three dimensions," Int. J. Oral Maxillofac. Surg., Nov. 2019, doi: 10.1016/j.ijom.2019.10.012.

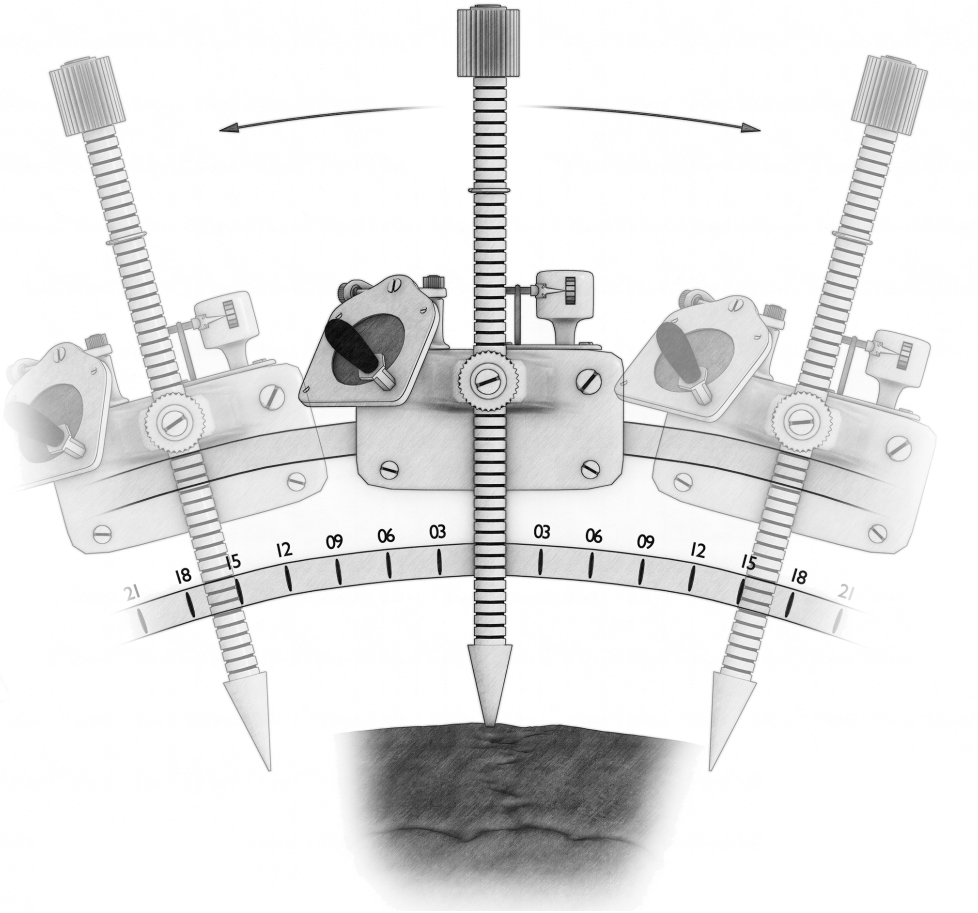

ABSTRACT

Background: Insight in the growth and development of the normal newborn's cranial shape is essential to monitor cranial development, to detect and diagnose abnormal skull shapes and for the long-term follow-up of craniosynostosis surgery. The aim of this study was to analyse the growth pattern of the cranial shape of infants during the first years of life using 3D stereophotogrammetry and 3D-CT with advanced 3D evaluation techniques.

Methods: A large set of 3D photographs (n=199) and CT-scans (n=183), taken between 0-54 months, was collected. Cranial shapes with artefacts and asymmetries were removed. Total volumes and intracranial volumes were obtained as well as 3D and 2D measurements including the cranial width, cranial length, cranial index and suture lengths. Furthermore, growthmaps were created for all modalities to indicate 3D growth over time.

Results: For the final analysis, a total of 130 3D photographs, 94 hard-tissue CT-scans and 75 soft-tissue CT-scans were used. The 3D and 2D measures, volumes, growthmaps and growth animations were obtained. A non-uniform growth was revealed by the 3D growhtmaps.

Conclusion: This study addresses the need for normative cranial evolution data to monitor healthy cranial development and for detection, follow-up and planning in craniosynostosis treatment.

INTRODUCTION

During the first years of a newborn's life, the cranium grows very rapidly[1]. Insight in this growth and development of the normal cranial shape is essential to monitor cranial development, detect abnormalities, and evaluate long-term results of craniosynostosis surgery [2].

Many studies have described the development of the cranial shape by reporting databases with craniometrics for different ages and populations. Craniometric data can be measured directly on the subjects' heads, using two dimensional (2D) measurement tools or can be derived from plain X-rays [3]–[6].

Since the introduction of three dimensional (3D) imaging, new accurate measurement methods for the evaluation of the cranium became available including 3D computed tomography (CT) and radiation-free 3D stereophotogrammetry [7]–[10]. Most studies, however, merely used 3D imaging techniques to create a database of 2D measurements. Yet, these 2D measurements and ratios fail to give an adequate, complete and detailed description of the cranial shape and its 3D evolution. Literature which describe a complete 3D evaluation of the skull during the first months of life is scarce [2].

The aim of this study was to analyse the growth pattern of the cranial shape of infants during the first years of life using 3D stereophotogrammetry and 3D CT with advanced 3D evaluation techniques. This insight can be used to describe normal cranial development, detect and diagnose cranial abnormalities and evaluate treatment of craniosynostosis.

PATIENTS AND METHODS

ACQUISITION AND SUBJECTS

A database with 3D craniometrics was established using 3D photographs and CT-scans of healthy infants. A 3D stereophotogrammetry set-up (3dMDCranial 3DMD, Atlanta, USA) with a five-pod configuration was used prospectively for the acquisition of 199 3D photographs of healthy infants. Ethical approval from the regional institutional review board of the institution was obtained for this study.

3D PHOTOGRAPHS

Three dimensional photographs of the healthy infants were taken at fixed time intervals (3, 6, 9, 12, 15, 18 and 24 months). Photographs with severe quality inconsistencies were excluded resulting in a set of 146 3D photographs. Furthermore, 3D photographs with a mild, moderate or severe asymmetry were excluded. To objectively determine asymmetry, the plagiocephalometry method described by Van Vlimmeren et al. was used [6] by calculating the ODDI (oblique diameter difference index) and CPI (cranial proportion index) for every 3D photograph. An ODDI <104.5 and a CPI < 90 was defined as normal. A total of 130 3D photographs of 49 infants were finally included in this study [Figure 1]. From this group 49% (n=63) were males.

COMPUTED TOMOGRAPHY

This study retrospectively used anonymized CT-scans of subjects which had a CT-scan in the Radboudumc Nijmegen or the Sint Luc University Medical Hospital Brussels. The CT-scans were performed on clinical indications (e.g. suspicion of head trauma). CT-scans of subjects between 0 and 54 months of age were screened and only included if no pathology or morphological changes were present. A part of the Radboudumc set was previously reported [11]. CT-scans not capturing the complete cranium or scanned with a slice thickness > 2 mm were excluded, resulting in a total of 183 CT-scans. The CT-scans were reconstructed to a 3D shape of the hard tissue (CT-HT) and soft tissue (CT-ST) in Maxilim (Medicim NV, Mechelen, Belgium). Three dimensional shapes with clear artefacts were removed from the CT-HT or CT-ST group. Since the plagiocephalometry method to exclude asymmetrical cranial shapes was designed for soft tissue only, a correlation and offset factor was calculated to make the plagiocephalometry method also applicable for hard tissue. Details of the plagiocephalometry method and offset calculation are given in the Appendix. Finally, a total of 94 CT-HT shapes and 75 CT-ST shapes were used in this study [Figure 1]. The CT-HT group contained 52% (n=49) males and the CT-ST group contained 50% (n=38) males. Distribution details are given in [Table

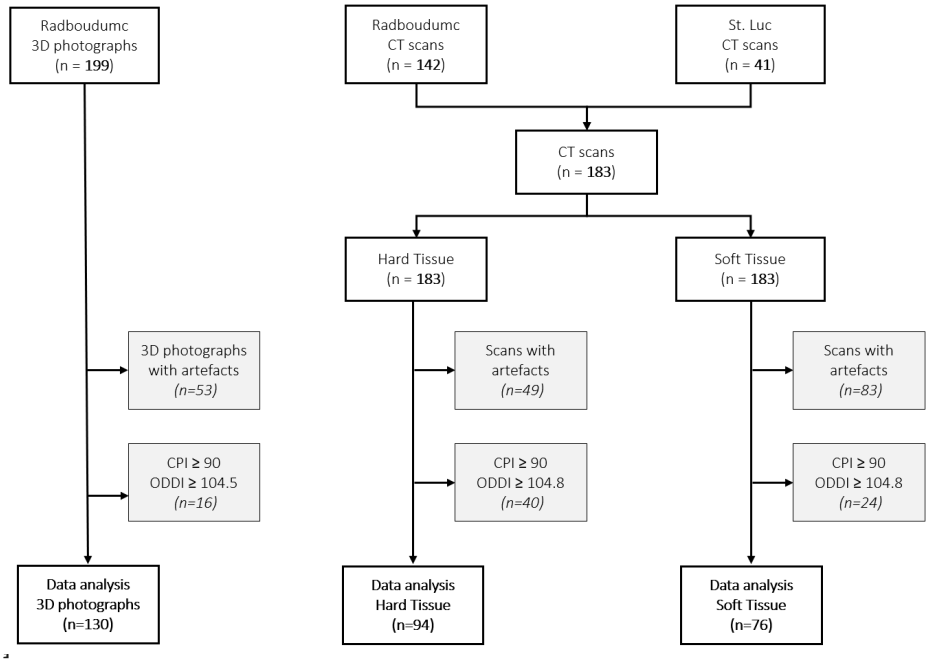

Figure 1: Flowchart of the study and the included 3D photographs and 3D-CT scans (CPI, cranial proportion index; ODDI, oblique diameter difference index).

DATA PROCESSING

The quality of all 3D photographs was assessed and minor artefacts were repaired using the MeshMixer 3D software (Autodesk MeshMixer, San Francisco, CA, USA). Similar to earlier presented methods, nine landmarks were manually marked on the textured 3D photographs [Table 2 and Figure 2] and used to automatically pre-align the 3D photographs in a reference frame (tragus-nasion orientation) [12]. The computed cranial focal point (CCFP) was used to automatically position the 3D photographs in identical reference frames (sella turcica -nasion orientation) using Matlab (MATLAB v2017a, The Mathworks Inc., Natick, MA, USA) [13]. The 3D photographs were checked for rotational or position variances and adjusted if necessary. For further analysis, all 3D photographs were normalized to create mesh data with the same number of vertices (data points) [11], [12].

An annotation tool was created in Unity (v5.6.0, Unity Technologies, San Francisco, USA) to manually position 21 landmarks on the CT-HT [Table 2]. Landmarks and the CCFP method was used to automatically position the 3D

shapes in the sella turcica-nasion orientation. Equal to the 3D photographs, rotational and positional differences were eliminated and the 3D CT shapes were normalized for further analysis.

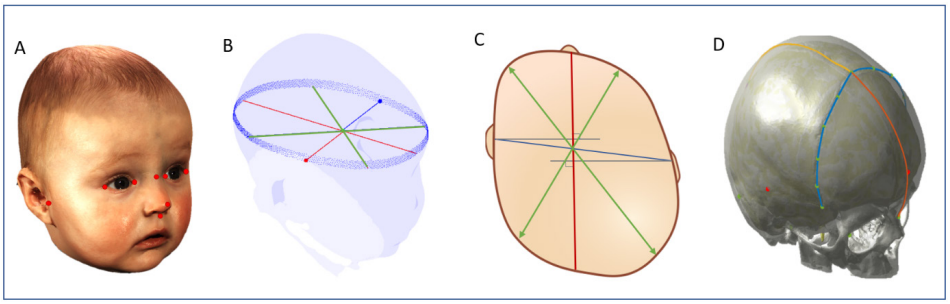

Figure 2: (A) Example of a 3D photograph with manually positioned landmarks (red). (B) The measurement plane was used to define the oblique diameters (green), cranial length, cranial width, and circumference (blue). (C) Illustration of the measurement method to determine the cranial asymmetry score and classification. (D) Lengths of the sutures measured over the CT-HT surface.

MEASUREMENTS

The 3D photographs were grouped in seven predefined age categories and the mean cranial shape was calculated for every group [11], [12]. The mean growth was calculated as the difference between a mean cranial shape and the consecutive mean cranial shape and visualized with a growthmap. The CT-HT shapes were grouped similar to the 3D photographs with two additional age groups of 36 and 48 months.

The cranial length was given by the most anterior and posterior point of the cranium. These two points were used to indicate a horizontal measuring plane on the cranial shapes [Figure 2]. The maximum cranial width was determined by a line perpendicular to the cephalic length. Cranial width divided by the cranial length and multiplied by 100 resulted in the cranial index (CI). The circumference was calculated using a plane crossing the points that define the cephalic length and cephalic width [Figure 2].

For all modalities, the volume measurements were performed above the sella turcica-nasion plane. Total volume (TV) was measured on 3D photographs, CT-HT and CT-ST. Intracranial volume (ICV) was measured on CT-HT group. The anterior and posterior component of the TV's were computed separately and divided at position of the sella turcica.

On the CT-HT scans, the metopic and sagittal suture lengths were measured over the surface in the midsagittal axis of the reference frame. The coronal suture length was determined using 11 landmarks, from the left pterion to the right pterion. The lateral orbital distance (LOD) was defined as the distance between the left and right lateral orbital wall.

IBM SPSS Statistics (IBM Germany GmbH, Ehningen, Germany) was used for descriptive statistics. The mean, standard deviation and 95%-confidence intervals were calculated for these results. A student's t-test was used to compare plagiocephalometry measurements on CT-HT and the CT-ST as well as any gender differences between the age groups.

Table 1: Sex distribution with mean age and standard deviation per age group for 3D photographs (3DP), CT hard tissue (CT-HT), and CT soft tissue (CT-ST).

	3D Photographs				CT hard tissue				CT soft tissue			
	n		Mean Age (SD)		n		Mean Age (SD)		n		Mean Age (SD)	
Group	Male	Female	Male	Female	Male	Female	Male	Female	Male	Female	Male	Female
1	14	12	3.1 (0.4	3.0 (0.2)	3	7	2.3 (1.2)	2.0 (1.6)	3	8	2.3(1.2)	2.0 (1.3)
2	10	12	6.4 (0.7)	5.9 (0.3)	2	1	5.5 (0.7)	6.0 (.)	1	0	6.0 (.)	
3	13	14	9.0 (0.4)	9.0 (0.2)	5	1	9.4 (0.9)	9.0 (.)	3	1	9.7 (0.6)	9.0 (.)
4	10	9	12.0 (0.4)	12.0 (0.2)	3	6	11.7 (1.2)	12.5 (0.5)	3	6	11.7 (1.2)	12.2 (0.8)
5	4	7	15.2 (0.3)	15.1 (0.5)	5	5	15.4 (0.9)	14.8 (0.8)	4	4	15.3 (1.0)	15.3 (0.5)
6	10	8	18.5 (0.8)	18.2 (0.1)	2	5	19.5 (2.1)	19.2 (1.5)	4	4	19.8 (1.5)	19.3 (1.7)
7	3	4	24.3 (0.3)	24.2 (0.1)	7	6	27.1 (2.8)	24.8 (2.2)	7	5	26.6 (2.5)	24.4 (2.3)
8					17	12	36.2 (3.0)	36.0 (2.8)	10	8	37.1 (2.6)	36.5 (3.1)
9					5	2	45.6 (4.8)	44.5 (0.7)	3	2	47.7 (5.5)	44.5 (0.7)

Table 2: Landmarks on 3D photographs and 3D CT.

3D photographs	3D CT
• Pretragion (left and right) • External cantion (left and right) • Internal cantion (left and right) • Nasal bridge • Nose tip • Subnasal landmark at the transition of the nose and upper lip	• Nasion • Sella turcica • Frontozygomatic suture • External acoustic meatus • Frontal intersection of the Pterion • Asterion • External occipital protuberance • Anterior Fontanelle • Posterior Fontanelle • 8 Additional landmarks over coronal suture

RESULTS

CRANIAL INDEX, WIDTH, LENGTH AND CIRCUMFERENCE

The CI, width, length and circumference measures over time for the 3D Photographs, CT-HT and the CT-ST are given in [Table 3] and [Figure 4]. The CI fluctuates within the first 24 months of age between 75 and 78 for all modalities. After this age the CI increases in both CT-HT and CT-ST. Both the cranial width and cranial length increase over time for all modalities. The CT-HT showed lower values compared to the other modalities. All modalities showed a sudden increase of both the cranial width and length around 18 months. The circumference, cranial width and cranial height all followed the same pattern of growth. For all measurements, differences between males and females were calculated [Table 3, Figure 3- Figure 5].

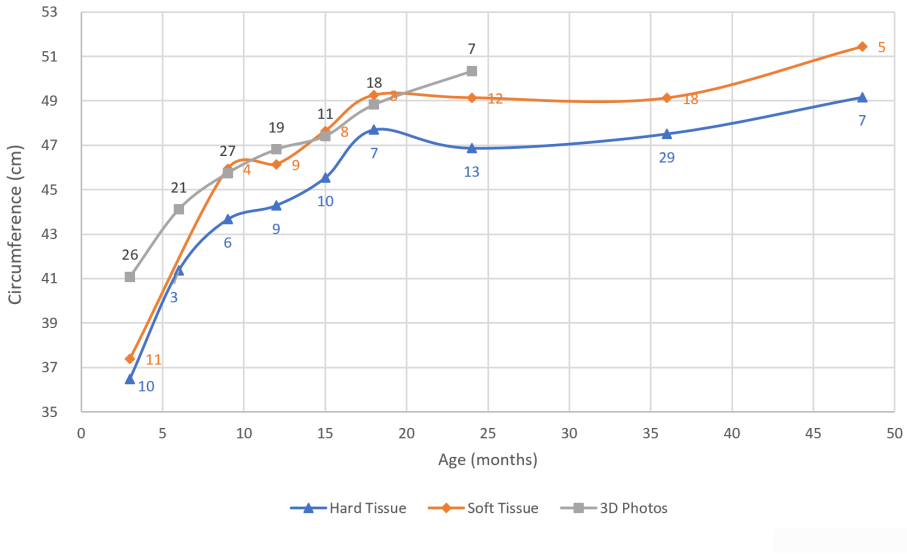

Figure 3: Circumference of all modalities. Coloured numbers indicate the number of subjects used for every age groups.

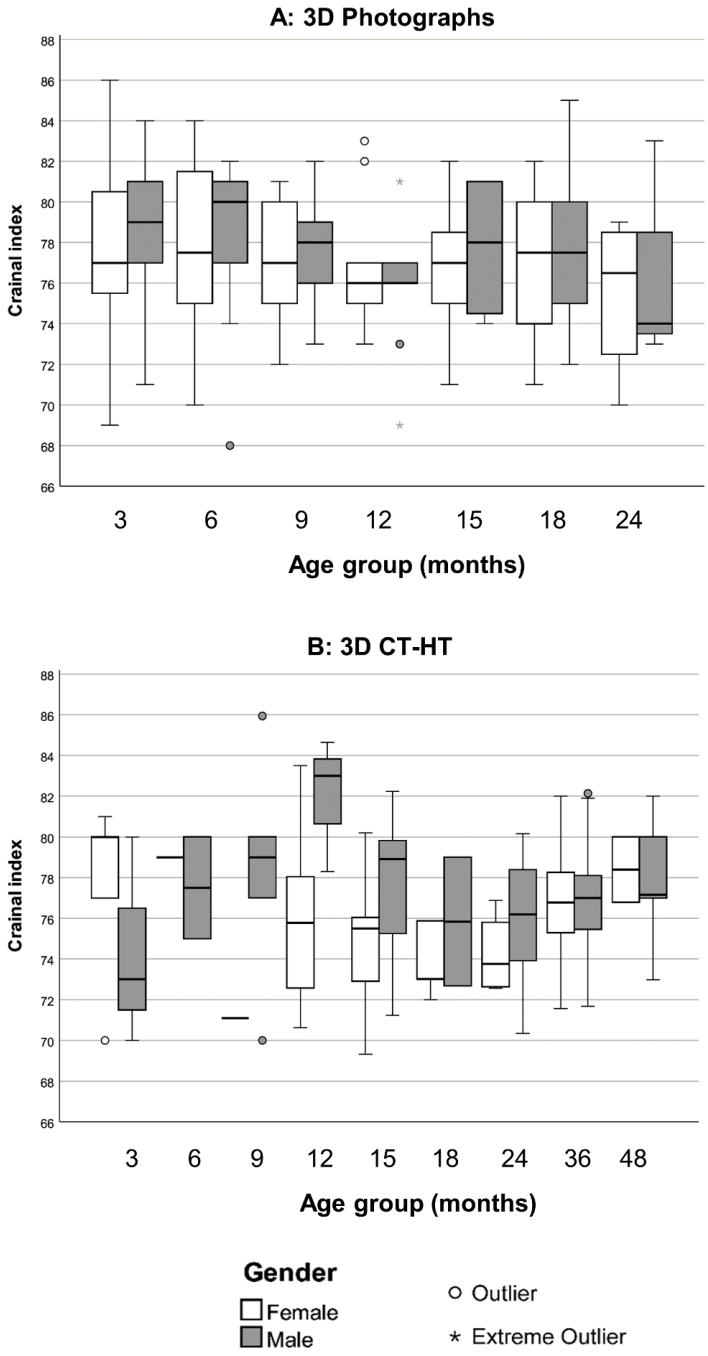

Figure 4: Cranial Index (CI) boxplots, illustrating the range of CI values and male – female ratio for the 3D photographs (A) and CT-HT (B).

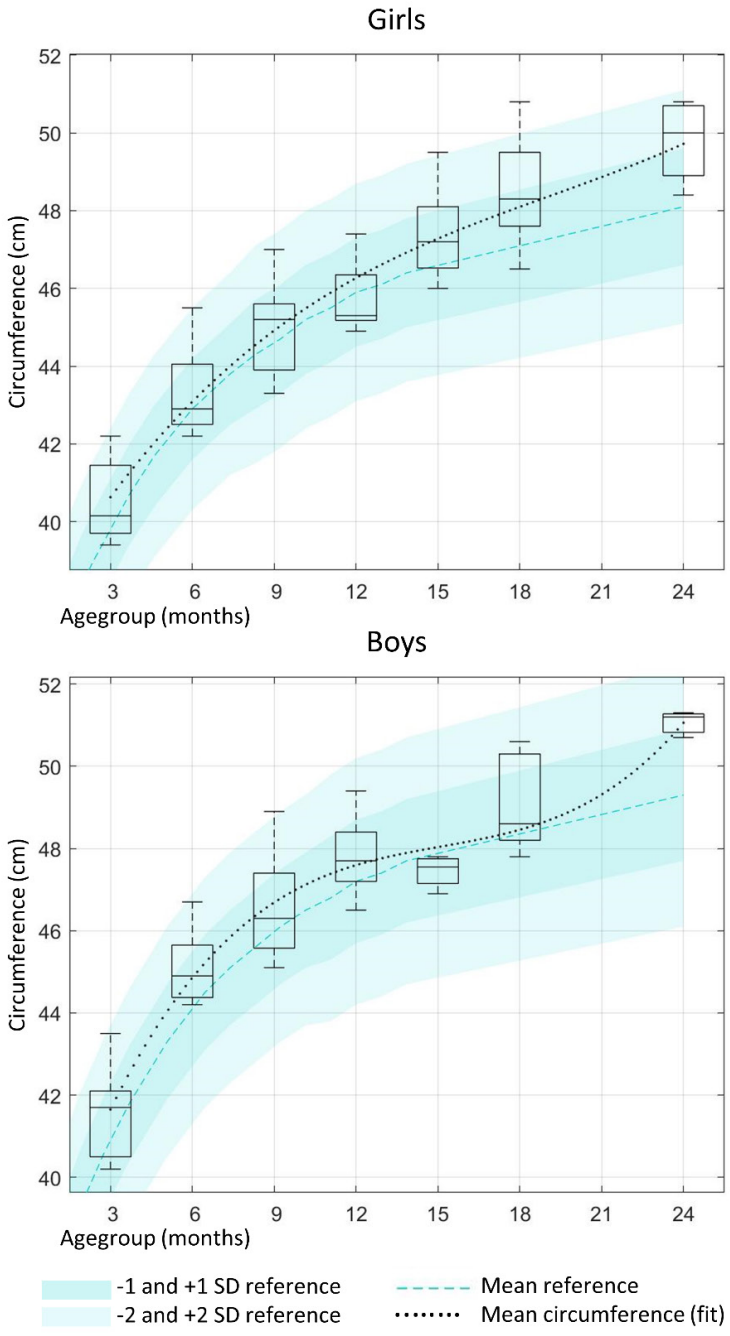

Figure 5: Boxplots of circumference measured on 3D photographs for boys (left) and girls (right). Circumference reference values based on the Dutch cross-sectional growth study was plotted in the background [14].

Table 3: The number of subjects per age group, per gender, per modality and the mean with standard deviation (SD) of the cranial index, cranial width, cranial length and circumference. CT-HT = Hard tissue CT scan, CT-ST = Soft tissue CT scan. * = statistical significant difference between means of male (M.) and female (F.) of given age group and modality ($p<0.05$).

		n		Cranial width (mm)				Cranial length (mm)				Cranial index				Circumference (mm)			
		M.	F.	Male		Female		Male		Female		Male		Female		Male		Female	
Group	age			Mean	SD	Mean	SD	Mean	SD	Mean	SD	Mean	SD	Mean	SD	Mean	SD	Mean	SD
3DP	3	14	12	114.4	3.6	111.4	6.0	146.0	5.3	143.6	4.5	78	4	78	5	*415.4	9.8	*405.3	9.9
	6	10	12	*124.8	5.3	*118.8	5.4	*159.9	4.1	*152.7	3.9	78	4	78	4	*451.1	8.1	*432.9	10.7
	9	13	14	*127.9	3.4	*122.6	4.2	*164.5	4.6	*159.6	4.8	78	2	77	3	*465.5	11.5	*450.1	11.4
	12	10	9	*129.3	3.2	*125.2	3.3	*171.0	4.4	*163.3	5.5	76	3	77	3	*477.5	8.8	*457.9	9.0
	15	4	7	131.1	4.1	129.4	4.1	168.3	3.4	168.3	5.6	78	4	77	4	474.5	4.0	474.0	11.9
	18	10	8	135.7	3.8	133.5	5.6	174.7	6.2	173.1	5.8	78	4	77	4	490.9	11.2	485.1	13.8
	24	3	4	139.7	6.8	134.9	5.8	182.4	4.6	178.7	5.1	77	6	76	4	510.7	3.2	498.0	11.2
CT-HT	3	3	7	95.9	12.0	100.4	11.1	128.1	11.6	129.8	17.8	74	5	78	4	360.8	37.4	366.5	46.2
	6	2	1	114.0	8.3	113.8	.	145.0	0.8	144.8	.	78	4	79	.	415.0	13.3	411.3	.
	9	5	1	119.6	4.7	114.1	.	151.5	6.3	160.4	.	78	6	71	.	435.3	8.9	443.6	.
	12	3	6	124.2	2.1	120.2	5.5	151.9	8.7	158.3	5.7	82	3	76	5	438.6	18.3	445.1	12.6
	15	5	5	125.3	4.2	120.6	6.5	161.9	6.6	161.3	6.1	78	4	75	4	458.8	13.4	452.0	15.4
	18	2	5	132.1	8.0	127.0	5.1	174.3	0.5	167.4	7.2	76	4	76	6	493.1	11.1	470.6	10.7
	24	7	6	128.1	6.5	124.0	3.8	168.8	3.5	167.1	7.2	76	4	74	2	472.4	10.2	464.5	16.2
	36	17	12	131.5	5.3	127.7	4.4	170.9	6.0	166.1	7.3	77	3	77	3	*480.7	15.3	*467.3	16.8
	48	5	2	134.9	3.9	135.9	3.0	174.9	3.9	177.1	4.1	78	3	78	2	491.6	6.2	491.9	13.2
CT-ST	3	3	8	99.9	12.8	102.3	9.7	135.2	9.7	131.3	11.6	73	6	78	6	377.2	32.5	372.7	32.3
	6	1	0	113.6	.	.	.	150.9	.	.	.	75	.	.	.	422.9	.	.	.
	9	3	1	125.4	7.6	119.0	.	161.3	4.6	166.4	.	77	8	72	.	459.2	3.5	459.9	.
	12	3	6	129.5	1.8	123.7	5.4	160.1	7.7	164.9	6.5	*81	3	*75	2	459.6	16.3	462.4	17.8
	15	4	4	132.5	2.0	124.7	7.6	168.0	7.5	171.2	6.3	*79	2	*73	2	478.1	16.4	474.8	18.6
	18	4	4	136.5	5.9	133.5	6.2	170.1	12.6	175.9	7.3	80	6	76	7	490.1	25.4	495.0	7.3
	24	7	5	134.8	5.7	131.5	4.1	176.3	3.7	175.6	7.3	77	3	75	2	493.6	9.8	488.2	16.3
	36	10	8	*137.9	5.5	*132.4	4.5	176.6	7.1	170.4	6.1	78	3	78	2	498.4	16.9	482.3	15.0
	48	3	2	144.2	2.7	141.9	1.5	182.7	6.1	183.2	1.2	80	3	79	2	516.4	9.6	511.3	7.1

VOLUMES

The intracranial volume (ICV) and the total volume (TV) for all modalities are shown in [Table 4] and [Figure 6]. The ICV of the CT-HT and TV of all modalities showed a near identical growth pattern compared to the corresponding circumference, cranial width and cranial length over time. The posterior volume showed a similar curve and had a near constant ratio towards the TV within 2.7%.

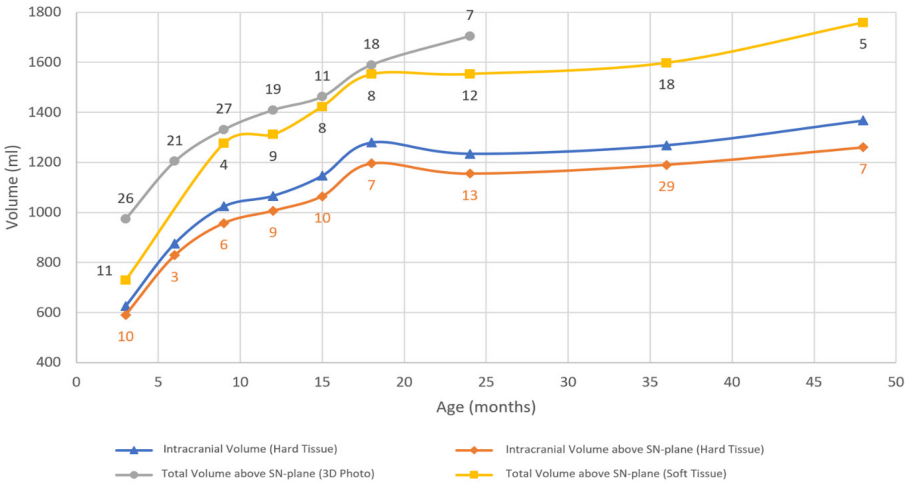

Figure 6: Volume measured on CT-HT, CT-ST and 3D photographs. Coloured numbers indicate the number of subjects used for every age groups.

SUTURE LENGTHS AND LATERAL ORBITAL DISTANCE

The 3D suture length measures for CT-HT over time are given in [Table 5] and [Figure 7]. The strongest increase for all sutures and LOD is within the first 9 months of age. At 12 months, the length of all the sutures and the LOD was equal or even smaller to the 9-months group. After a final increase in length at 15 months, no more growth was present in our dataset for all sutures and the LOD and the lengths remained the same.

Table 4: The number of subjects per age group per gender per modality as well as the average and standard deviation (SD) of the complete total volume, the intracranial volume above the S-N Plane, the total volume above the S-N Plane and the posterior total volume above the S-N Plane. S-N = Sella turcica-nasion, CT-HT = Hardtissue CT scan mesh, CT-ST = Softtissue CT scan mesh. * = statistical significant difference between means of male (M.) and female (F.) of given age group and modality ($p<0.05$).

		n		**Intracranial Volume** (ml)				**Intracranial Volume S-N** (ml)				**Total Volume S-N** (ml)				**Total Volume S-N Posterior** (ml)			
		M.	**F.**	**Male**		**Female**		**Male**		**Female**		**Male**		**Female**		**Male**		**Female**	
Group	age			Mean	SD	Mean	SD	Mean	SD	Mean	SD	Mean	SD	Mean	SD	Mean	SD	Mean	SD
3DP	3	14	12									*1002	54	*940	64	*630	29	*592	38
	6	10	12									*1281	74	*1140	67	*793	40	*713	40
	9	13	14									1394	92	1272	73	*856	52	*785	43
	12	10	9									1477	87	1334	62	*903	49	*824	40
	15	4	7									1474	54	1456	69	910	34	903	38
	18	10	8									1611	90	1563	126	992	49	962	72
	24	3	4									1770	44	1657	78	1097	30	1023	49
CT-HT	3	3	7	608	196	633	230	576	179	597	220	641	202	687	255	380	100	450	167
	6	2	1	882	153	862	.	833	163	820	.	928	166	932	.	580	81	599	.
	9	5	1	1025	34	1022	.	957	50	959	.	1103	47	1114	.	680	25	719	.
	12	3	6	1020	114	1089	77	959	108	1030	70	1111	135	1187	86	681	83	752	45
	15	5	5	1179	55	1114	124	*1114	56	*1014	60	*1305	71	*1193	59	820	78	779	99
	18	2	5	1395	88	1233	23	*1319	52	*1146	25	*1570	52	*1349	57	*957	64	*852	34
	24	7	6	1259	115	1204	92	1173	105	1134	72	1378	124	1322	86	894	53	838	103
	36	17	12	1302	112	1219	153	1215	100	1153	141	1451	106	1372	147	903	85	874	102
	48	5	2	1345	58	1423	111	1245	43	1300	67	1515	48	1556	81	970	27	1013	63
CT-ST	3	3	8									740	200	724	164	457	121	464	110
	6	1	0									925	.	.	.	591	.	.	.
	9	3	1									1290	49	1238	.	779	9	791	.
	12	3	6									1278	125	1328	141	778	78	835	88
	15	4	4									1483	100	1363	79	923	87	897	99
	18	4	4									1574	199	1531	62	975	95	968	28
	24	7	5									1565	134	1537	84	1007	64	968	91
	36	10	8									1654	130	1527	169	1010	96	953	101
	48	3	2									1755	71	1764	27	1110	53	1132	31

Table 5: The number of subjects per age group per gender per modality as well as the average and standard deviation (SD) of the 2D & 3D Distances measured on the CT-HT. * = statistical significant difference between means of male and female of given age group and modality ($p<0.05$).

	n		**Lateral Orbital Distance** (mm)				**3D Distance Metopica** (mm)				**3D Distance Coronal** (mm)			
	Male	**Female**	**Male**		**Female**		**Male**		**Female**		**Male**		**Female**	
Group			Mean	SD	Mean	SD	Mean	SD	Mean	SD	Mean	SD	Mean	SD
3	3	7	65.5	7.6	64.6	6.8	86.8	10.2	86.8	11.3	181.5	25.4	180.5	19.8
6	2	1	72.3	4.8	74.1	.	98.9	5.2	99.5	.	205.1	15.1	207.3	.
9	5	1	77.3	1.3	78.4	.	106.9	4.5	108.1	.	216.8	7.9	213.9	.
12	3	6	75.7	3.9	76.7	3.1	103.1	9.8	109.1	5.8	215.2	12.7	212.8	7.0
15	5	5	*83.1	2.0	*78.5	2.2	114.3	4.9	114.6	5.4	229.0	7.2	221.0	6.9
18	2	5	85.2	3.0	80.5	2.5	*121.0	1.7	*115.1	2.7	*255.6	14.1	*221.8	5.6
24	7	6	82.1	1.8	80.3	2.5	116.2	8.4	115.8	6.3	227.6	11.4	220.9	9.1
36	17	12	81.5	3.6	80.6	3.3	121.9	7.4	118.7	6.8	230.1	12.6	222.7	12.6
48	5	2	83.8	4.3	84.4	4.9	122.9	3.0	127.3	5.2	237.5	5.4	227.9	13.3

	n		**3D Distance Sagittal** (mm)				**3D Distance Posterior Fontanelle - Occiput** (mm)				**3D Distance Nasion - Occiput** (mm)			
	Male	**Female**	**Male**		**Female**		**Male**		**Female**		**Male**		**Female**	
Group			Mean	SD	Mean	SD	Mean	SD	Mean	SD	Mean	SD	Mean	SD
3	3	7	101.7	6.0	100.0	10.9	46.9	11.4	48.0	16.2	235.4	25.2	234.7	35.2
6	2	1	109.9	1.0	106.4	.	52.0	10.3	55.4	.	260.7	14.4	261.4	.
9	5	1	116.3	6.1	109.1	.	60.1	6.8	72.0	.	283.2	7.6	289.2	.
12	3	6	114.8	7.4	113.8	5.6	58.8	2.0	65.9	13.9	276.5	10.8	288.9	13.8
15	5	5	117.8	12.6	120.9	9.4	63.8	11.1	59.9	6.8	295.8	8.4	295.3	16.5
18	2	5	127.2	0.4	126.7	8.4	65.5	3.0	62.1	6.1	313.8	1.6	304.0	9.2
24	7	6	122.6	11.5	124.9	6.2	64.2	10.5	55.9	9.0	303.0	13.2	296.6	14.3
36	17	12	121.5	8.5	121.7	7.7	64.8	15.7	60.8	9.4	308.2	11.3	301.2	19.4
48	5	2	123.1	6.9	129.5	0.6	70.0	11.5	66.9	7.2	316.0	7.8	323.7	11.8

GROWTHMAPS

The growthmaps showed the evolution of the cranial shape. Most growth (in mm) was seen between 3 and 6 months in the frontal and parietal region, for both 3D photographs and the CT-HT. Between 6 and 12 months, growth was more prominent in the anterior part of the skull resulting in an elongation of the head. The posterior part of the skull developed more rapidly between 12 and 18 months. After 12 months the overall growth reduced compared to the first 12 months. Therefore, a longer time-interval of 12 to 24 months was used to create a growthmap which revealed that most growth was present in the frontal and the occipital region [Figure 8 and Figure 9]. Two supplementary video files demonstrate the evolution of the cranium in 3D for the 3D photographs and CT-HT [online via https://doi.org/10.1016/j.ijom.2019.10.012].

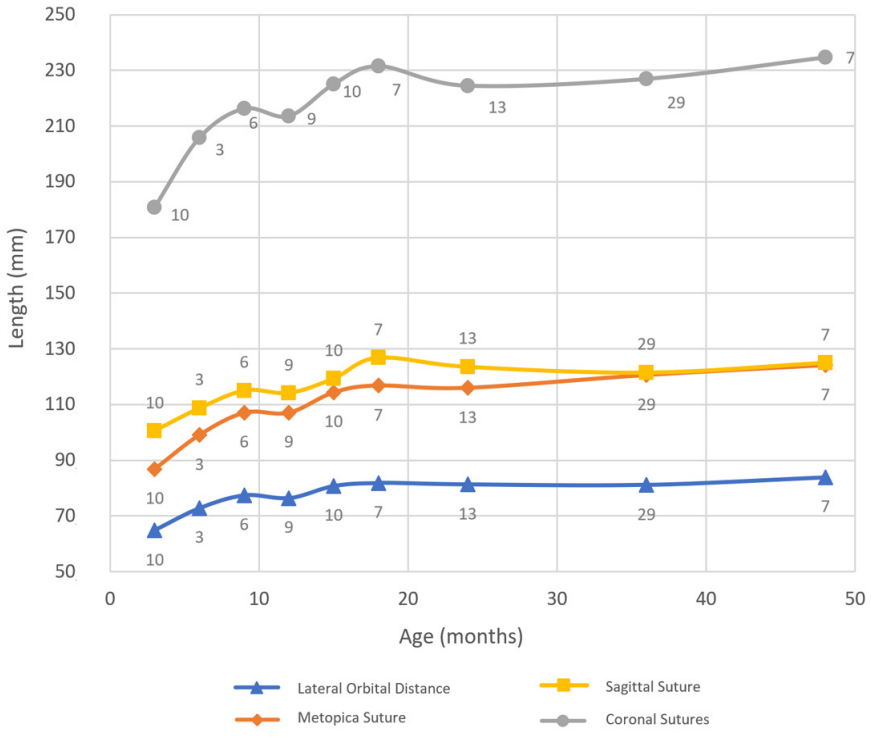

Figure 7: Suture length measured on the CT-HT. Coloured numbers indicate the number of subjects used for every age groups.

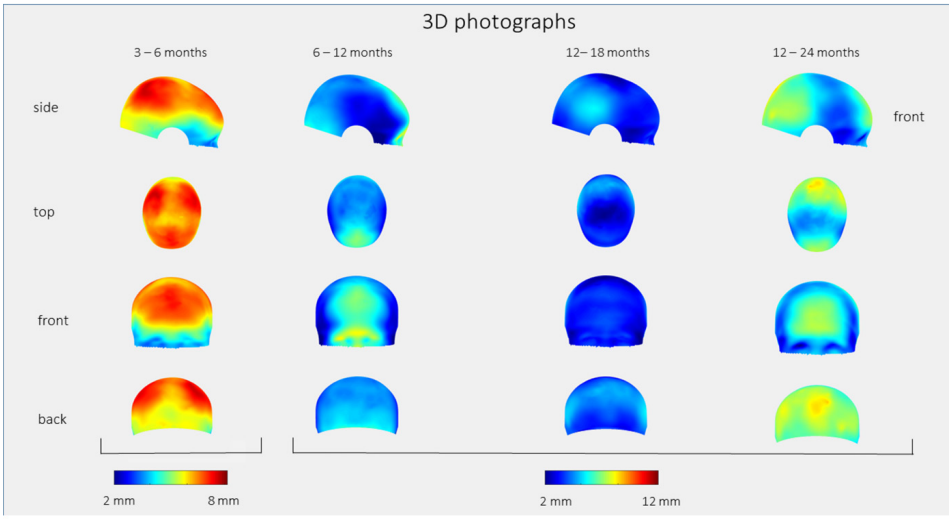

Figure 8: Growthmaps of 3D photographs, illustrating the focus of growth between different time-intervals.

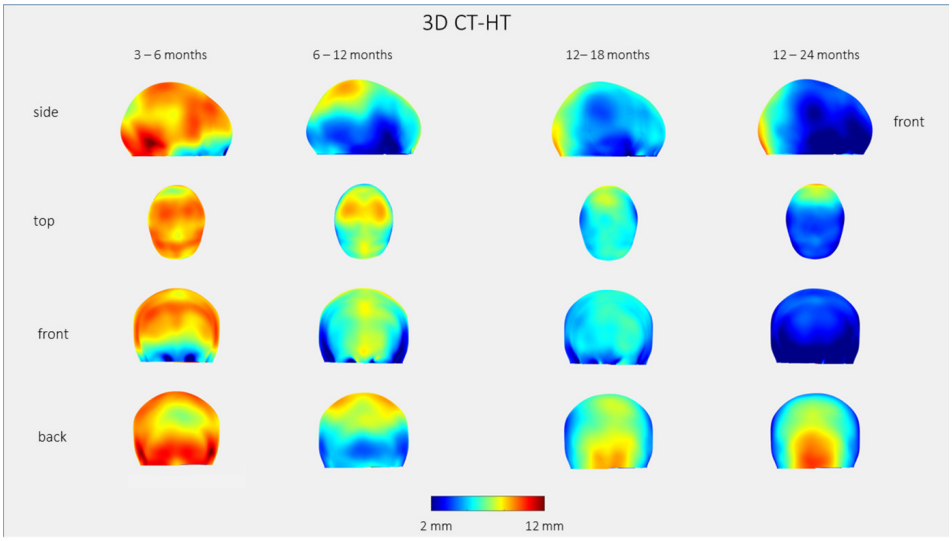

Figure 9: Growthmaps of 3D-CT, illustrating the focus of growth between different time-intervals.

DISCUSSION

The normal growth of the cranium was extensively evaluated by the use of 3D stereophotogrammetry and 3D-CT during the first years of life in this study. Early detection is key in endoscopically assisted craniosynostosis surgery, and normative reference data can be used for adequate and early detection of abnormalities [2], [12]. In addition, this reference data can be used by clinical experts to make follow-up during remodelling helmet therapy more objective [2], [15]. Also, this data provides a reference for preoperative planning of open reconstructive craniosynostosis surgery in which a virtual reconstruction of the new cranial shape and volume is made [16]. Therefore, this study addresses the need for normative cranial evolution data for detection, follow-up and planning in craniosynostosis.

GROWTHMAPS

Consistent with literature, the growthmaps of the 3D photographs and CT-HT revealed a fast expansion of the cranium in the younger age groups [1], [10], [17]. Between 3 and 6 months, a strong focus of growth was located in the frontal region and in the central parietal regions, indicating the growth kernels. The locations of the sagittal and coronal sutures were clearly indicated by the colours of the growthmaps emphasizing the importance of sutures for the growth of the cranium [18], [19]. According to the 12 – 24 months growthmap, the growth focus was located in the occipital head region, close to the site of the cerebellum. The timing of the cerebellum's volume increase corresponds with the timing of infantsstarting to walk and develop their balance and muscle coordination functions. Although the relation between brain functionality and volume is not clear, brain volume might influence brain development and this might be an explanation for the volume increase in this region [20]. Using MRI data, a disproportionate enlargement of the cerebellum during the first two years was also described by Knickmeyer et al., although this enlargement was even more prominent in the first year [21].

In the 12 - 24 months interval, the 3D photographs demonstrated 3-4 mm more frontal growth compared to the CT-HT group. Population and age differences as well as more and longer hair might have resulted in more volume at the back of the head. This larger posterior volume can result in a more posteriorly located CCFP. Consequently, this would lead to a more anterior alignment of

the cranial shapes and thus erroneously demonstrate more frontal growth.

The mean cranial shapes created in this study can additionally be used for the evaluation of individual cases. The average cranial shape of a specific age group can directly be compared to 3D photographs or 3D CT-scans of patients and allows a direct evaluation of the cranial shape in 3D. In addition to the graphs and tables, the supplementary videos provided optimal insight and understanding of the normal evolution over time. An enormous increase of the cranial size can be noted while the colours highlighted the difference in growth focus during the first 24 months of life. To the best of our knowledge, this is the first study which used this high amount of time intervals to evaluate cranial growth in 3D.

MEASUREMENTS

All CI measurements were in the range of 75 and 78 within the first 24 months of age. In line with literature, the 3D photographs, CT-HT and CT-ST all demonstrated lower values at 24 months [10], [22]. After this period, the CT-HT and CT-ST respectively showed an increase of CI up until the age of 48 months towards 78 and 80 which is in line with the findings of Farkas and Dekaban et al. [4], [23]. The results of CI are lower compared to the findings of Meyer-Marcotty et al. who established an average CI of 84 and 82 measured on 3D photographs of healthy infants of 6 and 12 months respectively [9]. Likus et al. presented also a larger CI of 83 on average, measured on CT-scans [1]. Delye et al. found a mean CI of 83 and 84 measured on CT of healthy infants of 6 and 12 months respectively. This indicates that the subjects used in this study have slightly more elongated head shapes [7]. We therefore believe it is important to establish reference measurements obtained from a population that is a good representation to the population of patients that are treated in a local centre.

Head circumference measured on 3D photographs showed almost identical trends when compared to the nationwide growth study in the Netherlands which included 14500 boys and girls of Dutch origin [Figure 5] [14]. Only the 24-months group of both sexes in our data showed a +1 SD higher circumference which can also be a consequence of hair of the subjects at this age.

Since sexual dimorphism is present in an early stage of life, a distinction between males and females was made in this study [24], [25]. Meyer-Marcotty et al. already described a significant larger value in males for length,

circumference and volume increase between 6 and 12 months of life [9], [10]. Joffe et al. measured slightly larger cranial circumferences at birth, at 6 months and at 12 months in males [26]. Although these studies used fewer time intervals, the sexual dimorphism with males presenting larger values is in line with the findings in this study for the 3D photographs during the first 12 months of life [Table 3 and Figure 5]. After this period, our results did not reveal a significant difference between males and females. This is in contrast with studies that stated that sexual dimorphism become more pronounced with later age [24]. This discrepancy might be explained by the smaller sample size of the 18- and 24-months age group in our study or by the fact that 3D photographs are more prone to artefacts at a later age because of the hair volume. Nevertheless, in contrast to our expectations we were not able to find a significant difference in the CT-HT and CT-ST groups [Table 3]. One explanation may be the smaller sample size of these groups compared to the 3D photographs.

VOLUME

Volume measurements based on head circumference has been frequently described [27], [28]. A strong correlation between head circumference and the ICV was found in this study and can be calculated using Equation 1. The high correlation of r=0.987($p<0.001$) makes this method also usable for bedside measures. The total volume graph [Figure 6] demonstrates a clear correlation on increase for the TV of the 3D photographs and CT-HT and CT-ST. Because of the soft tissue, the CT-ST and 3D photographs displayed a larger volume. The latter showed even slightly higher volumes which can be explained by artefacts such as hair.

$$\textit{Equation 1:} V_{intracranial} = 6 * 10^{-5} l_{circumference}^{2.7272}$$

The total ICV and the ICV above the sella turcica-nasion plane showed a strong and significant correlation (r=0.993, $p<0.001$). The TV above the sella turcica-nasion plane and the ICV above the sella tursica-nasion plane also had a strong significant correlation (r=0.987, $p<0.001$) making these volumes good estimates of each other. Comparing the ICV, other studies presented identical growth curves for the first 12 months although Kamdar et al. measured

smaller volumes of around 200 ml for all ages on CT-scans [17], [29], [30]. Our data suggests more rapid growth in the first 18 months of life with a peak at 18 months. However, the 18-months groups only included seven scans and might therefore be less accurate compared to the 15- and 24-months age groups. In addition, a similar peak for the 18-months group was seen for suture lengths and the circumference measurements based on the CT datasets. This suggests that relatively large heads were included in this group.

Cranial volume is an important factor for evaluation of cranial surgery. However, different populations, methods and results are presented in literature [29], [31], [32]. Therefore, it is important to interpret the volume data according their methodology of image acquisition and analysis. This study used different image modalities, yet the same analysis methods were used. This makes evaluation and follow-up more adequate and emphasizes the importance of this study.

LIMITATIONS

In this study, a total of 382 3D photographs and CT-scans were selected for initial inclusion. Due to strict exclusion criteria's, only 299 subjects were used for final analysis which resulted in certain age groups with smaller numbers. The 6-month CT-ST group contained only one scan and was therefore excluded from further analysis. In addition, distinction between males and females resulted in even more samples which were too small to analyse. Yet, the benefit and importance of using stringent exclusion criteria was a clean and pure dataset describing only normal cranial shapes and is therefore appropriate for surgical evaluation and follow-up.

CONCLUSION

This study analysed the growth pattern of the cranial shape of infantsduring the first years of life using 3D stereophotogrammetry and 3D-CT. Advanced 3D evaluation demonstrated a focus of growth of the anterior region of the head in the first year of life and more posterior growth after the age of 1 year. Normative data was presented which is of multidisciplinary interest and can be used by paediatricians and maternity consultation clinics to evaluate the growth and shape of infants' heads.

APPENDIX

OBLIQUE DIAMETER DIFFERENCE INDEX AND CRANIAL PROPORTION INDEX

The oblique diameter difference index (ODDI) and cranial proportion index (CPI) described in the plagiocephalometry method by van Vlimmeren et al. was used in this study to exclude asymmetrical cranial shapes [6]. The general exclusion criteria presented in that study were applicable for soft tissue only. However, since the soft tissue (CT-ST) shapes in this study were more prone for artefacts, the hard tissue (CT-HT) shapes were instead used to determine exclusion. Because it was expected that the effect of ODDI and CPI can be structurally different when measured on CT-HT, a correlation and offset factor between the artefact-free CT-ST and CT-HT was calculated for the ODDI and CPI measurements. In total, 97 CT-scans were used to determine the ODDI and CPI on both the CT-HT and the CT-ST shapes and a possible correlation and offset was investigated.

The mean ODDI was 103.1 (SD=2.3) for the CT-HT scans and 102.8 (SD=2.2) for the corresponding CT-ST scans. The paired correlation showed a statistically significant ($p<0.001$) and strong positive correlation for both the ODDI ($r=0.968$) and CPI ($r=0.984$). There was a statistically significant average difference for the ODDI ($t_{96}=4.456$, $p< 0.001$) but no statistical significant average difference for the CPI ($t_{96}=1.961$, $p=0.053$). Therefore, only an offset for the ODDI was applied which was based on the difference of the mean (+0.3). This resulted in a new ODDI of 104.8 and a CPI of 90 to be used as a cut-off for the CT-HT scans.

SUPPLEMENTARY MATERIALS

Table 6: Overview of all mean CCFP-offset values in the nasion-sella turcica orientation with the SD and 95% confidence interval as separated by modality and age-group. The sella turcica is positioned at (0,0,0).

	Age (mo.)	n	CCFP-X (mm)			CCFP-Y (mm)			CCFP-Z (mm)		
			Mean	SD	95% conf. int	Mean	SD	95% conf. int	Mean	SD	95% conf. int
CT-HT	3	10	-0.4	0.8	-0.9 - 0.2	13.6	3.9	10.8 - 16.3	28.4	3.3	26.1 - 30.8
	6	3	-1.2	1.0	-3.6 - 1.3	14.0	2.5	7.9 - 20.1	29.9	4.1	19.7 - 40.1
	9	6	-0.6	0.7	-1.3 - 0.1	13.3	4.0	9.2 - 17.5	32.4	3.7	28.5 - 36.3
	12	9	-0.5	0.8	-1.1 - 0.1	13.7	3.8	10.8 - 16.6	33.2	2.2	31.5 - 34.9
	15	10	0.1	0.9	-0.6 - 0.8	15.9	6.1	11.5 - 20.3	33.1	3.9	30.4 - 35.9
	18	7	-0.1	1.0	-1.1 - 0.8	14.7	3.7	11.3 - 18.0	34.4	3.6	31.1 - 37.7
	24	13	-0.6	1.1	-1.3 - 0.1	16.6	5.5	13.3 - 20.0	34.4	3.9	32.1 - 36.8
	36	29	-0.5	1.6	-1.1 - 0.1	14.5	5.0	12.6 - 16.4	35.2	3.1	34.0 - 36.4
	48	7	-0.2	0.5	-0.6 - 0.3	17.1	3.4	13.9 - 20.3	33.1	2.4	30.8 - 35.3
CT-ST	3	11	-0.4	0.6	-0.9 - 0.0	13.9	2.9	11.9 - 15.8	27.5	3.3	25.3 - 29.8
	9	4	-0.6	0.8	-1.9 - 0.7	13.5	4.2	6.8 - 20.3	31.3	1.0	29.7 - 32.9
	12	9	-0.5	0.8	-1.1 - 0.2	14.2	3.5	11.5 - 16.9	31.5	2.2	29.8 - 33.2
	15	8	-0.1	1.0	-0.9 - 0.8	17.2	5.9	12.3 - 22.2	31.2	4.5	27.4 - 34.9
	18	8	-0.1	1.5	-1.4 - 1.2	15.5	3.4	12.7 - 18.3	31.7	3.4	28.8 - 34.6
	24	12	-0.4	1.1	-1.2 - 0.3	17.3	4.8	14.3 - 20.3	32.7	4.4	29.9 - 35.5
	36	18	0.0	1.9	-1.0 - 0.9	14.0	5.2	11.4 - 16.6	34.4	3.2	32.8 - 36.0
	48	5	0.3	0.8	-0.7 - 1.3	17.3	2.1	14.7 - 20.0	31.2	1.8	28.9 - 33.5

REFERENCES

[1] W. Likus, G. Bajor, J. Baron, J. Markowski, D. Milka, and T. Lepich, "Cephalic Index in the First Three Years of Life: Study of Children with Normal Brain Development Based on Computed Tomography," *Sci. World J.*, vol. 2014, pp. 1–6, 2014.

[2] H. Delye *et al.*, "Creating a normative database of age-specific 3D geometrical data, bone density, and bone thickness of the developing skull: a pilot study," *J. Neurosurg. Pediatr.*, vol. 16, no. 6, pp. 687–702, Dec. 2015.

[3] A. Mcgarry, M. T. Dixon, R. J. Greig, D. R. L. Hamilton, S. Sexton, and H. Smart, "Head shape measurement standards and cranial orthoses in the treatment of infants with deformational plagiocephaly," *Developmental Medicine and Child Neurology*, vol. 50, no. 8. pp. 568–576, Aug-2008.

[4] A. S. Dekaban, "Tables of cranial and orbital measurements, cranial volume, and derived indexes in males and females from 7 days to 20 years of age," *Ann. Neurol.*, vol. 2, no. 6, pp. 485–491, Dec. 1977.

[5] M. Bastir, A. Rosas, and P. O'Higgins, "Craniofacial levels and the morphological maturation of the human skull," *J. Anat.*, vol. 209, no. 5, pp. 637–654, Oct. 2006.

[6] L. A. Van Vlimmeren, T. Takken, L. N. A. Van Adrichem, Y. Van Der Graaf, P. J. M. Helders, and R. H. H. Engelbert, "Plagiocephalometry: A non-invasive method to quantify asymmetry of the skull; a reliability study," *Eur. J. Pediatr.*, vol. 165, no. 3, pp. 149–157, Mar. 2006.

[7] E. J. van Lindert *et al.*, "Validation of cephalic index measurements in scaphocephaly.," *Childs. Nerv. Syst.*, vol. 29, no. 6, pp. 1007–14, Jun. 2013.

[8] W. Likus, G. Bajor, J. Baron, J. Markowski, D. Milka, and T. Lepich, "Cephalic Index in the First Three Years of Life: Study of Children with Normal Brain Development Based on Computed Tomography," *Sci. World J.*, vol. 2014, pp. 1–6, 2014.

[9] P. Meyer-Marcotty, H. Böhm, C. Linz, J. Kochel, A. Stellzig-Eisenhauer, and T. Schweitzer, "Three-dimensional analysis of cranial growth from 6 to 12 months of age," *Eur. J. Orthod.*, vol. 36, no. 5, pp. 489–496, Oct. 2014.

[10] P. Meyer-Marcotty *et al.*, "Cranial growth in infants—A longitudinal three-dimensional analysis of the first months of life," *J. Cranio-Maxillofacial Surg.*, vol. 46, no. 6, pp. 987–993, Jun. 2018.

[11] G. de Jong *et al.*, "Radiation-free 3D head shape and volume evaluation after endoscopically assisted strip craniectomy followed by helmet therapy for trigonocephaly," *J. Cranio-Maxillofacial Surg.*, vol. 45, no. 5, pp. 661–671, May 2017.

[12] J. W. Meulstee *et al.*, "A new method for three-dimensional evaluation of the cranial shape and the automatic identification of craniosynostosis using 3D stereophotogrammetry," *Int. J. Oral Maxillofac. Surg.*, vol. 46, no. March, pp. 819–826, Jul. 2017.

[13] G. A. de Jong, T. J. J. Maal, and H. Delye, "The computed cranial focal point," *J. Cranio-Maxillofacial Surg.*, vol. 43, no. 9, pp. 1737–1742, 2015.

[14] A. M. Fredriks *et al.*, "Continuing positive secular growth change in The Netherlands 1955-1997.," *Pediatr. Res.*, vol. 47, no. 3, pp. 316–23, Mar. 2000.

[15] H. H. K. . Delye *et al.*, "Endoscopically assisted craniosynostosis surgery (EACS): The craniofacial team Nijmegen experience," *J. Cranio-Maxillofacial Surg.*, vol. 44, no. 8, pp. 1029–1036, 2016.

[16] H. Chim, N. Wetjen, and S. Mardini, "Virtual surgical planning in craniofacial surgery.," *Semin. Plast. Surg.*, vol. 28, no. 3, pp. 150–8, Aug. 2014.

[17] M. R. Kamdar, R. A. Gomez, and J. A. Ascherman, "Intracranial Volumes in a Large Series of Healthy Children," *Plast. Reconstr. Surg.*, vol. 124, no. 6, pp. 2072–2075, Dec. 2009.

[18] L. A. Opperman, "Cranial sutures as intramembranous bone growth sites," *Dev. Dyn.*, vol. 219, no. 4, pp. 472–485, Dec. 2000.

[19] S.-W. Jin, K.-B. Sim, and S.-D. Kim, "Development and Growth of the Normal Cranial Vault : An Embryologic Review.," *J. Korean Neurosurg. Soc.*, vol. 59, no. 3, pp. 192–6, May 2016.

[20] A. Leingartner *et al.*, "Cortical area size dictates performance at modality-specific behaviors," *Proc. Natl. Acad. Sci.*, vol. 104, no. 10, pp. 4153–4158, Mar. 2007.

[21] R. C. Knickmeyer *et al.*, "A structural MRI study of human brain development from birth to 2 years.," *J. Neurosci.*, vol. 28, no. 47, pp. 12176–82, Nov. 2008.

[22] J.-F. Wilbrand *et al.*, "Normal Head Shape Parameters in the First 2 Years of Life and Effect of Helmet Therapy," *Neuropediatrics*, vol. 48, no. 06, pp. 432–441, Dec. 2017.

[23] L. G. Farkas, J. C. Posnick, and T. M. Hreczko, "Anthropometric Growth Study of the Head," *Cleft Palate-Craniofacial J.*, vol. 29, no. 4, pp. 303–308, Jul. 1992.

[24] E. Bulygina, P. Mitteroecker, and L. Aiello, "Ontogeny of facial dimorphism and patterns of individual development within one human population," *Am. J. Phys. Anthropol.*, vol. 131, no. 3, pp. 432–443, Nov. 2006.

[25] H. Matthews, T. Penington, I. Saey, J. Halliday, E. Muggli, and P. Claes, "Spatially dense morphometrics of craniofacial sexual dimorphism in 1-year-olds," *J. Anat.*, vol. 229, no. 4, pp. 549–559, 2016.

[26] T. H. Joffe *et al.*, "Fetal and infant head circumference sexual dimorphism in primates," *Am. J. Phys. Anthropol.*, vol. 126, no. 1, pp. 97–110, Jan. 2005.

[27] M. Martini, A. Klausing, G. Lüchters, N. Heim, and M. Messing-Jünger, "Head circumference - a useful single parameter for skull volume development in cranial growth analysis?," *Head Face Med.*, vol. 14, no. 1, p. 3, Jan. 2018.

[28] A. A. Lindley, J. E. Benson, C. Grimes, T. M. Cole, and A. A. Herman, "The relationship in neonates between clinically measured head circumference and brain volume estimated from head CT-scans.," *Early Hum. Dev.*, vol. 56, no. 1, pp. 17–29, Sep. 1999.

[29] A. H. Abbott *et al.*, "CT-determined intracranial volume for a normal population.," *J. Craniofac. Surg.*, vol. 11, no. 3, pp. 211–23, May 2000.

[30] M.-L. C. van Veelen *et al.*, "Volume measurements on three-dimensional photogrammetry after extended strip versus total cranial remodeling for sagittal synostosis: A comparative cohort study," *J. Cranio-Maxillofacial Surg.*, vol. 44, no. 10, pp. 1713–1718, Oct. 2016.

[31] C. Freudlsperger, S. Steinmacher, H. Bächli, E. Somlo, J. Hoffmann, and M. Engel, "Metopic synostosis: Measuring intracranial volume change following fronto-orbital advancement using three-dimensional photogrammetry," *J. Cranio-Maxillofacial Surg.*, vol. 43, no. 5, pp. 593–598, 2015.

[32] R. Seeberger *et al.*, "Intracranial volume (ICV) in isolated sagittal craniosynostosis measured by 3D photocephalometry: A new perspective on a controversial issue," *J. Cranio-Maxillofacial Surg.*, vol. 44, no. 5, pp. 626–631, 2016.

Chapter 6

Longitudinal 3D Follow-up and surgical Safety outcomes after endoscopic and open scaphocephaly surgery

G. de Jong*, J. Meulstee*, E.J. van Lindert, W. Borstlap, T. Maal, H. Delye

*G. de Jong and J. Meulstee contributed equally as co-first authors

Adapted from: the submitted manuscript to Journal of Cranio-Maxillofacial Surgery on September 2020.

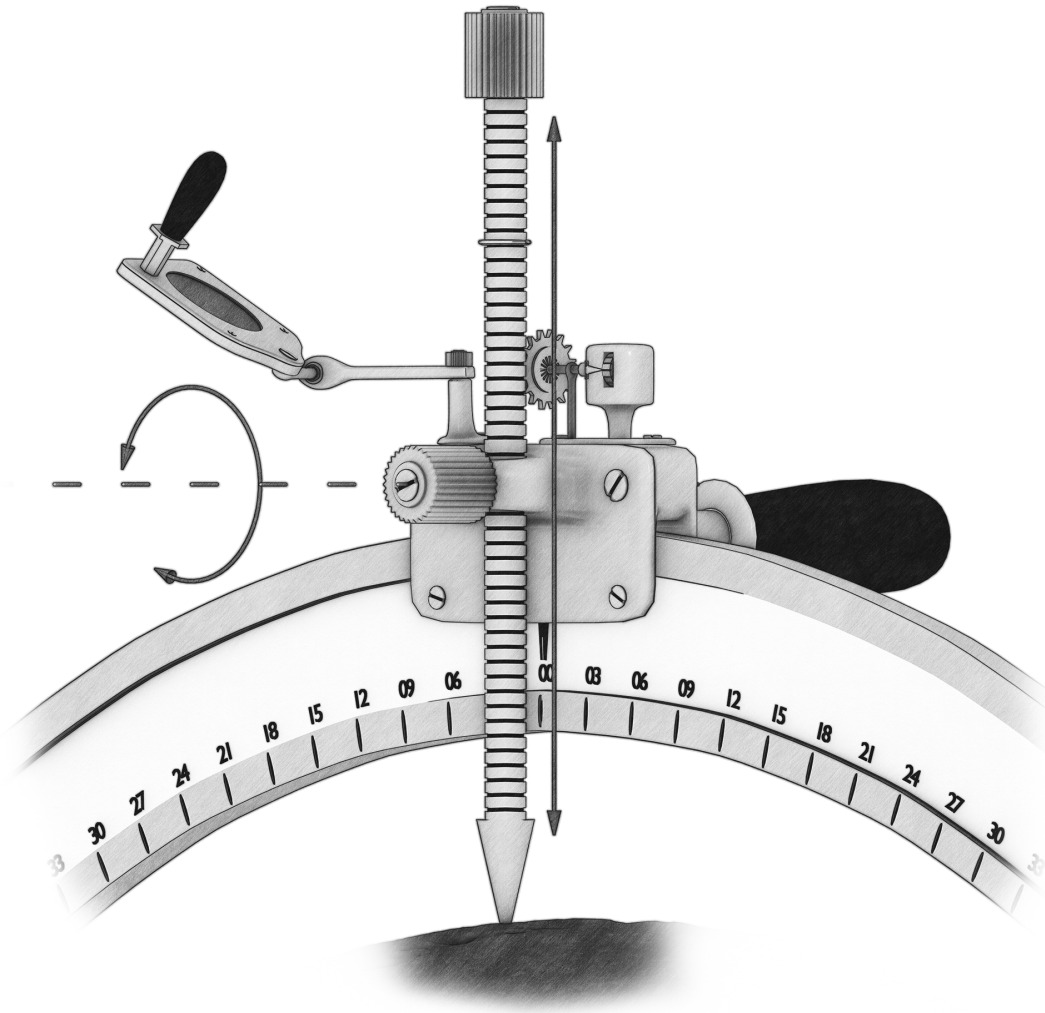

ABSTRACT

Background: Two commonly used surgical techniques for treating scaphocephaly are endoscopically assisted craniosynostosis surgery (EACS) or open cranial vault reconstruction (OCVR). However, the longitudinal 3D cranial shape developments after these surgery remains unknown. The aim of this study was primarily to evaluate the longitudinal 3D cranial shape developments and secondly the surgical safety outcomes after EACS and OCVR.

Methods: Longitudinal 3D photos (n=492) were collected from 140 infants who underwent EACS or OCVR with reference 3D photos (n=130) of healthy infants. The 3D cranial shape measurements and color-coded distance maps of growth and surgical changes were calculated and compared between the groups over time. Surgical safety outcomes were determined and compared for 150 EACS and OCVR patients.

Results: Both surgical techniques showed their strongest changes and growth direct after surgery. Most 3D measurements were not significantly different between groups at later ages. Comparison of EACS and OCVR for children aged 24 months, showed differences less than ± 2mm between head shapes. EACS was superior over OCVR in nearly all safety outcomes.

Conclusion: Comparison showed near identical results in the 3D measurements and distance maps between EACS and OCVR, however EACS showed superior surgical safety outcomes. EACS is the recommended treatment option.

INTRODUCTION

Scaphocephaly is the result of premature fusion of the sagittal suture and is characterized by esthetical features such as an elongated head, a wide and prominent forehead, and a narrow occiput [1]. Scaphocephaly is the most common type of craniosynostosis with a prevalence of around 45-50% in relation to other forms; it occurs in 1.5-4 of 10.000 live births worldwide [2]–[6].

Treatment of scaphocephaly aims to correct cranial deformities, prevent increased intracranial pressure, and reduce the risk of developmental delay [7]. There are a wide variety of treatment options, including open cranial vault reconstruction (OCVR), spring mediated cranioplasty, modified-pi reconstruction, and endoscopically assisted craniosynostosis surgery (EACS) with redressing helmet therapy [8]. Although OCVR is the most commonly used procedure [7], [9], there is a trend for minimal invasive treatment options since the initial introduction of the endoscopic technique which showed positive results [10]. Studies show that the endoscopic technique reduced complication and mortality rates, decreased blood loss, shortened hospital stay, and lowered healthcare costs [4], [8], [10]–[12]. However, the aesthetic and morphological outcome of treatment options is often not described in literature or is based on subjective measures [13], [14] which makes it challenging to determine the optimal surgical procedure.

Three-dimensional (3D) imaging techniques such as 3D stereophotogrammetry can be used to determine the pre- and post-surgery cranial shape. 3D Photos can be taken quickly and without harmful radiation at different moments before, during and after treatment. This allows a more objective long-term follow-up of the patients' cranial shape morphology.

The primary aim of this study was to evaluate the cranial shape development of scaphocephaly patients with objective 3D analysis methods. Secondly, the surgical safety outcomes of these type of patients were evaluated.

MATERIALS AND METHODS

PATIENTS

Unisutural non-syndromic scaphocephaly patients aging up to 56 months who underwent either EACS or OCVR between 2005 and 2019 at our institute were included in this study. A part of this patient sample was presented in an earlier

study regarding some of the surgical safety outcomes and 3D measurements (64 EACS patients) [12]. All data were anonymized prior to analysis. Patients older than 14 months at the time of surgery are rare in our institution and were excluded to prevent outliers. Approval with an informed consent waiver from the regional institutional review board was obtained for this study (2020-6128). This study was conducted in compliance with the World Medical Association Declaration of Helsinki on medical research ethics.

TREATMENT

During EACS, the fused sagittal suture is removed and biparietal and bitemporal stave osteotomies are performed. Helmet therapy is initiated two weeks after EACS for all patients and continued for a period of approximately 10 months. EACS for the preferred treatment for children younger than 6 months. In case EACS is not possible OCVR is performed. Since 2013, a virtual surgical planning is created to determine the best surgical strategy for all OCVR treated patients.

3D PHOTO ACQUISITION

3D Photos of the cranial shape were acquired using the 3DMD Cranial System (3dMDCranial, 3dMD, Atlanta, USA) in a prospective setup. The 3D photos of patients who underwent EACS or OCVR were distributed in the nearest age group (3, 6, 9, 12, 15, 18, 24, 36 and 48 months) and placed in the groups pre-surgery and post-surgery.

3D PHOTO PROCESSING

The same data acquisition and processing protocols were followed for the 3D photos as described in our earlier work [15]–[17]. All 3D photos underwent quality control and were excluded in case of incomplete craniums. 3D Photos with small artefacts were repaired. All 3D Photos were oriented in a similar position for further analysis in three steps. Firstly, nine landmarks for pre-alignment in the tragus-nasion orientation were manually indicated [15]. Secondly, within the tragus-nasion orientation, the Computed Cranial Focal Point (CCFP) was calculated. Finally, using the specific CCFP-offset values and the CCFP, the 3D photos were placed in their final position [16], [18].

The scaphocephaly CCFP-offset values were determined using 20 pre-surgery CT-scans of scaphocephaly patients with the method of an earlier study [16]. Reference CCFP-offset values were similarly acquired using 183 CT-scans of infants aged 0-48 months [15]. All 3D photos for the pre-surgery group were positioned using the scaphocephaly-specific CCFP-offset. Both the post-surgical OCVR 3D photos and the reference group 3D photos were positioned using the reference age-specific CCFP-offset values due to the head being modelled towards normal shaped heads. The post-surgery EACS 3D photos used scaphocephaly CCFP-offset values interpolated towards the reference value from 6 - 18 months of age. After 18 months, the reference CCFP values were used for the EACS 3D photos.

3D PHOTO MEASUREMENTS

For all 3D photos, the cranial length was measured from the most anterior point to the most posterior point of the cranium [15]. Dividing cranial width by cranial length resulted in the cephalic index (CI). Circumference was measured on the cranial shapes at the crossing points of the cranial width and length. The volume above the sella turcica – nasion plane was calculated. Results were split on gender, type of surgery, and pre or post-surgery status.

COLOR-CODED DISTANCE MAPS

Growth and shape comparison maps were created to visualize the shape changes of the head for each specific group using color-coded distance maps; these were also used to compare between groups. Asymmetries in the head can naturally occur but give a distorted image of the shape changes over time. Therefore, prior to calculating these distance maps, the 3D photos were mirrored over the midsagittal axis. The original 3D photo and the mirrored counterpart were both sampled using ray casting [15] and subsequently averaged. These averaged 3D photos will be used for the distance map computation. Male and female patients were grouped together for each age and treatment group.

The distribution data of the distance maps for the analysis are shown in [Table 2]. These visualize the difference between two head shapes in two sequential age groups or between two treatment groups. Finally, to investigate the long-term outcome of both surgical strategies the EACS7 and OCVR7 groups were compared. EACS patients usually no longer wear the remodeling helmet at that age.

Table 1: The overview of pre to post-surgery distance maps and post to post-surgery distance maps created for the EACS and OCVR patients.

Pre to Post-surgery distance maps			Post to Post-surgery distance maps		
Group 1 (Pre)		**Group 2 (Post)**	**Group 1 (Post)**		**Group 2 (Post)**
EACS 1	➔	EACS 2	EACS 2	➔	EACS 3
EACS 2	➔	EACS 3	EACS 3	➔	EACS 4
OCVR 1	➔	OCVR 2	EACS 4	➔	EACS 5
OCVR 2	➔	OCVR 3	EACS 5	➔	EACS 6
OCVR 3	➔	OCVR 4	EACS 6	➔	EACS 7
OCVR 4	➔	OCVR 5	EACS 7	➔	EACS 9
			EACS 7	➔	OCVR 7

ACQUISITION OF SURGICAL SAFETY OUTCOMES

Surgical safety outcomes obtained included: age at surgery, gender, blood loss, surgery time, total anesthesia time, blood-transfusions (peri and post-surgery), hospital stay duration, and intensive care stay duration. Helmet therapy duration was also obtained for EACS patients. The outcomes of 114 EACS patients (92 males) and 36 OCVR patients (29 males) were collected. This population largely overlaps the population of which the 3D photos were obtained.

STATISTICAL ANALYSIS OF GROWTH DATA

For all 3D photo measurements, the mean and standard deviation were computed per dataset per group using mixed model analysis; fixed effects of the age group, intervention, and gender for post-surgery were determined. A significant p-value for the fixed effect of a cranial 3D photo measurement indicates that the given measurement value changes differently between two groups over time. Two-tailed t-tests for 3D measurements between age groups per intervention and gender were conducted based on the mixed model results. The same tests were conducted for the reference groups to compare with the intervention groups.

Means and standard deviations were given for normally distributed data. Medians and the range were given for non-normally distributed data. Statistical significance for determining differences was assumed $p<0.05$. For statistical analyses, we used IBM SPSS Statistics version 25 (IBM Germany GmbH, Ehningen, Germany).

RESULTS

ACQUISITION OF 3D PHOTOS

A total of 384 3D photos from 106 infants were used for EACS, and a total of 108 3D photos from 34 infants were used for OCVR. The EACS and OCVR groups contained 84 males (79%) and 29 (85%) respectively. A total of 130 reference 3D photos with 64 males (49%) up to the age of 24-months were obtained from an earlier study [15]. The 3D photo distribution is shown in[Table 2].

Table 2: The number of 3D photos per age-group (months) over pre and post-surgery for EACS and OCVR groups. All groups were divided in male (M) and female (F).

		Pre-surgery				Post-surgery					
		EACS		OCVR		EACS		OCVR		References	
Group	Age (mo.)	M	F	M	F	M	F	M	F	M	F
1	3	52	13	4	1	4	2			14	12
2	6	18	3	8		33	3	1	1	10	12
3	9			8		47	11	4		13	14
4	12			8	2	47	13	7		10	9
5	15					26	6	9	1	4	7
6	18					12	3	10	3	10	8
7	24					37	8	17	2	3	4
8	36					8	2	4	2		
9	48					29	7	15	1		

SURGICAL SAFETY OUTCOMES

The male-female ratio was 4 to 1 in both the EACS and OCVR groups [Table 1]. For EACS patients, less blood loss and a shorter surgery and total anesthesia time were found [Table 3] and the overall length of stay was shorter [Table 4]. In the EACS group, only one case (1%) was treated in the ICU for a period of 3 days. In the OCVR group, 25 cases (61%) were admitted to the ICU for one day each. The remodeling helmet was worn 9.6 months on average (SD=2.4, range =3.9-16.1) after EACS.

Fewer blood transfusions were given during EACS [Table 6] and the amount of blood given was significantly lower in the EACS group. The only outcome parameter not significantly different between both groups was the number of post-surgery blood transfusions.

Table 3: Gender and age at surgery distribution for the EACS and OCVR groups.

	Totals (n (%))		**Age** (months)		
Group	**Male**	**Female**	**Median**	**Min**	**Max**
EACS	92 (81%)	22 (19%)	3.9	2.4	6.6
OCVR	29 (81%)	7 (19%)	9.2	4.0	14.0
p-value	0.985		<0.001		

Table 4: Blood loss, surgery time and total anesthesia time for the EACS and OCVR groups

	Blood loss (ml)			**Surgery time** (mins)			**Total anesthesia time** (mins)		
Group	**Median**	**Min**	**Max**	**Median**	**Min**	**Max**	**Median**	**Min**	**Max**
EACS	18	0	160	56	34	113	136	98	325
OCVR	100	15	300	131	89	283	250	167	394
p-value	<0.001			<0.001			<0.001		

Table 5: Length of stay and post-surgery days for EACS and OCVR surgery.

	Total (days)			**Post-Surgery** (days)		
Group	**Median**	**Min**	**Max**	**Median**	**Min**	**Max**
EACS	3	2	7	2	1	5
OCVR	5	4	9	5	3	8
p-value	<0.001			<0.001		

Table 6: The blood transfusion rate and total amount (in case of at least one transfusion) for the EACS and OCVR group. The adjusted p-value for chi-square statistical significance is computed as p≤0.008. Note that due to rounding of the percentages the sum can exceed 100%.

	Surgery Transfusions (n (%))				**Total Amount** (ml)		
Group	**None**	**Peri-surg.**	**Post-surg.**	**Both**	**Median**	**Min**	**Max**
EACS	93 (82%)	0 (0%)	19 (17%)	2 (2%)	90	65	190
OCVR	7 (19%)	17 (47%)	7 (19%)	5 (14%)	130	30	250
p-value	<0.001	<0.001	0.701	0.003	<0.001		

3D MEASUREMENTS

[Table 7] shows the results of the fixed effects test for the cranial measurements. A significant p-value indicates that the given measurement changes (pattern) over time are different between two groups. In general, most outcomes for males showed a different pattern over time in EACS as compared to OCVR and the Controls. OCVR showed this in lesser extend as compared to the Controls. Most differences in females were found between EACS and the Controls. In general the EACS growth patterns showed more deviations from the Controls.

The pre-surgery and post-surgery (cranial shape) measurements for the male and female patients are shown in [Tables 8-11] The graphs of the means and standard error of mean of the cranial index, cranial length, and circumference is shown in [Figure 1]. Almost all pre-surgery values were significantly different from the reference groups in both genders.

Table 7: P-values from the test of fixed effects on the cranial measurements based on interaction of overlapping age groups and treatment as separated by gender. A significant p-value indicates that the given measurement value changes over time are different between two groups.

Treatment groups		Gender	Cranial Width	Cranial Length	Cranial Index	Circumference	Volume
EACS	**OCVR**	**Male**	0.917	<0.001*	0.002*	0.001*	0.004*
		Female	0.043*	0.818	0.059	0.899	0.644
Control	**EACS**	**Male**	0.067	<0.001*	<0.001*	<0.001*	0.024*
		Female	0.062	<0.001*	0.772	<0.001*	0.004*
Control	**OCVR**	**Male**	0.011*	0.113	0.384	0.020*	0.015*
		Female	0.999	0.164	0.750	0.276	0.357

* = significant difference between treatment groups

Both the EACS and OCVR groups showed an increase of the CI from pre to post surgery. The CI in the reference groups was higher in both males and females compared to the surgery groups. The EACS patients showed an increase in the first months after surgery in both males and females, followed by a decline at around 9-12 months. OCVR patients have a constant post-surgery CI over time (around 69-71). The CIs of EACS patients showed a decline to approximately that of the OCVR CI values over time, which finally resulted in no significant differences between the EACS and OCVR groups.

Cranial width varied but had no clear pattern regarding the significant differences between the surgery groups themselves, and between the surgery groups and controls. The cranial length in the references remained shorter compared to the surgery groups over time. For males, a strong increase in the cranial length in OCVR was noted up to 24-months followed by a slower increase; EACS showed a steady increase until 36-48 months of age. The cranial length of both surgery groups got closer over time until no between-group significant differences existed.

The circumference of the EACS and OCVR groups were significantly larger than the references in the earlier post-surgery age groups, while becoming equal in the later age groups. Significant differences for the circumference between the surgery groups occurred at 15 and 36 months of age in the male population.

The volume differences between EACS, OCVR and the controls showed no clear pattern especially when considering male and female distributions.

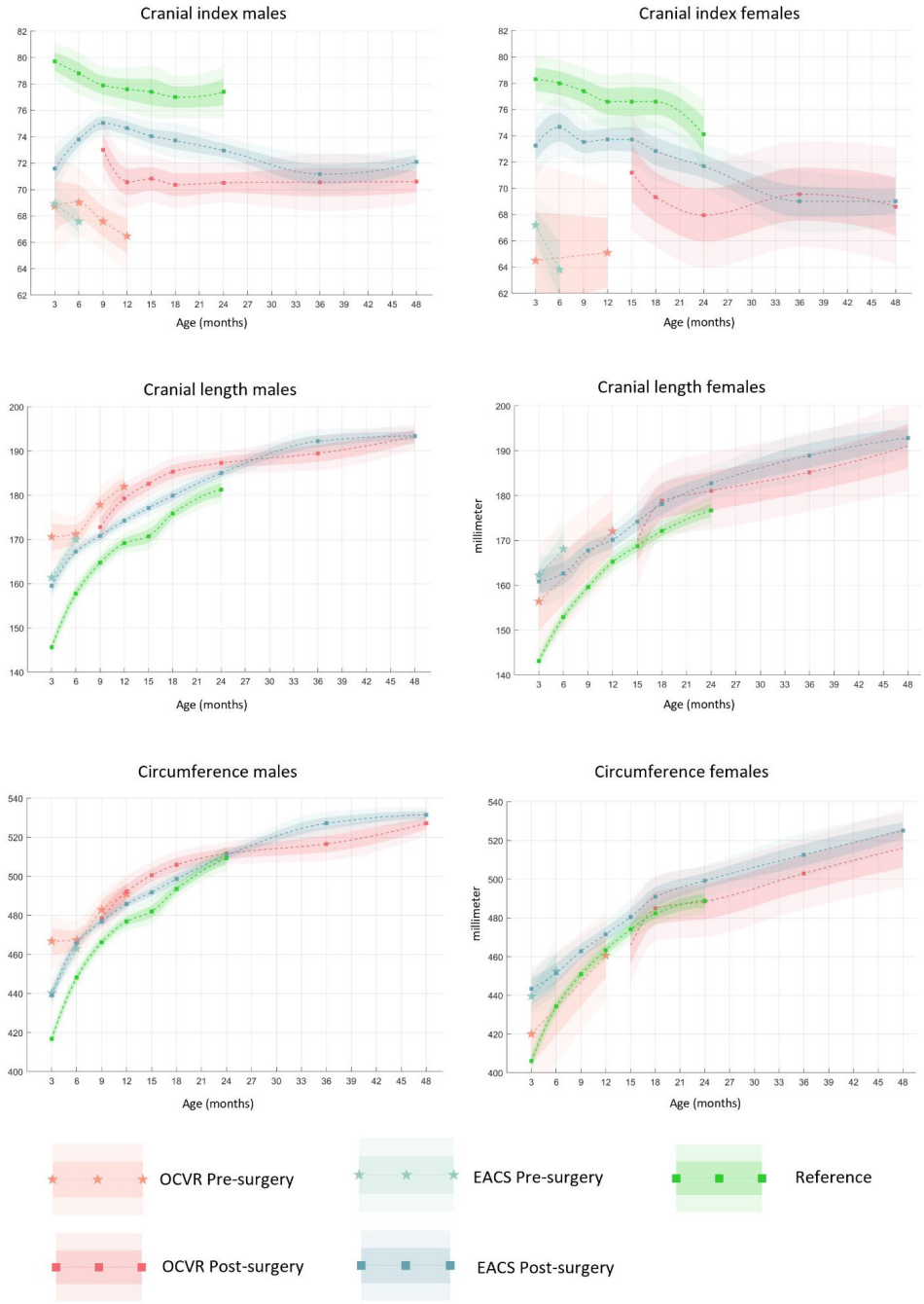

Figure 1: Graphs of the mean and standard error of mean of the cephalic index, cranial length and circumference after EACS and OCVR for scaphocephaly at given ages in months.

COLOR-CODED DISTANCE MAPS

The distance maps of EACS patients from pre to post surgery for age groups 1 (3 months) and 2 (6 months) are shown in [Figure 2]. A strong parietal growth of up to 10 mm was found in both groups. The frontal and occipital growth for the first age group were around 0 and 4 mm respectively. For the second age group, both frontal and occipital growth were approximately 0 mm.

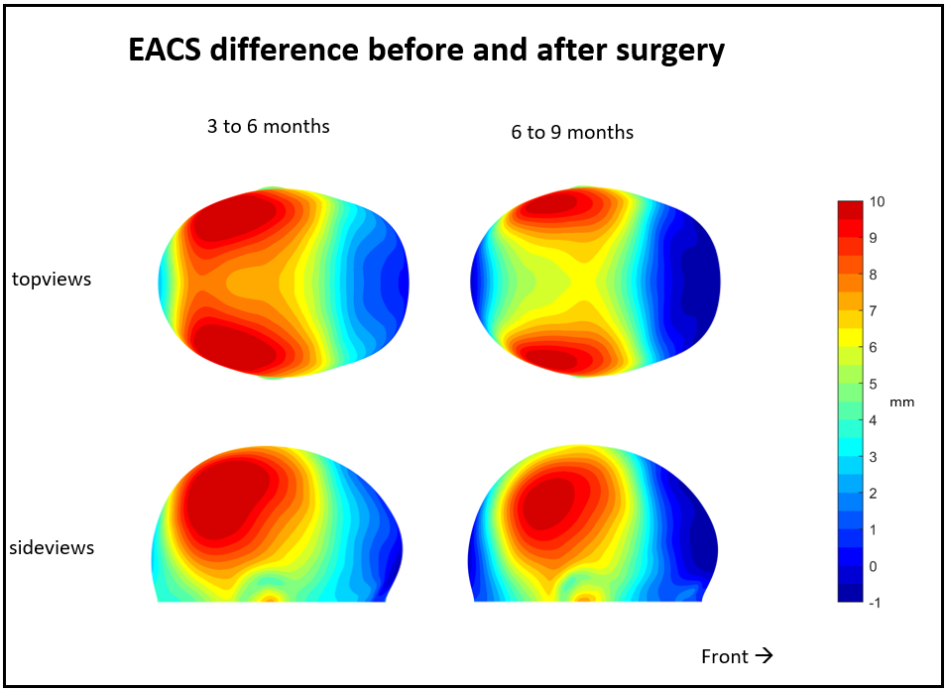

Figure 2: Distance maps indicating the mean head shape differences (in mm) from pre to post-EACS surgery for 3 - 6 months and 6 - 9 months of age. Note the color scaling (0.5 mm/ unique color).

The OCVR pre to post surgery distance maps are shown in [Figure 3]. Parietal changes up to 10 mm can be seen. In contrast to EACS, occipital growth up to 10 mm is present between 6 - 12 months; frontal changes remain limited in all age (OCVR) groups. More temporal widening can be observed compared to EACS patients.

Figure 3: Distance maps indicating the mean head shape differences (in mm) from pre to post-OCVR surgery for 3 - 6 months until 15 - 18 months of age. Note the color scaling (0.5 mm/ unique color).

The post-surgery follow-ups for EACS patients are shown in [Figure 4]. From 6 - 9 months of age, a prominent upper parietal growth of 5 mm is noted, with lower parietal growth around 3 mm. Frontal areas grow up to 4 mm. The frontotemporal region only shows 1-2 mm of growth. From 9 - 12 months, only 0-1 mm frontotemporal growth, up to 3 mm occipital growth and a midline growth up to approximately 2.5 mm was noted. Nearly identical growth is present between 9 - 18 months. However, growth at 18 months is more prominent around the occipital and frontal area (up to 5 mm). Between 18 - 24 months, only frontoparietal growth and some lower occipital growth up to 2.5 mm is present. Between 18 - 24 months, some frontotemporal growth (up to 3 mm) is dominant.

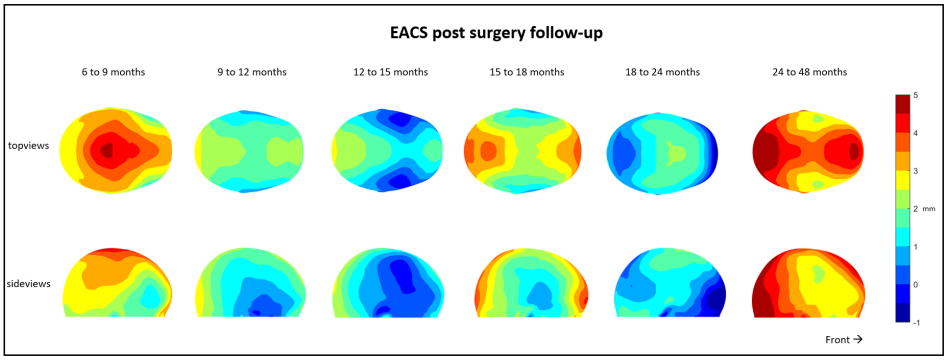

Figure 4: Distance maps indicating the mean head shape differences (in mm) post-EACS surgery for 3 - 6 months until 24 - 48 months of age. Note the color scaling (0.5 mm/ unique color).

The head shape comparisons at 24 months between EACS and OCVR are shown in [Figure 5]. The maximum differences are within the range -2 mm and +2 mm. Typically, OCVR treated patients have a more elongated head with a growth focus around the frontal and occipital areas, a somewhat narrow lower temporal region, and a wider lower parietal region. Furthermore, the vertex of the OCVR is slightly lower.

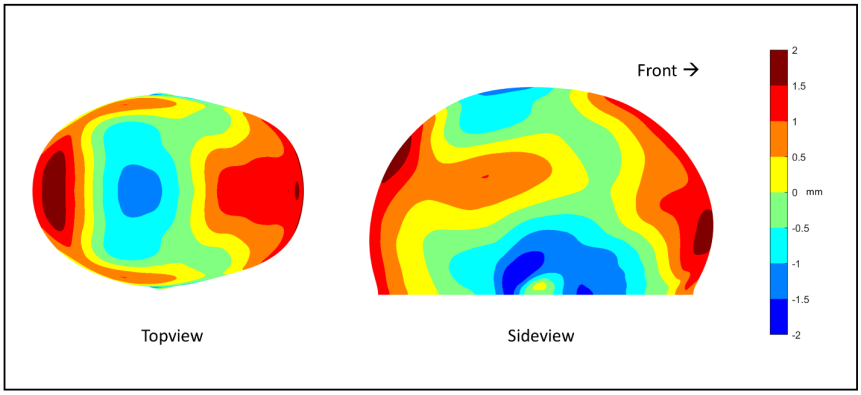

Figure 5: Distance maps indicating the mean head shape differences (in mm) between EACS and OCVR at 24 months of age (post-surgery). The length of the EACS is shorter while the vertex is higher. The EACS head shape is baseline. A positive value indicates that the OCVR head shape has localized additional volume over that of EACS. Note the color scaling (0.5 mm/ unique color).

DISCUSSION

SURGICAL SAFETY OUTCOMES

EACS performed equal or better than the OCVR in all aspects of the surgical safety outcomes. Only one EACS case was admitted to the ICU for a period of 3 days. This patient had additional non-craniosynostosis-related surgery within the same session which resulted in a complication requiring ICU admittance. This suggests that there were no EACS induced ICU admittances in contrast to 25 cases (61%) for OCVR. The mean age differences can be explained due to the preference of our institution to perform EACS in combination with helmet treatment in children under 6 months.

Surgery times are not always well defined in the literature as these can be reported with or without anesthesia time. Therefore, some of the reported values have to be interpreted with care. The statistically lower EACS surgery

time is comparable with earlier reports [19]–[23]; the overall surgery times for EACS and OCVR are in line with those in the literature [4], [19]–[28]. Anesthesia time only or surgery time including anesthesia is occasionally reported, but both are comparable with other endoscopic techniques for scaphocephaly correction [25] or when combining all strip craniectomy surgery types [28]. Shorter surgery and anesthesia times are factors noted in the literature that can contribute to reducing costs of EACS compared with OCVR [4], [28], [29].

Length of stay is also associated with higher costs [29]. Most studies describe a length of stay of 1-2 days for EACS patients which is in line with our study [19], [22], [26], [28], [30]. This is considering that in our institution patients are admitted one day prior to the surgery. The 3-6 days length of stay for OCVR patients included in this study is also comparable with literature [24], [26], [30].

The OCVR blood loss levels in our study seemed lower than reported in other studies [23], [24], [27], [30] whereas for EACS, the blood loss values are similar to earlier reporting [4], [12], [23], [30]. Overall blood loss was significantly lower in EACS group and was in the same range as reported values [4], [23], [26], [30]. Our OCVR patients were, on average, older than our EACS patients which resulted in a higher body mass and subsequently a higher circulation blood volume. Although body weight or circulation blood volume was not reported in this study, other studies have shown differences in these normalized values favoring EACS over OCVR regarding the amount of blood loss during surgery [22], [31].

Blood transfusions also add to general treatment cost [32]. In infants, it is preferable to minimize the number of blood transfusions as blood transfusion-related complications have a greater incidence [29]. At 18%, our post-surgery transfusion rates for EACS patients were slightly higher compared to those reported in other studies [4], [26], [30]. As blood loss volume was comparable to other studies, our higher transfusion rate may be explained by the fact that a blood transfusion was given more easily in earlier EACS procedures in our institution [12]. However, the transfusion rate in this study is currently lower compared to our earlier reports. The post-surgery transfusion rate was not significantly different between EACS and OCVR despite the two-fold differences (18% versus 37%). Regarding OCVR, the literature greatly varies with respect to peri or post-surgery transfusion rates, with reports of up to 100% [24], [29], [30].

3D MEASUREMENTS

The average number of 3D photos per patient was 3.8 and 3.2 in EACS and OCVR respectively. This is logical, given that follow-up is more frequent during helmet therapy in the first year.

Reports of true longitudinal follow-up after craniosynostosis surgery spanning over multiple years, especially regarding 2D & 3D measurements, are limited in the literature. This makes comparison with other studies less straightforward. Some studies report the 3D measurements using percentiles or Z-scores rather than e.g. millimeters or milliliter/cc [8], [10], [19], [28], [33]. Reporting of percentiles or Z-scores limits comparison with other studies due to the unavailability of the original or the reference group measurements.

The growth patterns of EACS were more deviant than those of OCVR as compared to the controls. OCVR aims for direct surgical reconstruction of the skull while EACS aims for a more natural growth after creating artificial sutures. However, in OCVR the natural sutures can be affected by the surgery itself limiting potential further natural growth. The differences in the surgical technique can explain the differences of the growth patterns over time.

Cranial width and length are only reported occasionally [34]. In our study, cranial width shows a strong increase post-surgery in especially EACS but lacks strong additional growth over time, suggesting an inability of the skull to expand laterally. A more common scaphocephaly measure is the CI. Pre-surgery studies report CI values in the range of 67-70 which is in line with our findings [22], [23]. Most of the post-surgery CI values for scaphocephaly correction remain around the 75-85 range which are higher than ours [8], [10], [19], [22], [23], [35], [36]. However, our results are more in line with earlier reports of the (Dutch) normal population [12], [37]. This may be due to a demographic difference in the patient population or to the measuring method [11], [37]. Therefore, using the same measuring methods and a representative control population is essential for objective and relevant research. Reference values for CI in similar populations using the same measuring technique still remain higher and significant at all times for both EACS and OCVR [15]. The trend of CI over time is in line with longitudinal studies [19], [23], [38]. Overall, CI in the EACS group remains higher than in the OCVR, and is significantly different for earlier age groups. For the later age groups, the effect diminishes in both males and females, with a CI near to 70.

The circumference directly after OCVR differs little from the pre-surgery situation [34]. The longitudinal circumference changes were in line with other reporting and did not differ between OCVR and EACS [8], [19].

Volume measurements differ per study due to the lack of consensus on volume measuring methods in craniosynostosis [39]. Interpretations of the volumes with regard to the measuring methods show similar volumes and changes for OCVR [40].

Early correction, as is the case in EACS, seems to be favorable for surgical safety outcomes. It is uncertain whether early correction with OCVR would yield similar results. To our best knowledge, no studies have been conducted specifically on the timing of EACS alone and their effect on 3D outcome measurements. Since untreated scaphocephaly leads to more extreme differences as compared to the references as caused by the compensatory growth [Figure 1, Table 8, Table 10] it might be possible that treating EACS patients as early as possible yields the best results.

DISTANCE MAPS

No post-surgery to post-surgery comparison for OCVR was done due to the limited number of 3D photos in the post-surgery OCVR group. Due to the number of 3D photos available for post-surgery EACS in group 8, the EACS group 7 was compared with EACS group 9 [Table 1].

In [Figure 2-Figure 4], an impressive increase in cranial growth can be seen in the distance maps. A clear increase of lateral expansion and vertex height can be noticed resulting in a proper lateral profile for both treatment options. In [Figure 5], the cranial length of the OCVR is greater compared to the EACS group. This can be explained by the fact that OCVR patients have more and longer compensatory growth in the anterior-posterior direction. The vertex height of the EACS group is slightly higher than that of the OCVR group and showed a natural and appealing spherical shape of the crania. This contrasts with Le et al. who reported that EACS results in a lower vertex height compared to OCVR [8]. Head height is occasionally reported as an outcome value or as a measure to compute an outcome value and could have been a valuable additional 3D measurement [8], [11], [13], [33]. Especially because this could be used for the comparison of other minimal invasive surgical techniques such as spring-mediated cranioplasties.

It is interesting (and promising) that the mean head shapes at 24-months were similar between OCVR and EACS [Figure 5]. This suggests only marginal differences between EACS and OCVR over time at that age.

During the first months after EACS, the majority effect of the growth appears to expand and enlarge the skull [Figure 2 & Figure 4]. After the first 3-6 months post-surgery, this expansion is mainly found in the head widening limits. However, the helmet therapy usually lasts until around 9 months after surgery. Based on our data, we are unsure whether the helmet therapy still benefits the surgical outcomes after this 3-6 month period. Yet, helmet therapy seems to benefit the CI positively, regardless of being implemented before or without surgery, although it raises concerns regarding intracranial pressure [36], [41]–[43]. The increase in head length growth around 15-18 months of age coincides more or less with end of helmet therapy, considering that helmets are worn for an average of 9.6 months. This may suggest that stopping of the helmet therapy gives rise to a relapse of increased head length growth. However, an increase of head length around 15-18 months was found in the reference group as well which suggest that, instead of having a relapse, patients may rather shift towards a normal and healthy cranial growth pattern after EACS and helmet therapy [15]. It would be very interesting to see whether other groups could confirm these findings, as this might suggest that early re-opening of a fused suture could invoke restoration of the normal growth pattern of the skull.

LIMITATIONS

The collection of 3D photos is dependent on the follow-up appointments in our institution. Due to logistic reasons not all follow-up moments allow the capture of a 3D photo, resulting in non-continuous follow-up. Furthermore, 3D photos can sometimes be unusable due to technological or patient-specific reasons, thus limiting the number of 3D photos. More consistent 3D photo captures would result in better analysis of 3D measurements and growth maps.

The patients surgical safety outcomes and the patients for the 3D photos had a largely overlapping population but held some differences. Due to the scope of the project these populations were not linked. It is recommended to have fully matched populations if the surgical outcomes need to be directly linked to e.g. the 3D measurements or growth distance maps.

The 3D photos of the reference group were only for infants aged up to 24-months, making direct comparison with the final age group difficult. Moreover, the reference groups were approximately 50% male and female, while the scaphocephaly groups were approximately 80% male, also limiting comparison.

The 3D photo growth maps had combined genders due to the amount of data. Separating the data would result in unrealistic representations of the growth maps. The higher dimensionality and use techniques of mixed models allowed gender separation for the 3D measurement outcomes. However, these techniques cannot be used for the entire growth maps. The mixed genders therefore make comparison with growth maps from earlier studies impossible.

There is a certain bias towards EACS due to our institution's policy. Patients that are older than 6 months are no longer eligible for EACS and subsequently will always receive OCVR in our institution. This has resulted in limited data for OCVR cases; we were therefore unable to create the longitudinal growth maps of OCVR cases. Some of the OCVR patients that were younger than 6 months of age had a more limited degree of reconstruction, yet more invasive than EACS, to reduce the risk and potential complications. Due to the variations in the degree of reconstruction for this subgroup of patients (n=5) we did not differentiate these in our analysis.

The CCFP-offset values were chosen based on the availability of the CT-data they were derived from. This resulted in choices for interpolation and reference values. As our follow-up protocol does not include a post-surgery CT-scan, there is no certainty if these CCFP-values are the best possible values despite CCFP robustness [16], [18].

CONCLUSION

The primary goal of our study was to evaluate the cranial shape development of scaphocephaly patients using objective 3D analysis methods. Looking at the 3D measurements and growth maps of OCVR and EACS, we see differences between the two treatments, but they diminish over time. This is also true when comparing the reference 3D measurements, with the exception of the CI; the EACS and OCVR growth maps show only a 2 mm difference at most, making the resulting cranial shapes of both treatments comparable. EACS treated patients tend to have a less elongated and a higher, more spherical shaped head compared to OCVR treated patients.

Secondly, we evaluated the surgical safety outcomes of these patients to determine whether our treatment was comparable to those described by others. Regarding surgery time, total anesthesia time, length of stay, blood loss, and blood transfusions, EACS is significantly better compared to OCVR. The absolute surgical outcomes were nearly all comparable with earlier reported literature values. Considering the effects of surgery times, length of stay, blood loss, and blood transfusions on the clinical care and associated costs, EACS is the preferred treatment option if applicable.

Given the near identical results in the 3D measurements and distance maps between OCVR and EACS combined with the superior EACS surgical safety outcomes, we conclude that EACS before the age of 6 months is the preferred treatment option for scaphocephaly. We therefore recommend early diagnostics and referral for suspected craniosynostosis.

REFERENCES

[1] Y. Heuzé *et al.*, "New insights into the relationship between suture closure and craniofacial dysmorphology in sagittal nonsyndromic craniosynostosis," *J. Anat.*, vol. 217, no. 2, pp. 85–96, Jun. 2010, doi: 10.1111/j.1469-7580.2010.01258.x.

[2] A. V Ciurea, C. Toader, and C. Mihalache, "Actual concepts in scaphocephaly : (an experience of 98 cases).," *J. Med. Life*, vol. 4, no. 4, pp. 424–31, Nov. 2011.

[3] Nederlandse Vereniging van Plastische Chirurgie, "Richtlijn Behandeling en zorg voor craniosynostose," 2010.

[4] C. C. Cartwright, D. F. Jimenez, C. M. Barone, and L. Baker, *Endoscopic strip craniectomy: a minimally invasive treatment for early correction of craniosynostosis.*, vol. 35, no. 3. 2003, pp. 130–138.

[5] M. . Cornelissen *et al.*, "Increase of prevalence of craniosynostosis," *J Craniomaxillofac Surg*, vol. 44, no. 9, pp. 1273–1279, 2016, doi: 10.1016/j.jcms.2016.07.007.

[6] H. Q. Lee *et al.*, "Changing epidemiology of nonsyndromic craniosynostosis and revisiting the risk," *J. Craniofac. Surg.*, vol. 23, no. 5, pp. 1245–1251, 2012, doi: 10.1097/SCS.0b013e318252d893.

[7] G. D. Doumit, F. A. Papay, N. Moores, and J. E. Zins, "Management of sagittal synostosis: a solution to equipoise.," *J. Craniofac. Surg.*, vol. 25, no. 4, pp. 1260–5, Jul. 2014, doi: 10.1097/SCS.0b013e3182a24635.

[8] M.-B. Le *et al.*, "Assessing long-term outcomes of open and endoscopic sagittal synostosis reconstruction using three-dimensional photography.," *J. Craniofac. Surg.*, vol. 25, no. 2, pp. 573–6, 2014, doi: 10.1097/SCS.0000000000000613.

[9] B. S. Lee *et al.*, "Management options of non-syndromic sagittal craniosynostosis," *J. Clin. Neurosci.*, vol. 39, pp. 28–34, May 2017, doi: 10.1016/J.JOCN.2017.02.042.

[10] D. F. Jimenez, C. M. Barone, M. E. McGee, C. C. Cartwright, and C. L. Baker, "Endoscopy-assisted wide-vertex craniectomy, barrel stave osteotomies, and postoperative helmet molding therapy in the management of sagittal suture craniosynostosis," *J. Neurosurg. Pediatr.*, vol. 100, no. 5, pp. 407–417, May 2004, doi: 10.3171/ped.2004.100.5.0407.

[11] L. A. Dvoracek *et al.*, "Comparison of traditional versus normative cephalic index in patients with sagittal synostosis: Measure of scaphocephaly and postoperative outcome," *Plast. Reconstr. Surg.*, vol. 136, no. 3, pp. 541–548, Sep. 2015, doi: 10.1097/PRS.0000000000001505.

[12] H. H. K. Delye *et al.*, "Endoscopically assisted craniosynostosis surgery (EACS): The craniofacial team Nijmegen experience," *J. Cranio-Maxillofacial Surg.*, vol. 44, no. 8, pp. 1029–1036, Aug. 2016, doi: 10.1016/j.jcms.2016.05.014.

[13] J. Marcus and T. Stokes, "Quantitative and qualitative assessment of morphology in sagittal synostosis: mid-sagittal vector analysis," *J. Craniofacial …*, vol. 17, no. 4, pp. 680–6, Jul. 2006, Accessed: Jul. 23, 2014. [Online]. Available: http://www.ncbi.nlm.nih.gov/pubmed/16877914.

[14] H. Delye, T. Clijmans, M. Y. Mommaerts, J. Vander Sloten, and J. Goffin, "Creating a normative database of age-specific 3D geometrical data, bone density, and bone thickness of the developing skull: a pilot study," *J. Neurosurg. Pediatr.*, vol. 16, no. 6, pp. 687–702, Dec. 2015, doi: 10.3171/2015.4.PEDS1493.

[15] J. W. Meulstee, G. A. de Jong, W. A. Borstlap, G. Koerts, T. J. J. Maal, and H. Delye, "The normal evolution of the cranium in three dimensions," *Int. J. Oral Maxillofac. Surg.*, Nov. 2019, doi: 10.1016/j.ijom.2019.10.012.

[16] G. de Jong *et al.*, "Radiation-free 3D head shape and volume evaluation after endoscopically assisted strip craniectomy followed by helmet therapy for trigonocephaly," *J. Cranio-Maxillofacial Surg.*, vol. 45, no. 5, pp. 661–671, May 2017, doi: 10.1016/j.jcms.2017.02.007.

[17] J. W. Meulstee *et al.*, "A new method for three-dimensional evaluation of the cranial shape and the automatic identification of craniosynostosis using 3D stereophotogrammetry," *Int. J. Oral Maxillofac. Surg.*, vol. 46, no. 7, pp. 819–826, Jul. 2017, doi: 10.1016/j.ijom.2017.03.017.

[18] G. A. de Jong, T. J. J. Maal, and H. Delye, "The computed cranial focal point," *J. Cranio-Maxillofacial Surg.*, vol. 43, no. 9, pp. 1737–1742, Nov. 2015, doi: 10.1016/j.jcms.2015.08.023.

[19] E. B. Ridgway, J. Berry-Candelario, R. T. Grondin, G. F. Rogers, and M. R. Proctor, "The management of sagittal synostosis using endoscopic suturectomy and postoperative helmet therapy," *J. Neurosurg. Pediatr.*, vol. 7, no. 6, pp. 620–626, 2011, doi: 10.3171/2011.3.peds10418.

[20] D. F. Jimenez and C. M. Barone, "Endoscopic craniectomy for early surgical correction of sagittal craniosynostosis.," *Journal of neurosurgery*, vol. 88, no. 1. pp. 77–81, 1998, doi: 10.3171/jns.1998.88.1.0077.

[21] C. M. Barone and D. F. Jimenez, "Endoscopic craniectomy for early correction of craniosynostosis.," *Plast. Reconstr. Surg.*, vol. 104, no. 7, pp. 1965–73; discussion 1974-5, 1999, doi: 10.3171/jns.1998.88.1.0077.

[22] M. N. N. Shah, A. A. A. Kane, J. D. D. Petersen, A. S. S. Woo, S. D. D. Naidoo, and M. D. D. Smyth, "Endoscopically assisted versus open repair of sagittal craniosynostosis: The St. Louis Children's Hospital experience - Clinical article," *J. Neurosurg. Pediatr.*, vol. 8, no. 2, pp. 165–170, 2011, doi: 10.3171/2011.5.PEDS1128.

[23] P. A. Gerety, M. N. Basta, J. P. Fischer, and J. A. Taylor, "Operative management of nonsyndromic sagittal synostosis: A head-to-head meta-analysis of outcomes comparing 3 techniques," *J. Craniofac. Surg.*, vol. 26, no. 4, pp. 1251–1257, 2015, doi: 10.1097/SCS.0000000000001651.

[24] R. Toma *et al.*, "Quantitative morphometric outcomes following the Melbourne method of total vault remodeling for scaphocephaly.," *J. Craniofac. Surg.*, vol. 21, no. 3, pp. 637–43, May 2010, doi: 10.1097/SCS.0b013e3181d841d9.

[25] L. R. David, P. Proffer, W. J. Hurst, S. Glazier, and L. C. Argenta, "Spring-mediated cranial reshaping for craniosynostosis," *J. Craniofac. Surg.*, vol. 15, no. 5, p. 370, 2004, doi: 10.1097/00001665-200409000-00021.

[26] D. F. Jimenez, C. M. Barone, C. C. Cartwright, and L. Baker, "Early management of craniosynostosis using endoscopic-assisted strip craniectomies and cranial orthotic molding therapy.," *Pediatrics*, vol. 110, no. 1 Pt 1, pp. 97–104, 2002, doi: 10.1542/peds.110.1.97.

[27] G. M. Zakhary, D. M. Montes, J. E. Woerner, C. Notarianni, and G. E. Ghali, "Surgical correction of craniosynostosis. A review of 100 cases," *J. Cranio-Maxillofacial Surg.*, vol. 42, no. 8, pp. 1684–1691, 2014, doi: 10.1016/j.jcms.2014.05.014.

[28] C. P. P. Riordan *et al.*, "Minimally Invasive Endoscopic Surgery for Infantile Craniosynostosis: A Longitudinal Cohort Study," *J. Pediatr.*, vol. 216, pp. 142-149.e2, 2020, doi: 10.1016/j.jpeds.2019.09.037.

[29] H. Yan *et al.*, "A systematic review and meta-analysis of endoscopic versus open treatment of craniosynostosis. Part 1: The sagittal suture," *J. Neurosurg. Pediatr.*, vol. 22, no. 4, pp. 352–360, 2018, doi: 10.3171/2018.4.PEDS17729.

[30] A. Goyal, V. M. Lu, Y. U. Yolcu, M. Elminawy, and D. J. Daniels, "Endoscopic versus open approach in craniosynostosis repair: a systematic review and meta-analysis of perioperative outcomes," *Child's Nerv. Syst.*, vol. 34, no. 9, pp. 1627–1637, 2018, doi: 10.1007/s00381-018-3852-4.

[31] M. M. Abbott, G. F. Rogers, M. R. Proctor, K. Busa, and J. G. Meara, "Cost of treating sagittal synostosis in the first year of life," *J. Craniofac. Surg.*, vol. 23, no. 1, pp. 88–93, 2012, doi: 10.1097/SCS.0b013e318240f965.

[32] I. Abraham and D. Sun, "The cost of blood transfusion in Western Europe as estimated from six studies," *Transfusion*, vol. 52, no. 9, pp. 1983–1988, 2012, doi: 10.1111/j.1537-2995.2011.03532.x.

[33] J. A. Fearon, E. B. McLaughlin, and J. C. Kolar, "Sagittal craniosynostosis: Surgical outcomes and long-term growth," *Plast. Reconstr. Surg.*, vol. 117, no. 2, pp. 532–541, 2006, doi: 10.1097/01.prs.0000200774.31311.09.

[34] C. Linz *et al.*, "3D stereophotogrammetric analysis of operative effects after broad median craniectomy in premature sagittal craniosynostosis," *Child's Nerv. Syst.*, vol. 30, no. 2, pp. 313–318, 2014, doi: 10.1007/s00381-013-2253-y.

[35] M. R. Proctor, "Endoscopic craniosynostosis repair," *Transl. Pediatr.*, vol. 3, no. 3, pp. 247–258, 2014, doi: 10.3978/j.issn.2224-4336.2014.07.03.

[36] A. Hashmi, N. I. Marupudi, S. Sood, and A. Rozzelle, "Effect of Preoperative Molding Helmet in Patients with Sagittal Synostosis," *J. Craniofac. Surg.*, vol. 28, no. 4, pp. 898–903, 2017, doi: 10.1097/SCS.0000000000003512.

[37] E. J. van Lindert *et al.*, "Validation of cephalic index measurements in scaphocephaly," *Child's Nerv. Syst.*, vol. 29, no. 6, pp. 1007–1014, Jun. 2013, doi: 10.1007/s00381-013-2059-y.

[38] D. Agrawal, P. Steinbok, and D. D. Cochrane, "Long-term anthropometric outcomes following surgery for isolated sagittal craniosynostosis.," *J. Neurosurg.*, vol. 105, no. 5 Suppl, pp. 357–60, 2006, doi: 10.3171/ped.2006.105.5.357.

[39] R. Seeberger *et al.*, "Intracranial volume (ICV) in isolated sagittal craniosynostosis measured by 3D photocephalometry: A new perspective on a controversial issue," *J. Cranio-Maxillofacial Surg.*, vol. 44, no. 5, pp. 626–631, 2016, doi: 10.1016/j.jcms.2016.01.023.

[40] M.-L. C. van Veelen *et al.*, "Volume measurements on three-dimensional photogrammetry after extended strip versus total cranial remodeling for sagittal synostosis: A comparative cohort study," *J. Cranio-Maxillofacial Surg.*, vol. 44, no. 10, pp. 1713–1718, Oct. 2016, doi: 10.1016/j.jcms.2016.07.029.

[41] N. Pediatr, "Neurosurgical forum Helmets and synostosis," *J Neurosurg Pediatr.*, vol. 9, no. June, pp. 680–682, 2012.

[42] N. I. Marupudi, S. Sood, A. Rozzelle, and S. D. Ham, "Effect of molding helmets on intracranial pressure and head shape in nonsurgically treated sagittal craniosynostosis patients," *J. Neurosurg. Pediatr.*, vol. 18, no. 2, pp. 207–212, 2016, doi: 10.3171/2016.1.peds15569.

[43] S. Sood, A. Rozzelle, B. Shaqiri, N. Sood, and S. D. Ham, "Effect of molding helmet on head shape in nonsurgically treated sagittal craniosynostosis.," *J. Neurosurg. Pediatr.*, vol. 7, no. 6, pp. 627–32, Jun. 2011, doi: 10.3171/2011.4.PEDS116.

Chapter 7

Combining deep learning with 3D stereophotogrammetry for craniosynostosis diagnosis

G. de Jong, E. Bijlsma, J. Meulstee, M. Wennen, E. van Lindert, T. Maal, R. Aquarius, H. Delye

Adapted from: G. de Jong et al., "Combining deep learning with 3D stereophotogrammetry for craniosynostosis diagnosis," Sci. Rep., vol. 10, no. 1, p. 15346, Sep. 2020, doi: 10.1038/s41598-020-72143-y.

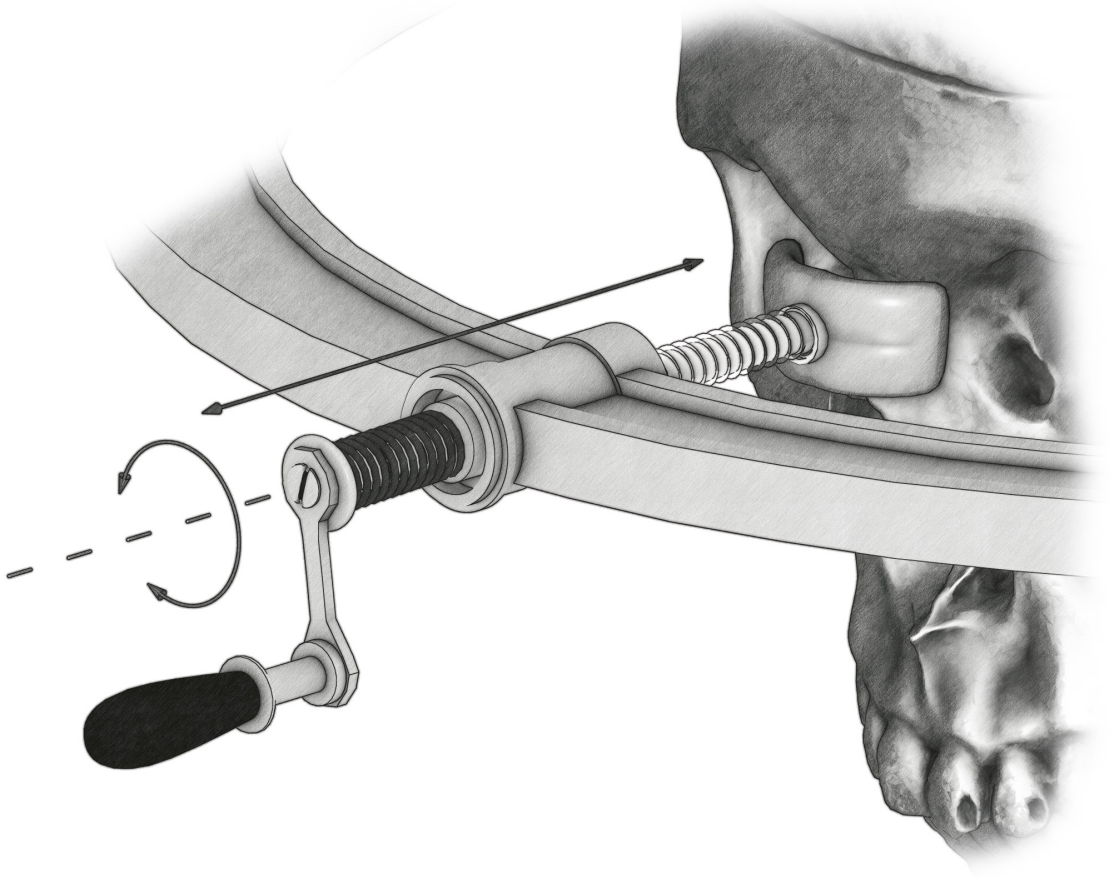

ABSTRACT

Background: Craniosynostosis is a condition in which cranial sutures fuse prematurely, causing problems in normal brain and skull growth in infants. To limit the extent of cosmetic and functional problems, swift diagnosis is needed. The goal of this study is to investigate if a deep learning algorithm is capable of correctly classifying the head shape of infants as either healthy controls, or as one of the following three craniosynostosis subtypes; scaphocephaly, trigonocephaly or anterior plagiocephaly.

Methods: In order to acquire cranial shape data, 3D stereophotographs were made during routine pre-operative appointments of scaphocephaly (n=76), trigonocephaly (n=40) and anterior plagiocephaly (n=27) patients. 3D Stereophotographs of healthy infants (n=53) were made between the age of 3-6 months. The cranial shape data was sampled and a deep learning network was used to classify the cranial shape data as either: healthy control, scaphocephaly patient, trigonocephaly patient or anterior plagiocephaly patient. For the training and testing of the deep learning network, a stratified 10-fold cross validation was used.

Results: During testing 195 out of 196 3D stereophotographs (99,5%) were correctly classified. **Conclusion:** This study shows that trained deep learning algorithms, based on 3D stereophotographs, can discriminate between craniosynostosis subtypes and healthy controls with high accuracy.

INTRODUCTION

Craniosynostosis is defined as the premature fusion of one or more cranial sutures. This results in cranial malformation and can lead to facial asymmetry, as well as functional consequences such as increased intracranial pressure, deafness, visual impairment and cognitive deficits [1], [2]. The prevalence of isolated, non-syndromic craniosynostosis is 3.14 to 6 per 10.000 live births [3], [4]. The three most common forms of isolated, non-syndromic craniosynostosis are scaphocephaly, trigonocephaly and anterior plagiocephaly which correspond to the premature fusion of the sagittal suture, the metopic suture, and a unilateral coronal suture, respectively [3], [5]–[7].

Early diagnosis and intervention is important as it often leads to more therapeutic options for surgeons and the best cosmetic results for patients[1], [2]. Currently, computed tomography (CT) is the primary image technique used in craniosynostosis diagnosis [8], [9]. CT is proven to be an accurate diagnostic tool in craniosynostosis, but exposes the infant to ionizing radiation, which can pose a health risk for radiation induced cancer [9]–[11]. Therefore a safer alternative diagnostic tool is needed.

Experts within tertiary healthcare centers can diagnose craniosynostosis quite accurately by visual examination of the shape of the head [8]. However, in the primary and secondary healthcare sectors, misdiagnosis of craniosynostosis still occurs due to the lack of expertise [12]. It therefore makes sense to study the potential of an imaging technique based on visual information: 3D stereophotogrammetry of the cranium. 3D stereophotogrammetry is a fast, radiation-free and patient-friendly method to evaluate the 3D morphology of the cranial shape [13]. 3D stereophotogrammetry has previously been used in combination with principal component analysis, a common machine learning technique, to characterize relevant aspects of the cranial shapes of trigonocephaly patients, scaphocephaly patients and healthy infants (controls) [14]. However, this technique cannot automatically classify these cranial shapes as scaphocephaly, trigonocephaly, anterior plagiocephaly or as a healthy child, which makes it irrelevant for clinical implementation.

To overcome this limitation, we suggest combining 3D stereophotogrammetry with the more modern machine learning technique ‘deep learning’. This facilitates direct classification of cranial shapes and makes clinical implementation more feasible. Deep learning has shown promising results

in various fields of research, including medical image analysis [15]–[18]. Some benefits of deep learning prediction models are the possibility to evaluate complex patterns as well as non-linear patterns in data sets, effectively increasing the learning and classifying capacity of the model.

The goal of this study is to investigate if deep learning algorithms are capable to correctly classify the head shape of infants on 3D stereophotographs as healthy control or as a craniosynostosis patient with the accompanying subtype; scaphocephaly, trigonocephaly or anterior plagiocephaly.

MATERIALS AND METHODS

DATA ACQUISITION

A total of 160 CT-confirmed craniosynostosis patients and 53 healthy controls were retrospectively collected for this study. Healthy infants (controls) were selected based on their age (3 to 6 months old), which was similar to the age-range of the craniosynostosis patients. Some of the healthy controls have been previously included in a study for determining the normal evolution of the cranium in three dimensions [19]. 3D Stereophotogrammetry (3dMDCranial 3DMD, Atlanta, USA) with a five-pod configuration was used for image acquisition. 3D Stereophotographs were acquired by trained 3D photographers.

All craniosynostosis patients selected for this study were treated in the Radboudumc between July 2009 and September 2019 and diagnosed with isolated, non-syndromic premature closure of sutures, which was confirmed by CT as part of standard treatment protocol. Inclusion of patients was based on the availability of clinical pre-surgery 3D stereophotographs. We excluded 10 scaphocephaly, 4 trigonocephaly and 3 plagiocephaly patients due to the absence of a pre-surgery 3D stereophotograph or the presence of unremovable or unfixable imaging artefacts on the 3D stereophotograph. Unfixable imaging artefacts included the loss of anatomical landmarks or a large portion of the cranium. This resulted in the following craniosynostosis subtypes distribution in the included patients: scaphocephaly (n=76), trigonocephaly (n=40) and anterior plagiocephaly (n=27). One 3D stereophotograph per patient or healthy reference was included.

The mean age and the standard deviation were computed for each group. A One-way ANOVA was performed to determine statistical significant differences

between the mean ages of each group. A Levene's test for homogeneity of variances was conducted. Finally a Dunnett T3 post-hoc test was performed to determine which groups were statistical significant different. Statistically significant differences were assumed at $p<0.05$. All statistical data analyses were performed using SPSS version 25.0 (Armonk, NY: IBM Corp, 2017).

All research was performed in accordance with relevant guidelines and regulations. This study did not fall within the remit of the Medical Research Involving Human Subjects Act (WMO). This study was approved by the medical ethical review board of the Radboud University Medical Centre Nijmegen, The Netherlands (no. 2020-6128). The study has been reviewed by the ethics committee (Commissie Mensgebonden Onderzoek regio Arnhem – Nijmegen, Netherlands) on the basis of the Dutch Code of conduct for health research, the Dutch Code of conduct for responsible use, the Dutch Personal Data Protection Act and the Medical Treatment Agreement Act. Informed consent was waived by this same ethics committee (Commissie Mensgebonden Onderzoek regio Arnhem – Nijmegen, Netherlands). Furthermore, the 3D stereophotographs of the 53 healthy controls were collected as part of an ongoing program to form a large reference cohort for future studies and was approved by the medical ethical review board of the Radboud University Medical Centre Nijmegen, The Netherlands (no. 2018-4935).

DATA SAMPLING

Prior to data sampling, each 3D stereophotograph was manually positioned in the sella turcica-nasion orientation using the age specific computed cranial focal point [5], [20]. Subsequently, data sampling was performed to ensure a standardized representation of each 3D stereophotograph. We used a raycasting algorithm for each 3D stereophotograph, utilizing a reference hemi-icosphere (r = 1mm) consisting of 751 vertices. The center of the hemi-icosphere was placed on the location of the computed sella turcica and each ray was cast outward in the direction of each of the 751 vertices until the intersection with the 3D stereophotograph was reached [Figure 1]. The 751 vertices were the result of an optimization in which the raycasting algorithm was able to accurately capture the shape of the head while minimizing the amount of potential of overfitting features. Each raycast length, from the sella turcica to the intersection with the 3D stereophotograph, was stored for deep learning.

Because specific asymmetries in the collected cranial shapes can exist and can lead to potential underperformance of the deep learning model due to overfitting, data augmentation steps were used. A commonly used data augmentation step is image mirroring [21]. We mirrored each 3D stereophotograph over the mid-sagittal axis. Both the regular and the mirrored datasets were combined for deep learning model creation. Finally, for each ray the mean and standard deviation was computed over all the subjects. Each ray was then standardized by subtracting the per-ray mean and scaling using the per-ray unit variance [22]. This feature scaling technique was applied to correct for size differences and to amplify features of all subjects.

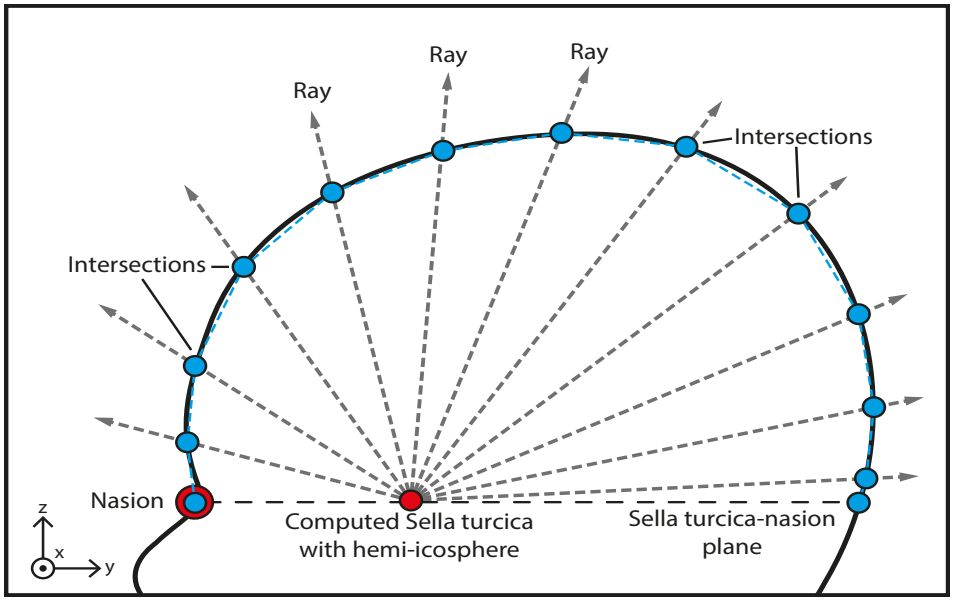

Figure 1: 2D schematic representation of the head shape raycasting technique using a hemi-icosphere to determine the ray length from the sella turcica to the intersection of the outer surface of the 3D stereophotograph of the head.

DEEP LEARNING

We used a deep learning network with a categorical outcome, which classified the data of each subject as one of the following: healthy, scaphocephaly, trigonocephaly, anterior plagiocephaly. The used network was a conventional, feed-forward neural network holding respectively 192, 128, 64 and 32 nodes within the hidden layers. Activations within the hidden layers consisted of the Leaky Rectified Linear unit (Leaky ReLu), a variation on the Rectified Linear

unit (ReLu) [23], with an alpha of 0.2. The used regularization techniques were dropout [24] (rate = 0.5), batch normalization [25] (momentum = 0.8) and added gaussian noise (std=0.5) on the input during training. The output layer had a softmax activation function with 4 nodes for healthy, scaphocephaly, trigonocephaly and anterior plagiocephaly. Training was performed using the Adam optimizer [26] with a learning rate of $1*10^{-3}$, a decay of $1*10^{-6}$ and a clip/gradient normalization of 0.001. Batch sizes during training consisted of 256 samples and training was performed for up to 1000 epochs. The categorical cross entropy is evaluated for the validation set and used as a stopping criterium. If no improvement of the validation categorical cross entropy was found for 50 epochs training was halted.

For the training and testing of the deep learning network, a stratified 10-fold cross validation was used. A subject's original 3D stereophotograph and its mirrored counterpart stayed linked throughout training and testing of the deep learning network [Figure 2]. This ensures that one subject is only present in either the training or test dataset to preventing cross-over and misleading outcomes of the deep learning model.

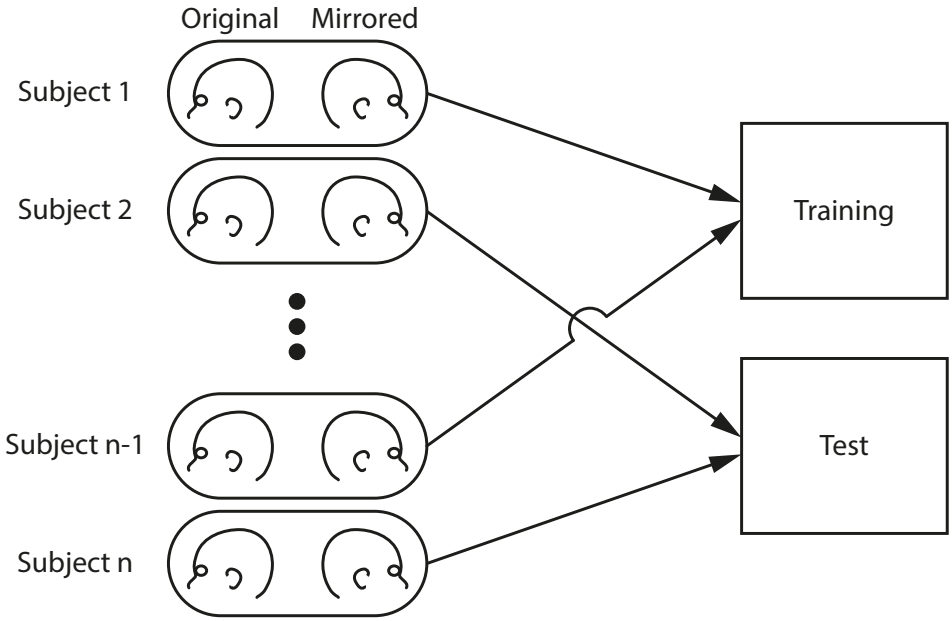

Figure 2: A subject's original 3D stereophotograph and its mirrored counterpart stay linked throughout training and testing of the deep learning network to prevent cross-over.

The outcome of the deep learning network was a confusion matrix of the test dataset. Furthermore, the recall and sensitivity (true positive / (true positive + false negative)), precision (true positive / (true positive + false positive)) and specificity (true negative / (true negative + false positive) were computed based on the confusion matrix.

The software used for the deep learning network creation was Keras [27] with the Tensorflow [28] backend. The software used for statistical analysis of the deep learning results and preprocessing of the data was Scikit-learn [29].

RESULTS

The mean age at the acquisition of the 3D stereophotograph of the subjects was 5.1 months (SD: 3.0), 4.0 months (SD: 1.5), 6.9 months (SD: 4.7) and 4.6 months (SD: 1.6) for scaphocephaly patients, trigonocephaly patients, anterior plagiocephaly patients and healthy controls, respectively. There was a statistically significant difference between the group means as determined by one-way ANOVA($F(3,192) = 6.315$, $p<0.001$) Equal variances were not assumed based upon the Levene's Test ($p<0.001$). The Dunnett T3 post-hoc test showed a statistically significant difference between the mean ages of the trigonocephaly and plagiocephaly patients ($p=0.027$). The differences between the mean ages of the trigonocephaly and scaphocephaly patients approached but did not reach statistical significant differences ($p=0.051$).

DEEP LEARNING NETWORK

Out of 196 patients and healthy controls, 195 subjects (99,5%) were correctly classified. One anterior plagiocephaly patient was classified as a healthy control [Table 1]. Sensitivity and specificity was 100% in all cases except for plagiocephaly which had a sensitivity of 96.3% and the healthy cases which had a specificity of 99.2%.

Table 1 The confusion matrix of the test set with computed recall/sensitivity, precision and specificity.

		Predicted				
		Scaphocephaly	**Trigonocephaly**	**Anterior Plagiocephaly**	**Healthy**	**Sensitivity/ Recall**
Actual	**Scaphocephaly**	**76**	0	0	0	100,0%
	Trigonocephaly	0	**40**	0	0	100,0%
	Anterior Plagiocephaly	0	0	**26**	1	96,3%
	Healthy	0	0	0	**53**	100,0%
	Precision	100,0%	100,0%	100,0%	98,1%	
	Specificity	100,0%	100,0%	100,0%	99,2%	

DISCUSSION

In this study, we demonstrate that 3D stereophotogrammetry combined with deep learning can provide a basis to accurately classify cranial shapes of healthy controls, scaphocephaly patients, trigonocephaly patients and anterior plagiocephaly patients.

Our study is in line with results from a previous study, in which 3D stereophotographs were used to distinguish healthy subjects from subjects with scaphocephaly and trigonocephaly [14]. Both our study and the study of Meulstee et al. underline the feasibility of diagnosing craniosynostosis using 3D stereophotogrammetry, a non-invasive technique without the risk of exposing the patient to ionizing radiation. Other machine learning techniques have also shown the potential in the classification of (parts of) craniosynostosis on 3D stereophotographs with additional statistical analysis or preprocessing [30]–[32].

Although the overall performance of the models presented in this study is good, there was one discrepancy between the prediction and the actual diagnosis. In the test dataset, one anterior plagiocephaly patient was classified as a healthy control. Anterior plagiocephaly cases were the least abundant within our dataset (n=27), which means that the deep learning network had only a limited opportunity to learn the key features in the cranial shape associated with this craniosynostosis subtype. Furthermore, one of our experts reviewed the case and classified it as mild anterior plagiocephaly.

Deep learning algorithms tend to perform better when large datasets are used during training [17]. However, due to the low prevalence of isolated, non-syndromic craniosynostosis (3.14 to 6 per 10.000 live births) [3], [4], it is difficult to obtain large datasets for each craniosynostosis subtype. Smaller datasets can lead to suboptimal results because of overfitting, a process in which a network learns to recognize certain aspects specific to only the training cases, which negatively impacts the ability of the model to accurately classify new cases.

Several techniques have been used in this study to minimize the effect of overfitting. First, all 3D stereophotographs were sampled in the same orientation. This severely reduced heterogeneity and size of the data other than the actual shape differences. By removing this unwanted noise, neural

networks need smaller databases to properly learn the key features of 3D stereophotographs to discriminate between the different subtypes of craniosynostosis. Second, there was an optimization in the number of vertices in the raycasting algorithm to minimize the amount of potential of overfitting features. Third, we applied feature scaling to correct for size differences and to amplify features of all subjects, which was desirable because of the differences in age between some of the groups. Fourth, we mirrored each 3D stereophotograph to decrease the impact of specific asymmetries in the collected cranial shapes, which can also lead to overfitting. Fifth, regularization techniques were used in the neural networks to further prevent overfitting. Finally, 10-fold cross validation was used to determine the validity of each prediction model. The training and test results show a near identical distributions within the confusion matrices over all the folds suggesting good generalization of the model [Supplementary Table 1].

We applied a stratified 10-fold cross validation setup without a separate test-set to determine the validity of each prediction model. Inclusion of a test-set could further establish the validity of a trained prediction model. Ideally a test-set should comprise a collection of externally collected 3D-stereophotographs and this could be the starting point for further research.

As mentioned before, larger datasets would be beneficial for craniosynostosis research. The rise of smartphone 3D stereophotogrammetry technology [33], [34] can aid in generating larger craniosynostosis datasets in the future. However, in the meantime data could be artificially generated based on the existing training data. This can be done by using a Generative Adversarial Network (GAN), which is another deep learning technique [35]. A GAN can generate data similar to the input of the network, thereby offering the possibility to synthetically enhance an existing dataset. This technique has previously been applied in medical images [36]–[39] and also in improving accuracy in experiments with small-sized training datasets [38]–[41]. Due to the small size of the current 3D stereophotogrammetry dataset, GAN implementation could be of great value for future projects. The feasibility of the use of GANs in generating fictive datasets of trigonocephaly cases has been explored by our group but is not used within this study [42].

3D photogrammetry is not the only radiation-free imaging modality that can be used to diagnose craniosynostosis as systematic physical examination,

ultrasound and MRI-scan also be utilized and have led to good results in the past [7], [9], [11], [43], [44]. It would be interesting to see if a deep learning algorithm would perform similarly when using images from another modality. Although each method has its own advantages, 3D stereophotogrammetry remains one of the fastest radiation-free methods for capturing the cranial shape for such diagnosis. Furthermore, 3D stereophotogrammetry technology is rapidly evolving, enabling the use smart-phone technology to make accurate 3D stereophotographs [33], [34].

CONCLUSION

This study shows that trained deep learning algorithms, based on 3D stereophotographs, can discriminate between craniosynostosis subtypes and healthy controls with high accuracy.

APPENDIX

Table 1: The confusion matrix of the training sets with computed recall/sensitivity, precision and specificity. Due to the use of the 10-fold cross-validation method, training numbers are 9 times higher than the number of patients.

		Predicted				
		Scaphocephaly	**Trigonocephaly**	**Anterior Plagiocephaly**	**Healthy**	**Sensitivity/ Recall**
Actual	**Scaphocephaly**	**684**	0	0	0	100,0%
	Trigonocephaly	0	**360**	0	0	100,0%
	Anterior Plagiocephaly	0	0	**242**	1	99,6%
	Healthy	0	0	1	**476**	99,8%
	Precision	100,0%	100,0%	99,6%	99,8%	
	Specificity	100,0%	100,0%	99,9%	99,9%	

REFERENCES

[1] R. E. Bristol, G. P. Lekovic, and H. L. Rekate, "The effects of craniosynostosis on the brain with respect to intracranial pressure," *Semin. Pediatr. Neurol.*, vol. 11, no. 4, pp. 262–267, 2004, doi: 10.1016/j.spen.2004.11.001.

[2] J. J. Delashaw JB, Persing JA, Broaddus WC, "Cranial vault growth in craniosynostosis," *J. Neurosurg.*, no. 70, pp. 159–65, 1989.

[3] A. Shuper, P. Merlob, M. Grunebaum, and S. H. Reisner, "The Incidence of Isolated Craniosynostosis in the Newborn Infant," *Arch. Pediatr. Adolesc. Med.*, vol. 139, no. 1, p. 85, Jan. 1985, doi: 10.1001/archpedi.1985.02140030091038.

[4] H. Q. Lee *et al.*, "Changing epidemiology of nonsyndromic craniosynostosis and revisiting the risk," *J. Craniofac. Surg.*, vol. 23, no. 5, pp. 1245–1251, 2012, doi: 10.1097/SCS.0b013e318252d893.

[5] G. A. de Jong, T. J. J. Maal, and H. Delye, "The computed cranial focal point," *J. Cranio-Maxillofacial Surg.*, vol. 43, no. 9, pp. 1737–1742, Nov. 2015, doi: 10.1016/j.jcms.2015.08.023.

[6] D. Krakow, "Craniosynostosis," *Obstet. Imaging Fetal Diagnosis Care Second Ed.*, vol. 53, pp. 301-304.e1, 2017, doi: 10.1016/B978-0-323-44548-1.00062-0.

[7] M. L. Cunningham and C. L. Heike, "Evaluation of the infant with an abnormal skull shape.," *Curr. Opin. Pediatr.*, vol. 19, no. 6, pp. 645–51, Dec. 2007, doi: 10.1097/MOP.0b013e3282f1581a.

[8] J. A. Fearon, S. P. Beals, and J. C. Yu, "The Diagnosis and Treatment of Single-Sutural Synostoses: Are Computed Tomographic Scans Necessary?," *Plast Reconstr Surg.*, vol. Oct, no. 120(5), pp. 1327–1331, 2007, doi: 10.1097/01.prs.0000279477.56044.55.

[9] H. J. Kim, H. G. Roh, and I. W. Lee, "Craniosynostosis: Updates in radiologic diagnosis," *J. Korean Neurosurg. Soc.*, vol. 59, no. 3, pp. 219–226, 2016, doi: 10.3340/jkns.2016.59.3.219.

[10] J. P. Sheppard, T. Nguyen, Y. Alkhalid, J. S. Beckett, N. Salamon, and I. Yang, "Risk of Brain Tumor Induction from Pediatric Head CT Procedures: A Systematic Literature Review," *Brain Tumor Res. Treat.*, vol. 6, no. 1, p. 1, 2018, doi: 10.14791/btrt.2018.6.e4.

[11] T. Schweitzer, H. Böhm, P. Meyer-Marcotty, H. Collmann, R. I. Ernestus, and J. Krauß, "Avoiding CT scans in children with single-suture craniosynostosis," *Child's Nerv. Syst.*, vol. 28, no. 7, pp. 1077–1082, 2012, doi: 10.1007/s00381-012-1721-0.

[12] I. M. J. Mathijssen, *Guideline for Care of Patients with the Diagnoses of Craniosynostosis: Working Group on Craniosynostosis*, vol. 26, no. 6. 2015.

[13] C. L. Heike, K. Upson, E. Stuhaug, and S. M. Weinberg, "3D digital stereophotogrammetry : a practical guide to facial image acquisition," *Head Face Med.*, pp. 1–11, 2010.

[14] J. W. Meulstee *et al.*, "A new method for three-dimensional evaluation of the cranial shape and the automatic identification of craniosynostosis using 3D stereophotogrammetry," *Int. J. Oral Maxillofac. Surg.*, vol. 46, no. 7, pp. 819–826, Jul. 2017, doi: 10.1016/j.ijom.2017.03.017.

[15] G. Litjens *et al.*, "A survey on deep learning in medical image analysis," *Med. Image Anal.*, vol. 42, pp. 60–88, Dec. 2017, doi: 10.1016/j.media.2017.07.005.

[16] D. Shen, G. Wu, and H.-I. Suk, "Deep Learning in Medical Image Analysis," *Annu. Rev. Biomed. Eng.*, vol. 19, no. 1, pp. 221–248, Jun. 2017, doi: 10.1146/annurev-bioeng-071516-044442.

[17] A. Esteva *et al.*, "Dermatologist-level classification of skin cancer with deep neural networks," *Nature*, vol. 542, no. 7639, pp. 115–118, 2017, doi: 10.1038/nature21056.

[18] Y. Lecun, Y. Bengio, and G. Hinton, "Deep learning," *Nature*, vol. 521, no. 7553, pp. 436–444, 2015, doi: 10.1038/nature14539.

[19] J. W. Meulstee, G. A. de Jong, W. A. Borstlap, G. Koerts, T. J. J. Maal, and H. Delye, "The normal evolution of the cranium in three dimensions," *Int. J. Oral Maxillofac. Surg.*, Nov. 2019, doi: 10.1016/j.ijom.2019.10.012.

[20] G. de Jong *et al.*, "Radiation-free 3D head shape and volume evaluation after endoscopically assisted strip craniectomy followed by helmet therapy for trigonocephaly," *J. Cranio-Maxillofacial Surg.*, vol. 45, no. 5, pp. 661–671, May 2017, doi: 10.1016/j.jcms.2017.02.007.

[21] C. Shorten and T. M. Khoshgoftaar, "A survey on Image Data Augmentation for Deep Learning," *J. Big Data*, vol. 6, no. 1, 2019, doi: 10.1186/s40537-019-0197-0.

[22] A. K. Jain and R. C. Dubes, *Algorithms for Clustering Data*. USA: Prentice-Hall, Inc., 1988.

[23] V. Nair and G. E. Hinton, "Rectified Linear Units Improve Restricted Boltzmann Machines," in *Proceedings of the 27th International Conference on Machine Learning (ICML-10), June 21-24, 2010, Haifa, Israel*, 2010, pp. 807–814, [Online]. Available: https://icml.cc/Conferences/2010/papers/432.pdf.

[24] N. Srivastava, G. Hinton, A. Krizhevsky, I. Sutskever, and R. Salakhutdinov, "Dropout: A Simple Way to Prevent Neural Networks from Overfitting," *J. Mach. Learn. Res.*, vol. 15, pp. 1929–1958, 2014, doi: 10.1214/12-AOS1000.

[25] S. Ioffe and C. Szegedy, "Batch normalization: Accelerating deep network training by reducing internal covariate shift," *32nd Int. Conf. Mach. Learn. ICML 2015*, vol. 1, pp. 448–456, 2015.

[26] D. P. Kingma and J. Ba, "Adam: A Method for Stochastic Optimization," Dec. 2014, [Online]. Available: http://arxiv.org/abs/1412.6980.

[27] F. Chollet and others, "Keras." GithHub, 2015, [Online]. Available: https://github.com/fchollet/keras.

[28] M. Abadi *et al.*, "TensorFlow: A System for Large-Scale Machine Learning TensorFlow: A system for large-scale machine learning," *12th USENIX Symp. Oper. Syst. Des. Implement. (OSDI '16)*, pp. 265–284, 2016, doi: 10.1038/nn.3331.

[29] F. Pedregosa *et al.*, "Scikit-learn: Machine Learning in Python," *J. Mach. Learn. Res.*, vol. 12, pp. 2825–2830, Jan. 2012, [Online]. Available: http://arxiv.org/abs/1201.0490.

[30] M. J. Cho, R. R. Hallac, M. Effendi, J. R. Seaward, and A. A. Kane, "Comparison of an unsupervised machine learning algorithm and surgeon diagnosis in the clinical differentiation of metopic craniosynostosis and benign metopic ridge," *Sci. Rep.*, vol. 8, no. 1, pp. 4–10, 2018, doi: 10.1038/s41598-018-24756-7.

[31] A. R. Porras *et al.*, "Quantification of Head Shape from Three-Dimensional Photography for Presurgical and Postsurgical Evaluation of Craniosynostosis," *Plast. Reconstr. Surg.*, vol. 144, no. 6, pp. 1051e-1060e, 2019, doi: 10.1097/PRS.0000000000006260.

[32] R. Bhalodia, L. A. Dvoracek, A. M. Ayyash, L. Kavan, R. Whitaker, and J. A. Goldstein, "Quantifying the Severity of Metopic Craniosynostosis," *J. Craniofac. Surg.*, vol. 00, no. 00, p. 1, Jan. 2020, doi: 10.1097/SCS.0000000000006215.

[33] I. Barbero-García, J. L. Lerma, P. Miranda, and Á. Marqués-Mateu, "Smartphone-based photogrammetric 3D modelling assessment by comparison with radiological medical imaging for cranial deformation analysis," *Meas. J. Int. Meas. Confed.*, vol. 131, pp. 372–379, 2019, doi: 10.1016/j.measurement.2018.08.059.

[34] I. Barbero-García, J. L. Lerma, Á. Marqués-Mateu, and P. Miranda, "Low-Cost Smartphone-Based Photogrammetry for the Analysis of Cranial Deformation in Infants," *World Neurosurg.*, vol. 102, pp. 545–554, 2017, doi: 10.1016/j.wneu.2017.03.015.

[35] I. J. Goodfellow *et al.*, "Generative Adversarial Networks," pp. 1–9, Jun. 2014, [Online]. Available: http://arxiv.org/abs/1406.2661.

[36] J. M. Wolterink, K. Kamnitsas, C. Ledig, and I. Išgum, "Generative adversarial networks and adversarial methods in biomedical image analysis," pp. 1–29, Oct. 2018, [Online]. Available: http://arxiv.org/abs/1810.10352.

[37] S. Kazeminia *et al.*, "GANs for Medical Image Analysis," *Artif. Intell. Med.*, p. 101938, Sep. 2018, doi: 10.1016/j.artmed.2020.101938.

[38] O. Bailo, D. Ham, and Y. M. Shin, "Red blood cell image generation for data augmentation using Conditional Generative Adversarial Networks," Jan. 2019, [Online]. Available: http://arxiv.org/abs/1901.06219.

[39] H. Shin *et al.*, "Medical Image Synthesis for Data Augmentation and Anonymization using Generative Adversarial Networks," Jul. 2018, [Online]. Available: http://arxiv.org/abs/1807.10225.

[40] F. Calimeri, A. Marzullo, C. Stamile, and G. Terracina, "Biomedical Data Augmentation Using Generative Adversarial Neural Networks," in *Artificial Neural Networks and Machine Learning -- ICANN 2017*, Springer International Publishing, 2017, pp. 626–634.

[41] C. Bowles *et al.*, "GAN Augmentation: Augmenting Training Data using Generative Adversarial Networks," Oct. 2018, [Online]. Available: http://arxiv.org/abs/1810.10863.

[42] D. H. Sterkenburg A., de Jong G., Meulstee J., "ISCFS 2019 Abstract Supplement 19-3-240 | CRANIOSYNOSTOSIS/METOPIC | Generating fictive trigonocephaly data using a generative adversarial network to produce data to train deep learning algorithms," in *Plastic and Reconstructive Surgery – Global Open*, 2019, vol. 7, no. 8S–2, doi: 10.1097/01.GOX.0000584024.54456.21.

[43] K. Rozovsky, K. Udjus, N. Wilson, N. J. Barrowman, N. Simanovsky, and E. Miller, "Cranial Ultrasound as a First-Line Imaging Examination for Craniosynostosis," *Pediatrics*, vol. 137, no. 2, pp. e20152230–e20152230, Feb. 2016, doi: 10.1542/peds.2015-2230.

[44] K. A. Eley, S. R. Watt-Smith, F. Sheerin, and S. J. Golding, "'Black Bone' MRI: a potential alternative to CT with three-dimensional reconstruction of the craniofacial skeleton in the diagnosis of craniosynostosis," *Eur. Radiol.*, vol. 24, no. 10, pp. 2417–2426, Oct. 2014, doi: 10.1007/s00330-014-3286-7.

Chapter 8

General Discussion & Future Perspective

Guido A. de Jong

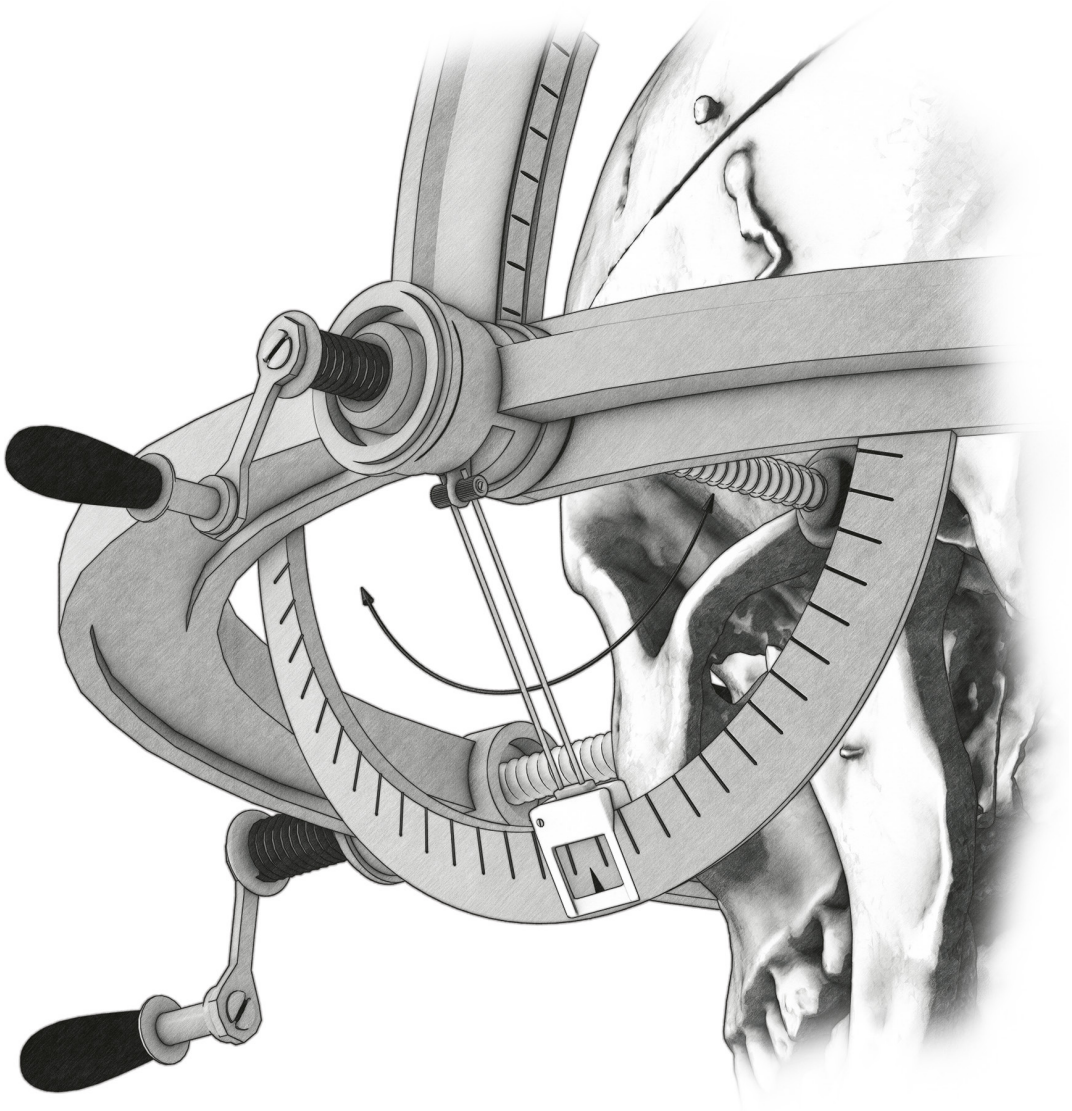

GENERAL DISCUSSION

The primary goal of this thesis was the creation of a new standardized method for objective longitudinal craniosynostosis evaluation using radiation-free methods. The new standardized method was supposed to provide the tools or alternatively a basis to help in the objective evaluation for the different forms of craniosynostosis treatment. The Computed Cranial Focal Point (CCFP) played a central role within this new standardized method [1]. A large section of the discussion will be dedicated towards the CCFP, the implementation, and the technical limitations.

THE COMPUTED CRANIAL FOCAL POINT

The introduction of the Computed Cranial Focal Point (CCFP) was essential for the primary goal and provided a basis to use 3D stereophotogrammetry (or 3D photos) in the longitudinal evaluation in craniosynostosis or healthy individuals [1]–[3]. The CCFP can act as a stable intracranial landmark in case bony landmarks are absent as is the case with 3D photos.

STRENGTHS

Historically one would have to rely on reference frames using X-rays or CT-scans for longitudinal follow-up of cranial development [4]–[10]. With the introduction of 3D stereophotogrammetry alternative references frames based upon surface landmarks were developed [10]–[16]. The CCFP can be used as an alternative intracranial landmark and additionally as a mean to compute the sella turcica for the use in reference frames [1].

The CCFP showed to be robust against deformations and missing data [1]. Due to this robustness good results were achieved in overlaying CT-scans and 3D photos in healthy adults, trigonocephaly cases, and scaphocephaly cases [1] [**Chapter 3**]. A different factor for good overlaying results, is the use of the population specific CCFP-offset. The CCFP-offset is the 3D position of the CCFP relative to the sella turcica in the sella turcica- nasion (StN) orientation. Computing the CCFP-offset is primarily performed using CT-scans. However, it could theoretically also be used in MRI-scans. This CCFP-offset can be used in case there is a need for determining the sella turcica position. Another application of the CCFP and the CCFP-offset values is in overlaying cranial scans of two different modalities [1], [2].

WEAKNESSES

It is important to realize that the CCFP-offset by itself is fairly stable within certain groups (e.g. healthy adults, untreated craniosynostosis patients, young children of similar age, etc.). However, the CCFP-offset will differ between these populations. Applying a non-population specific CCFP-offset in alignment will still be consistent, but will no longer accurately approximate the sella turcica **[Chapter 3]**. Furthermore, the CCFP-offset also changes over age and therefore requires the use of age specific CCFP-offsets [2], [3] **[Chapter 6]**. In two of our studies we made assumptions regarding the CCFP-offset age evolution after craniosynostosis repair [**Chapter 6**] [3]. The CCFP-offset changes over time showed to be fairly linear in nature. This allows for some interpolation and extrapolation of this offset in case we have missing values.

Determining the CCFP-offset after craniosynostosis treatment or for healthy individuals 4-18 years of age is still not performed [**Chapter 3, Chapter 6**]. The CCFP-offset after craniosynostosis treatment cannot be investigated within our institution without a dedicated study due to the lack of routine CT-scans or MRI-scans during follow-up. Instead, in our institution 3D photos are used in the standard follow-up after craniosynostosis repair. Unfortunately it is impossible to determine the CCFP-offset on 3D photos. A prospective study could be performed if other institutions are currently, or historically have been, assessing the craniosynostosis follow-up using CT-scans. Determining the CCFP-offset of healthy individuals (for the ages of 4-18 years old) could be investigated by using CT-scans made during general care. These scans have to be selected for being negative for pathologies, trauma, or morphological changes. However, until these CCFP-offset values are known we must keep in mind that the assumptions made regarding the values could to some extend influence the results.

CRANIOSYNOSTOSIS AND NORMATIVE OUTCOMES

The trigonocephaly study was the first study where the CCFP workflow was utilized to evaluate clinical outcomes [3]. The workflow proved to be a promising tool in the longitudinal follow-up after craniosynostosis treatment. However, in this study there was no 3D photo reference data of healthy controls available from our own institution at this time. Furthermore, there was no comparison between treatment options. The 3D heatmaps provided insight in how the trigonocephaly patients changed after treatment and over time.

Both absolute and relative shape changes were evaluated. The added value of these 3D heatmaps was present in visualizing the 3D growth in the affected regions of the head. The ratio between the anterior skull volume and the total volume skull volume was a different measure within this study with the goal to determine volume corrections in the affected region in trigonocephaly. However, while indicating the volume change in the affected and unaffected region, this measure would require reference data measured with the same methodology for full interpretation.

The normal evolution of the cranium in three dimensions was the second study where the CCFP workflow was utilized in clinical practice [2]. This study provided the reference data for the craniosynostosis (and other cranial development) studies. A more automated workflow, using primarily the CCFP, was set up to determine the cranial measurements and provide 3D growth maps of healthy reference cases. The cranial measurements were in-line with the literature and the growth maps showed similar patterns as observed in various other studies. This study was, to our best knowledge, the first study to capture the normal head growth using 3D photos. The normal head growth in 3D provides a good reference for craniosynostosis patients in other studies.

The scaphocephaly study [**Chapter 6**] was the first study that utilized the CCFP workflow for the comparison data of two different treatment options (endoscopically assisted craniosynostosis surgery and open cranial vault reconstruction) and healthy references. Additionally, the surgical (safety) outcomes were also registered. Within this workflow it was finally possible to provide an evidence-based treatment recommendation regarding both surgical outcomes and long-term cranial shape follow-up. Although the surgical outcome parameters were well described in other studies [17], [18] the longitudinal growth maps reporting on multiple stages after treatment were not described in literature yet to our best knowledge.

GENERAL LIMITATIONS

There are certain limitations of the studies described above. The main issue is the low number of cases, age distributions and gender differences. Craniosynostosis remains a rare disease. Our institution has over 15 years of experience in endoscopic craniosynostosis treatment and even longer in open craniosynostosis treatment. A registry including craniosynostosis patients was introduced in our institution in 2004. Approximately 300 craniosynostosis

patients in this registry which have been threated either using endoscopic or open surgery. In 250 patients a 3D photo was acquired before and/or after treatment as could be identified from the 3D photo database. However, only 143 patients could be used for further analysis based on the presence of a usable pre-treatment 3D photo with sufficient quality and exclusion of syndromic cases [**Chapter 7**]. In craniosynostosis there are three predominantly non-syndromic forms of which the largest group (scaphocephaly) occurs in roughly 50% of these cases. The majority of the cases are treated using endoscopically assisted craniosynostosis surgery (EACS). So even in the largest craniosynostosis group this leaves a very small fraction of children that are treated using the alternative treatment form of open cranial vault reconstruction (OCVR) [**Chapter 6**]. There are (potential) differences between male and female head growth patterns in infants [2], [19]. Furthermore, on average only 20-40% of the craniosynostosis cases are female to begin with [17], [18], [20]. This combination leads to even further thinning of usable 3D photos especially in female patients [**Chapter 6**].

Due to the low number of usable cases, age distributions, and the gender differences it was inevitable throughout this thesis to combine age and/or gender groups in certain analysis [3], [21], [22] [**Chapter 6**]. In order to create the purest form of data analysis for craniosynostosis follow-up cases should be separated based upon craniosynostosis subtype, treatment option, gender and age. Without additional cases using an eligible modality like 3D photos or CT-scans it will be very difficult to fully comprehend craniosynostosis follow-up.

The current lack of sufficient plagiocephaly patients and data is the prime reason these cases were not evaluated in a longitudinal study in this thesis. It is of uttermost importance to seek collaborations with institutions treating the same patients, especially if, for instance with craniosynostosis, multiple treatment options are available without consensus of the best treatment. Collaborations, open data sharing, and methodology sharing can also further help in defining the best outcome measures and treatment options.

One of the downsides of the 3D stereophotogrammetry system used in this thesis is the additional cost for an institution in obtaining such a system. Most of these systems cost between 6.000 to 100.000 euros which is a dedicated investment for specific patient groups. Despite their use outside the field of craniosynostosis, these 3D stereophotogrammetry systems are less versatile than the radiology devices like ultrasound, X-ray, CT-scanners or MRI-

scanners. The total amount of 3D stereophotogrammetry setups suitable for full cranial 3D scanning in the institutions globally remains limited to date. MRI-scans or CT-scans could be used in the use of the new standardized method for objective longitudinal craniosynostosis evaluation. However, these scans would not be ideal due to the use of general anaesthetics and/or the radiation dose (in CT-scans)[23]–[25].

FUTURE PERSPECTIVE

IN GENERAL

There are still some uncertainties regarding the CCFP and CCFP-offset to make it a validated technique for all craniosynostosis forms. The studies in this thesis proved that longitudinal follow-up was possible with good results but held some limitations as described above. It is recommended to collect the CCFP-offset variables from ages 4-18 years old and after craniosynostosis repair. As with any research it is also recommended to further enhance the dataset and perform external validation of the methods.

Collaborations, open data sharing, and methodology sharing can also further help in defining the best outcome measures and treatment options for craniosynostosis. Initiatives and collaborations like Eurocleft and Americleft [26], [27], or the MR CLEAN study (and all its derivatives/follow-up studies) [28] have shown the power in collaboration with an abundance of research in their respective fields as a result. It is recommended to also initiate such an international registry for craniosynostosis care. First steps in these collaborations for craniosynostosis care has been shown in development and behaviour after scaphocephaly [29]. However, collaborative national or international registries on surgery and shape outcomes for craniosynostosis are not available to our best knowledge. The creation and maintenance of such (online) registries can enhance collaboration between institutions and be a platform where diagnostics, treatment options and outcome prediction could be integrated. These integrations should be built to support a wide array of modalities like 3D photos, CT-scans, and MRI-scans. Having online tools that have these integrations will result in the best possible care for craniosynostosis patients especially if there are multiple treatment options available within a certain institute. The future of research is not based around individual researchers or single research groups, but rather nation-wide or

international consortia and collaborations. Additional positive effects caused by these consortia and collaborations is the ease of establishing consensus as well as keeping healthcare affordable. Duplicate research, expensive medical devices, costs caused by knowledge gaps, etc. can be partially tackled using this construction.

After the introduction of the static 3D stereophotography setups different dedicated handheld devices became available for capturing 3D surfaces of e.g. faces and heads [30], [31]. Additionally smartphone based photogrammetry options were recently introduced [32]. The handheld setups have an advantage over the static setups regarding the space requirements. Still, the 3D stereophotography setups are often capable of capturing the head surface (far) below one second while most handheld scanners take seconds to minutes to do a full capture. The resolutions of the handheld scanners can be theoretically as good as the static setups in ideal conditions. Nonetheless, the use of the handheld or smartphone based scanners could increase the availability of radiation-free capturing of the cranial 3D shape. This could, in combination with new tools, contribute to early detection and better follow-up when used in in the primary and secondary healthcare sectors. Early detection allows for early treatment which showed to be superior within our scaphocephaly study [**Chapter 6**].

ARTIFICAL INTELLIGENCE & DEEP LEARNING IN CRANIOSYNOSTOSIS

Artificial Intelligence (AI) will, without any doubt, severely impact clinical care and research throughout the entire field of medicine. Only one chapter in this thesis used AI in the form of deep learning. Yet, we were stunned by the incredible results of this techniques to classify craniosynostosis on 3D photos [22] . A part of this success (although not reported in detail) is the heavy use of standardization which was enabled using the CCFP workflow. Considering the success described in [22] [**Chapter 7**], deep learning techniques could be utilized to give an abstract score of “normality” on 3D photos of heads of patients that were treated for craniosynostosis. This would be the first step in an alternative method for optimizing craniosynostosis treatment. If a treated craniosynostosis case would still be classified as craniosynostosis after an extended period of time, in-depth analysis of the 3D photo could be performed by determining generic localizable features [33]. This would in essential create

heatmaps or distance maps that visualize the contribution to the classification or the "expected" differences from the normal head shape. These visualized contributions show the potential areas in which additional correction should take place. After these corrections would be performed the cranial shape will be classified as a healthy or "normal". These maps themselves are somewhat similar to those that show the difference between an average/generalized healthy case and the patients as used in this thesis other studies [1]–[3], [21], [34], [35]. However, there is a major difference between the distance/curvature map differences from these studies and the contribution/attention maps generated using deep learning. Deep learning is not limited to e.g. logistic or linear differences or regression analysis. Rather it can create arbitrary relations and correlations between any given set of datapoints provided.

The creation of these arbitrary relations and correlations between the data can be illustrated using trigonocephaly. Having a metopic ridge, which can be observed using 3D photos, is usually no guaranteed indication of trigonocephaly [36]–[38]. There are other factors like CT-scan based skull measurement angles which also present in trigonocephaly [39]. However, in moderate trigonocephaly these angles can be similar to those of healthy controls. The lateral supraorbital regions often represent a more inward expression as compared to healthy controls but again vary per healthy case or trigonocephaly patient [34]. An infant with a strong metopic ridge and inward expressed lateral orbital regions can still be a perfectly healthy infant, while an infant with only a mild metopic ridge and a certain cranial angle could be a severe trigonocephaly case. A single measurement or even a combination of measurements on a 3D photo is no guarantee for an adequate diagnosis. Furthermore, after trigonocephaly treatment, what combination of measurements defines if the head shape is comparable to that of a healthy individual. Luckily with deep learning we don't have to define these measures beforehand since the algorithm can determine these abstract measurements itself. Unfortunately, deep learning classification models often behave like so called black boxes; we know the input and the expected output but have no to limited understanding of its internal function/reasoning. Fortunately, we can still extract some information from this black box functioning for each individual case depending on the type of deep learning used. If we have highly accurate craniosynostosis classification models in deep learning we could theoretically determine what features contribute positively and negatively

to the given classification by reading the so called saliency maps or class activation maps [33], [40]. Since the deep learning models used in [22] [**Chapter 7**] were unsuitable for the creation of saliency maps or class activation maps we did not perform this analysis. Creation of these maps when they become available for the types of networks used, or re-training with networks that do allow these, is recommended in future research. This allows for better understanding of objective craniosynostosis classification and the required corrections for achieving normal head shapes.

AI can also contribute in a more straightforward fashion. Currently our objective longitudinal craniosynostosis evaluation using radiation-free methods has a workflow that is still dependant on manual pre-orientation using landmark placement. Conventional algorithms for 3D landmark detection is one option to further automate this process [41]–[43]. Alternatively, AI can also be utilized in 3D landmark detection, classification or point cloud registration/ orientation [44]–[46].

Prediction of craniosynostosis outcomes in 3D would also be within the realm of possibilities using AI. Face age progression is already achieved using AI [47]. Similar techniques for prediction of outcome after craniosynostosis treatment over time when enough data becomes available can be interesting to determine the optimum treatment.

Since craniosynostosis is a rare disease as mentioned in the general limitations it remains difficult to perform adequate analysis on all different groups (age, type, gender) due to the lack of data in certain groups. Besides additional data collection, AI can help with obtaining more "data". This data is artificially generated data which can be produced using Generative Adversarial Networks (GANs) which have been successfully used in medical imaging [48]. There are many applications in GANs. The main application to focus on is the creation of new original and realistic data without the use of conventional statistical or probabilistic models. With a GAN the data for the various craniosynostosis cases could be rapidly expanded. However, there is no guarantee that e.g. training a new deep learning classification model based upon this generated data will result in better classification performance. It is recommended to explore the use of GANs and the added value for craniosynostosis research.

FINAL REMARKS

The question if the methodology created in this thesis should be the new standardized method for objective longitudinal craniosynostosis evaluation using radiation-free methods is an interesting one to answer. A new standard should be evidence based and accepted via consensus within the field the standard applies to. So we could break this down in the evidence part and the consensus part.

The methodology has been refined over time and limitations have been identified. This lead to good results in especially the radiation-free trigonocephaly and scaphocephaly patient evaluation. Furthermore, clear future perspectives are set and can help in future goals in the objective longitudinal follow-up. In addition, the artificial intelligence approach became a possibility due to the high degree of standardization. This allows for a new line of research regarding craniosynostosis diagnosis, planning, predication and follow-up. Logically, changes in methodology should be accepted when it becomes updated, or more refined methods are found in the longitudinal follow-up. So in short the evidence, bounds, limitations and future perspective of the methodology are set.

The consensus component is a bit more complex. Within the Craniofacial Team Nijmegen the described methodologies are currently implemented in the dedicated stand-alone in-house software 3DMedX (3D Lab Radboudumc, Nijmegen, The Netherlands). This is currently used in the standard craniosynostosis follow-up for trigonocephaly and scaphocephaly. The implementation is a gigantic step in making the methodology available for use outside our institute. Earlier versions of the follow-up process relied on a mix of various programs which are all now combined in one simple piece of software. Additionally, the accessibility of 3D photography has increased due to the rise of cheaper 3D stereophotogrammetry setups. These absence of these factors have been a bottleneck in earlier collaborations with other institutes. Collaborations have now become easier with the availability of the software and hardware. However, this means that consensus with this methodology in mind so far has not been achieved outside our institute. In addition, no consensus on any methodology in longitudinal 3D head shape follow-up of craniosynostosis has been made to our best knowledge. It is therefore recommended to establish consensus on the use standardized methods in

follow-up by e.g. consortia and collaborations. Furthermore, these consortia and collaborations can result in the collection of data required which is useful in further methodology refinement.

So back to the question if the methodology created in this thesis should be the new standardized method for objective longitudinal craniosynostosis evaluation using radiation-free methods. Evidence has been provided, but no consensus exists outside our institution yet. So at this moment, it is the new standardized method only within our institution. I would like to encourage collaborations and consortia to evaluate and form consensus on the use these methods. Hopefully this thesis provides and evidence based standardized method for objective longitudinal craniosynostosis evaluation using radiation-free methods. Or alternatively, that this thesis sparks the sense of urgency and need to investigate these methods to provide the best possible craniosynostosis treatment and follow-up.

REFERENCES

[1] G. A. de Jong, T. J. J. Maal, and H. Delye, "The computed cranial focal point," *J. Cranio-Maxillofacial Surg.*, vol. 43, no. 9, pp. 1737–1742, Nov. 2015, doi: 10.1016/j.jcms.2015.08.023.

[2] J. W. Meulstee, G. A. de Jong, W. A. Borstlap, G. Koerts, T. J. J. Maal, and H. Delye, "The normal evolution of the cranium in three dimensions," *Int. J. Oral Maxillofac. Surg.*, Nov. 2019, doi: 10.1016/j.ijom.2019.10.012.

[3] G. de Jong *et al.*, "Radiation-free 3D head shape and volume evaluation after endoscopically assisted strip craniectomy followed by helmet therapy for trigonocephaly," *J. Cranio-Maxillofacial Surg.*, vol. 45, no. 5, pp. 661–671, May 2017, doi: 10.1016/j.jcms.2017.02.007.

[4] J. R. Marcus *et al.*, "Use of a three-dimensional, normative database of pediatric craniofacial morphology for modern anthropometric analysis.," *Plast. Reconstr. Surg.*, vol. 124, no. 6, pp. 2076–84, Dec. 2009, doi: 10.1097/PRS.0b013e3181bf7e1b.

[5] A. Björk, "Cranial base development: a follow-up x-ray study of the individual variation in growth occurring between the ages of 12 and 20 years and its relation to brain case," *Am. J. Orthod.*, 1955, doi: 10.1016/0002-9416(55)90005-1.

[6] B. Solow and A. Tallgren, "Head posture and craniofacial morphology," *Am. J. Phys. Anthropol.*, vol. 44, no. 3, pp. 417–435, 1976, doi: 10.1002/ajpa.1330440306.

[7] S. Pruzansky and E. F. Lis, "Cephalometric roentgenography of infants: Sedation, instrumentation, and research," *Am. J. Orthod.*, vol. 44, no. 3, pp. 159–186, Mar. 1958, doi: 10.1016/0002-9416(58)90012-5.

[8] W. M. Krogman, "Craniometry and cephalometry as research tools in growth of head and face," *Am. J. Orthod.*, vol. 37, no. 6, pp. 406–414, 1951, doi: 10.1016/0002-9416(51)90190-X.

[9] S. Dangi *et al.*, "Robust head CT image registration pipeline for craniosynostosis skull correction surgery," *Healthc. Technol. Lett.*, vol. 4, no. 5, pp. 174–178, 2017, doi: 10.1049/htl.2017.0067.

[10] N. R. Saber *et al.*, "Generation of normative pediatric skull models for use in cranial vault remodeling procedures.," *Childs. Nerv. Syst.*, vol. 28, no. 3, pp. 405–10, Mar. 2012, doi: 10.1007/s00381-011-1630-7.

[11] P. Meyer-Marcotty *et al.*, "Head orthesis therapy in infants with unilateral positional plagiocephaly: an interdisciplinary approach to broadening the range of orthodontic treatment," *J. Orofac. Orthop. / Fortschritte der Kieferorthopädie*, vol. 73, no. 2, pp. 151–165, Apr. 2012, doi: 10.1007/s00056-011-0070-z.

[12] L. H. Plank, B. Giavedoni, J. R. Lombardo, M. D. Geil, and A. Reisner, "Comparison of infant head shape changes in deformational plagiocephaly following treatment with a cranial remolding orthosis using a noninvasive laser shape digitizer," *J. Craniofac. Surg.*, vol. 17, no. 6, pp. 1084–1091, 2006, doi: 10.1097/01.scs.0000244920.07383.85.

[13] J.-F. Wilbrand *et al.*, "Objectification of cranial vault correction for craniosynostosis by three-dimensional photography," *J. Cranio-Maxillofacial Surg.*, vol. 40, no. 8, pp. 726–730, Dec. 2012, doi: 10.1016/j.jcms.2012.01.007.

[14] D. R. McKay *et al.*, "Measuring cranial vault volume with three-dimensional photography: A method of measurement comparable to the gold standard," *J. Craniofac. Surg.*, vol. 21, no. 5, pp. 1419–1422, 2010, doi: 10.1097/SCS.0b013e3181ebe92a.

[15] R. Toma *et al.*, "Quantitative morphometric outcomes following the Melbourne method of total vault remodeling for scaphocephaly.," *J. Craniofac. Surg.*, vol. 21, no. 3, pp. 637–43, May 2010, doi: 10.1097/SCS.0b013e3181d841d9.

[16] P. Meyer-Marcotty, H. Bohm, C. Linz, J. Kochel, A. Stellzig-Eisenhauer, and T. Schweitzer, "Three-dimensional analysis of cranial growth from 6 to 12 months of age," *Eur. J. Orthod.*, vol. 36, no. 5, pp. 489–496, Oct. 2014, doi: 10.1093/ejo/cjt010.

[17] H. Yan *et al.*, "A systematic review and meta-analysis of endoscopic versus open treatment of craniosynostosis. Part 1: The sagittal suture," *J. Neurosurg. Pediatr.*, vol. 22, no. 4, pp. 352–360, 2018, doi: 10.3171/2018.4.PEDS17729.

[18] A. Goyal, V. M. Lu, Y. U. Yolcu, M. Elminawy, and D. J. Daniels, "Endoscopic versus open approach in craniosynostosis repair: a systematic review and meta-analysis of perioperative outcomes," *Child's Nerv. Syst.*, vol. 34, no. 9, pp. 1627–1637, 2018, doi: 10.1007/s00381-018-3852-4.

[19] H. Delye, T. Clijmans, M. Y. Mommaerts, J. Vander Sloten, and J. Goffin, "Creating a normative database of age-specific 3D geometrical data, bone density, and bone thickness of the developing skull: a pilot study," *J. Neurosurg. Pediatr.*, vol. 16, no. 6, pp. 687–702, Dec. 2015, doi: 10.3171/2015.4.PEDS1493.

[20] P. A. Gerety, M. N. Basta, J. P. Fischer, and J. A. Taylor, "Operative management of nonsyndromic sagittal synostosis: A head-to-head meta-analysis of outcomes comparing 3 techniques," *J. Craniofac. Surg.*, vol. 26, no. 4, pp. 1251–1257, 2015, doi: 10.1097/SCS.0000000000001651.

[21] J. W. Meulstee *et al.*, "A new method for three-dimensional evaluation of the cranial shape and the automatic identification of craniosynostosis using 3D stereophotogrammetry," *Int. J. Oral Maxillofac. Surg.*, vol. 46, no. 7, pp. 819–826, Jul. 2017, doi: 10.1016/j.ijom.2017.03.017.

[22] G. de Jong *et al.*, "Combining deep learning with 3D stereophotogrammetry for craniosynostosis diagnosis," *Sci. Rep.*, vol. 10, no. 1, p. 15346, Dec. 2020, doi: 10.1038/s41598-020-72143-y.

[23] Y. Arlachov and R. H. Ganatra, "Sedation/anaesthesia in paediatric radiology," *Br. J. Radiol.*, vol. 85, no. 1019, 2012, doi: 10.1259/bjr/28871143.

[24] K. P. Mason *et al.*, "Infant Sedation for MR Imaging and CT: Oral versus Intravenous Pentobarbital," *Radiology*, vol. 233, no. 3, pp. 723–728, 2007, doi: 10.1148/radiol.2333031872.

[25] J. Pages, N. Buls, and M. Osteaux, "CT doses in children: A multicentre study," *Br. J. Radiol.*, vol. 76, no. 911, pp. 803–811, 2003, doi: 10.1259/bjr/92706933.

[26] W. C. Shaw *et al.*, "The Eurocleft project 1996-2000: Overview," *J. Cranio-Maxillofacial Surg.*, vol. 29, no. 3, pp. 131–140, 2001, doi: 10.1054/jcms.2001.0217.

[27] R. E. Long *et al.*, "The americleft study: An inter-center study of treatment outcomes for patients with unilateral cleft lip and palate part 1. Principles and study design," *Cleft Palate-Craniofacial J.*, vol. 48, no. 3, pp. 239–243, 2011, doi: 10.1597/09-180.1.

[28] O. A. Berkhemer *et al.*, "A Randomized Trial of Intraarterial Treatment for Acute Ischemic Stroke," *N. Engl. J. Med.*, vol. 372, no. 1, pp. 11–20, 2015, doi: 10.1056/nejmoa1411587.

[29] H. Care *et al.*, "Preliminary Analysis From the Craniofacial Collaboration United Kingdom Developmental Outcomes in Children With Sagittal Synostosis," *J. Craniofac. Surg.*, vol. 30, no. 6, pp. 1740–1744, 2019, doi: 10.1097/SCS.0000000000005575.

[30] A. Haleem and M. Javaid, "3D scanning applications in medical field: A literature-based review," *Clin. Epidemiol. Glob. Heal.*, vol. 7, no. 2, pp. 199–210, Jun. 2019, doi: 10.1016/j.cegh.2018.05.006.

[31] P. B. Shah and Y. Luximon, "Review on 3D Scanners for Head and Face Modeling," in *Computer Science*, vol. 1, no. September 2019, 2017, pp. 47–56.

[32] I. Barbero-García, J. L. Lerma, Á. Marqués-Mateu, and P. Miranda, "Low-Cost Smartphone-Based Photogrammetry for the Analysis of Cranial Deformation in Infants," *World Neurosurg.*, vol. 102, pp. 545–554, 2017, doi: 10.1016/j.wneu.2017.03.015.

[33] B. Zhou, A. Khosla, A. Lapedriza, A. Oliva, and A. Torralba, "Learning Deep Features for Discriminative Localization," *Proc. IEEE Comput. Soc. Conf. Comput. Vis. Pattern Recognit.*, vol. 2016-Decem, pp. 2921–2929, 2016, doi: 10.1109/CVPR.2016.319.

[34] R. Bhalodia, L. A. Dvoracek, A. M. Ayyash, L. Kavan, R. Whitaker, and J. A. Goldstein, "Quantifying the Severity of Metopic Craniosynostosis," *J. Craniofac. Surg.*, vol. 00, no. 00, p. 1, Jan. 2020, doi: 10.1097/SCS.0000000000006215.

[35] A. R. Porras *et al.*, "Quantification of Head Shape from Three-Dimensional Photography for Presurgical and Postsurgical Evaluation of Craniosynostosis," *Plast. Reconstr. Surg.*, vol. 144, no. 6, pp. 1051e-1060e, 2019, doi: 10.1097/PRS.0000000000006260.

[36] M. J. Cho, R. R. Hallac, M. Effendi, J. R. Seaward, and A. A. Kane, "Comparison of an unsupervised machine learning algorithm and surgeon diagnosis in the clinical differentiation of metopic craniosynostosis and benign metopic ridge," *Sci. Rep.*, vol. 8, no. 1, pp. 4–10, 2018, doi: 10.1038/s41598-018-24756-7.

[37] M. J. Cho, A. A. Kane, J. R. Seaward, and R. R. Hallac, "Metopic 'ridge' vs. 'craniosynostosis': Quantifying severity with 3D curvature analysis," *J. Cranio-Maxillofacial Surg.*, vol. 44, no. 9, pp. 1259–1265, 2016, doi: 10.1016/j.jcms.2016.06.019.

[38] T. Hicdonmez, "Children with metopic ridge," *Turk. Neurosurg.*, vol. 27, no. 4, pp. 585–589, 2017, doi: 10.5137/1019-5149.JTN.16886-15.2.

[39] J. S. Beckett, P. Chadha, J. a Persing, and D. M. Steinbacher, "Classification of trigonocephaly in metopic synostosis.," *Plast. Reconstr. Surg.*, vol. 130, no. 3, pp. 442e–7e, Sep. 2012, doi: 10.1097/PRS.0b013e31825dc244.

[40] K. Simonyan, A. Vedaldi, and A. Zisserman, "Deep Inside Convolutional Networks: Visualising Image Classification Models and Saliency Maps," *2nd Int. Conf. Learn. Represent. ICLR 2014 - Work. Track Proc.*, pp. 1–8, Dec. 2013, [Online]. Available: http://arxiv.org/abs/1312.6034.

[41] S. Filipe and L. A. Alexandre, "A comparative Evaluation of 3D keypoint detectors," in *Conference: 9th Conference on Telecommunications*, 2013, pp. 145–148, [Online]. Available: http://socia-lab.di.ubi.pt/~silvio/papers/Conftele_2013.pdf.

[42] F. Tombari, S. Salti, and L. Di Stefano, "Performance evaluation of 3D keypoint detectors," *Int. J. Comput. Vis.*, vol. 102, no. 1–3, pp. 198–220, 2013, doi: 10.1007/s11263-012-0545-4.

[43] H. Fadaifard, G. Wolberg, and R. Haralick, "Multiscale 3D feature extraction and matching with an application to 3D face recognition," *Graph. Models*, vol. 75, no. 4, pp. 157–176, 2013, doi: 10.1016/j.gmod.2013.01.002.

[44] Z. Zhang, Y. Dai, and J. Sun, "Deep learning based point cloud registration: an overview," *Virtual Real. Intell. Hardw.*, vol. 2, no. 3, pp. 3–222, 2020, doi: 10.1016/j.vrih.2020.05.002.

[45] Y. Guo, H. Wang, Q. Hu, H. Liu, L. Liu, and M. Bennamoun, "Deep Learning for 3D Point Clouds: A Survey," pp. 1–24, 2019, [Online]. Available: http://arxiv.org/abs/1912.12033.

[46] S. A. Bello, S. Yu, C. Wang, J. M. Adam, and J. Li, "Review: Deep learning on 3D point clouds," *Remote Sens.*, vol. 12, no. 11, 2020, doi: 10.3390/rs12111729.

[47] H. Yang, D. Huang, Y. Wang, and A. K. Jain, "Learning Face Age Progression: A Pyramid Architecture of GANs," *Proc. IEEE Comput. Soc. Conf. Comput. Vis. Pattern Recognit.*, pp. 31–39, 2018, doi: 10.1109/CVPR.2018.00011.

[48] X. Yi, E. Walia, and P. Babyn, "Generative adversarial network in medical imaging: A review," *Med. Image Anal.*, vol. 58, p. 101552, Dec. 2019, doi: 10.1016/j.media.2019.101552.

Chapter 9

Summary

Guido A. de Jong

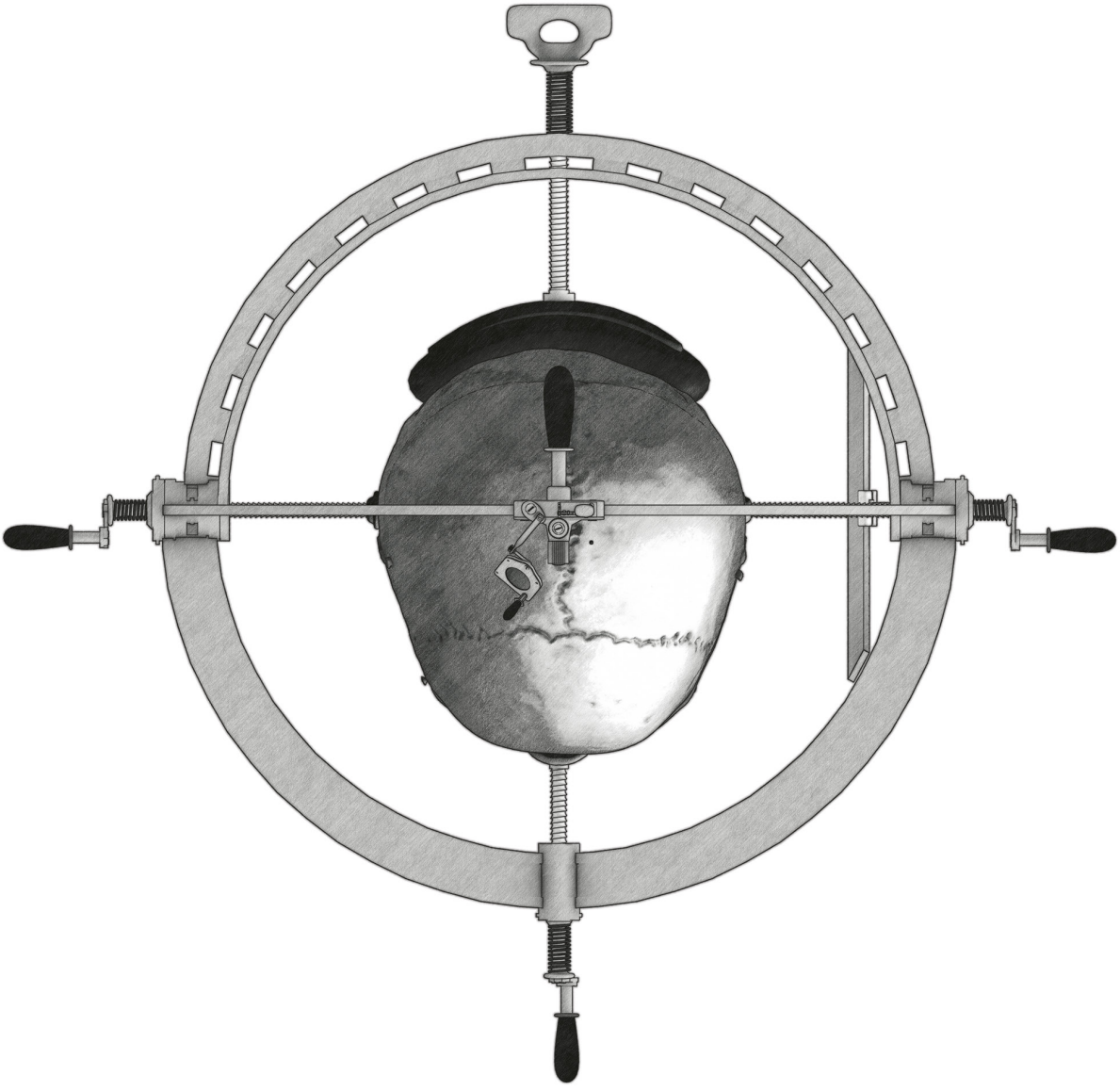

SUMMARY

In **Chapter 1**, we introduced the primary issues in longitudinal craniosynostosis follow-up. A short overview of the primary forms of non-syndromic craniosynostosis is given along with the various treatment options. Some of the follow-up techniques after craniosynostosis treatment with emphasis to the radiation-free 3D stereophotogrammetry technique are listed. A section of this chapter gives the importance and some variations of reference frames for 3D imaging techniques in craniosynostosis. The treatment options, and follow-up techniques with the variations in reference frames lead to the primary issue in the longitudinal follow-up after craniosynostosis treatment which are summarized to form the aim of the thesis. The primary goal of this thesis is defined as the creation of a new standardized method for objective longitudinal craniosynostosis evaluation using radiation-free methods.

We initially developed the Computed Cranial Focal Point (CCFP) and presented this in **Chapter 2**. Rather than being a point/landmark that is based upon hard or soft-tissue landmarks in 3D it is an intracranial landmark that is computed from the entire surface area of the head or skull. This is the point where all the surface normal of the head on average intersect. This computation method is initially tested on synthetic sphere-like shapes with deformations and craniosynostosis-like features. The method itself showed to be reliable and robust against missing data and deformations. The craniosynostosis shapes showed a deviant CCFP position as compared with the reference models or other craniosynostosis shapes giving the option to potentially identify/score the type. When looking at the adult population there is a stable position of the CCFP compared towards the sella turcica. Furthermore there is only a few millimeter difference between the position of the CCFP as computed using the skin or using the skull. This allows for computation of the position of the sella turcica using different modalities that either yield the skin or skull as a 3D mesh like 3D Photos or CT-scans. Alignment of multiple modalities using the CCFP was also tested and resulted in a near perfect match considering growth and additional volume caused by hair and the hairnet which is typically used during the acquisition of a 3D photograph. This chapter presents the foundation of the new standard for objective longitudinal craniosynostosis evaluation using radiation-free methods by the means of the CCFP.

Soft-tissue matching is one of the primary uses of the CCFP. Soft-tissue

matching is used to evaluate changes between 3D head shapes either longitudinally or with other cases and references. The true effect of the presence of scaphocephaly or trigonocephaly on the soft-tissue matching using the CCFP alignment technique was not investigated yet and therefore explored in **Chapter 3**. This alignment technique is based upon the CCFP-offset; the 3D position of the CCFP relative to the sella turcica in the sella-turcica nasion (StN) orientation. The mean CCFP-offset was determined in the 3D soft-tissue reconstruction of CT-scans in both scaphocephaly and trigonocephaly patients. Applying the CCFP alignment technique with the obtained CCFP-offset in these cases to perform soft-tissue matching between CT-scans and 3D photos yielded good results. This technique was similar to the one described in **Chapter 2**. It was also found that using a different (reference) CCFP-offset in both a CT-scan and 3D photo yielded similar soft-tissue matching patterns, but created an offset of the overall CT-scan and 3D photo. Depending on availability of a known CCFP-offset and the need of approximating the sella turcica position in 3D photos either a population specific CCFP-offset or a reference CCFP-offset could be used in the soft-tissue matching procedure. The second method is not recommended in longitudinal follow-up due to the CCFP-offset shift over time and/or after treatment of craniosynostosis. In short, within this chapter parts of the uncertainty that were present in the CCFP alignment method for scaphocephaly and trigonocephaly were investigated.

The first clinical evaluation of our institutes data concerning the follow-up of craniosynostosis is for the treatment of endoscopically assisted trigonocephaly. A radiation-free method was performed based on the CCFP and described in **Chapter 4**. The 3D cranial morphology of the craniosynostosis patients was evaluated using growth maps. The growth maps illustrate that within the first few months there is a strong growth from pre surgery to post surgery around the surgical site, but not at the location of the removed suture. This is followed by growth on the suture site. Head widening seems to occur on average between 24 and 36 months of age. No normative data was available at this time hampering further evaluation. This led to the need of reference data.

The CCFP Computation method and flow has since been improved for both CT-scans and 3D Photos. This improved workflow has first been described in the Appendix of **Chapter 4** [1]. The improved workflow has a higher degree of standardization and normalization of either CT-scans or 3D Photos. The new workflow is based upon pre-alignment using surface landmarks and includes

uniform sampling using half of an ico-sphere. The new workflow further includes gap fixing in case the CT-scan or 3D Photo has existing or sampling induced error gaps. Due to this workflow it is possible to easily compare large series of 3D Photos or CT-scans with their respective changes over time in a standardized workflow. Additionally within the workflow smoothing of small inconsistencies was added.

In **Chapter 5** the normal head growth in the first four years of age in 3D are assessed for CT-scans and up to two years for 3D Photos. This should provide in the need of normative reference data. Assessments of volume, cranial width, cranial length, cranial index, suture lengths and shape parameters were performed (when applicable). The 3D Photos are analyzed using the CCFP computation workflow while the CT-scans are determined using the native StN orientation with the sampling of the CCFP workflow. The growth maps show that there are specific regions of the head that differ in growth over time. These growth patterns are not directly clear when looking at only volumes, cranial widths/lengths/indices, etc. This roots for the use of growth maps for complete assessment of cranial growth over time. Thanks to **Chapter 5** we have insight in the normal 3D growth evolution of the head up to 2 and 4 years old for 3D photos and CT-scans respectively. This results in a reference 3D model which van be used to compare the growth of patients with pathologies like craniosynostosis.

In **Chapter 6** a longitudinal 3D shape development follow-up of scaphocephaly patients was performed. Within this study the CCFP alignment was used on the longitudinal 3D photos of these patients. Comparisons between the outcomes of two treatment options from our institution, endoscopically assisted craniosynostosis surgery (EACS) and open cranial vault reconstruction (OCVR), were made. Primarily, the 3D cranial shape measurements and color-coded distance maps were compared between the treatment groups and with healthy references. Secondly the surgical safety outcome values like length of stay, blood loss, surgery times and transfusion rates were compared between the treatment groups. Initially the 3D cranial shape measurements differed between the two treatment groups in earlier ages but mostly diminished over time. At 24 months of age the mean difference between the two treatment groups over the cranial shape was less than ±2 mm. Over time there were no consistent statistical significant differences for the 3D measurements between both treatment groups and the healthy references. The surgical outcomes

showed that EACS was superior in nearly all outcomes in comparison to OCVR. Considering the near identical results in the 3D measurements and distance maps between EACS and OCVR combined with the superior EACS surgical outcomes EACS is the recommended treatment option. Thanks to this chapter we were finally able to compare two treatment options with each other and healthy references and give evidence-based proof for the superiority of one treatment option over the other.

Besides conventional 3D measurements it is also possible to use deep learning in the diagnosis of craniosynostosis. **Chapter 7** explores the use of deep learning in the diagnosis of craniosynostosis based upon 3D photos. A set of 3D photos of the three most prominent craniosynostosis forms were collected. These include scaphocephaly, trigonocephaly and anterior plagiocephaly. A group of reference 3D photos of healthy infants in the same age were added to this set. All these 3D photos were aligned using the CCFP. A deep learning classification network was applied to these 3D photos. During testing only one 3D photo was misclassified in the entire set. This chapter shows that trained deep learning algorithms, based on CCFP aligned 3D photos, can discriminate between craniosynostosis subtypes and healthy controls with high accuracy. Thanks to this chapter there is a highly accurate diagnosis method on 3D photos with the use of deep learning. The exploration of diagnosis of craniosynostosis on 3D photos with the use of deep learning makes it feasible to also perform follow-up with the use of deep learning.

The general discussion and future perspective is given in **Chapter 8**. Since a new potential standard was introduced concerning the CCFP a large section of the general discussion was based around this subject. The strengths, limitations and alternative usages are given in that section. The patient and healthy reference studies are reflected on based upon history, methodology and outcome of those studies. Some of the more general limitations of the study and the applications of this study outside our institution are briefly discussed. The future perspectives show the need for additional research surrounding the CCFP computation method for certain use cases. An important section in the future perspective is the need for collaborations, open data sharing, and methodology sharing to further help in defining the best outcome measures and treatment options for craniosynostosis. Also the potential of artificial intelligence and deep learning in craniosynostosis is described in-depth. The final remarks reflect on the definition of success for this thesis itself.

Chapter 10

Thesis Appendix

Guido A. de Jong

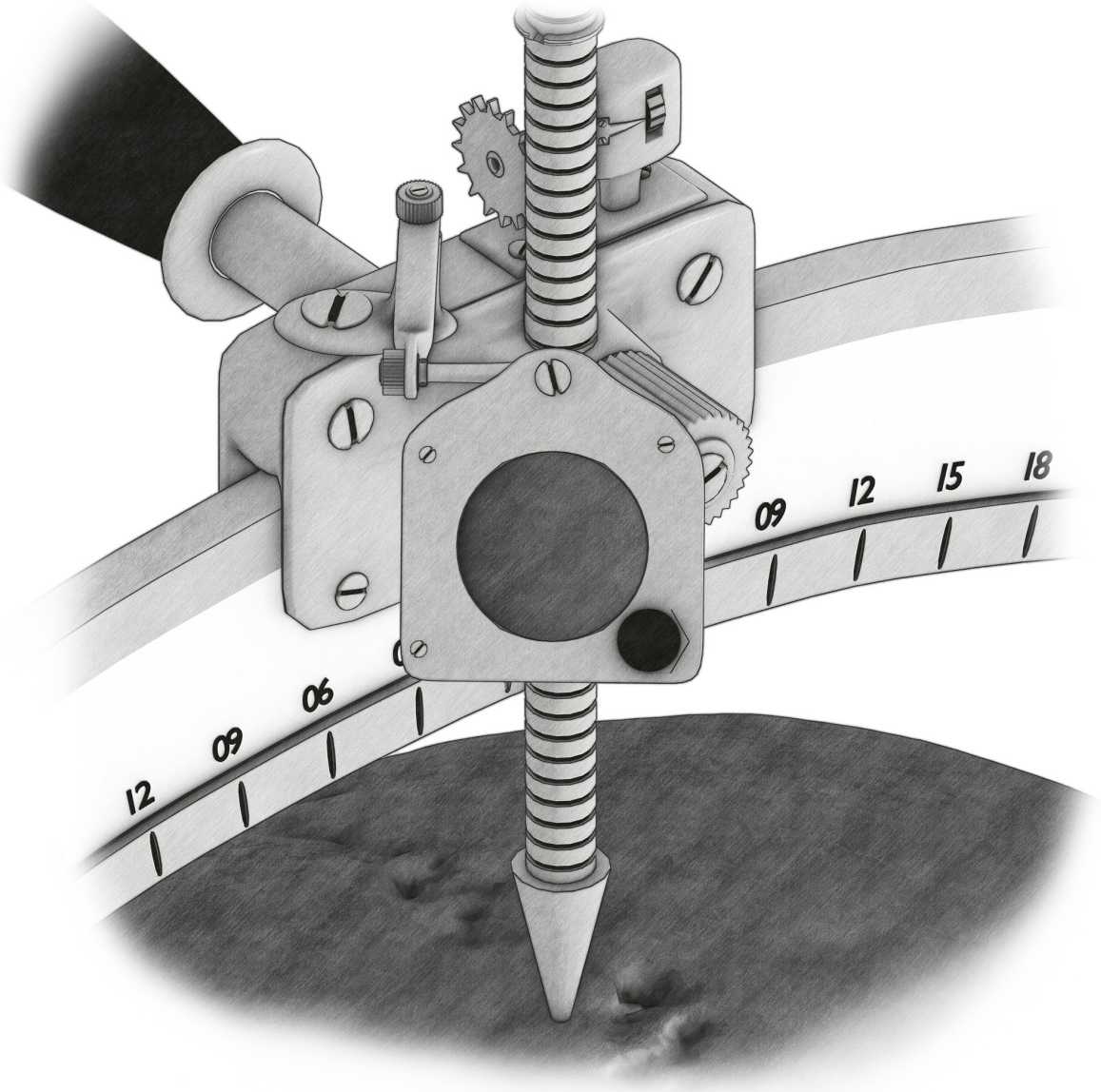

NEDERLANDSE SAMENVATTING

In **hoofdstuk 1** worden de primaire knelpunten in het langdurig opvolgen van craniosynostose geïntroduceerd. Middels een kort overzicht worden de basisvormen van niet-syndromale craniosynostose toegelicht samen met de meest voorkomende behandelmethoden. Daarnaast worden er een reeks technieken benoemd die gericht zijn op het opvolgen van craniosynostose na behandeling. Specifiek wordt er aandacht gegeven aan de stralings-vrije technieken van opvolgen door middel van 3D stereofotogrammetrie. In dit hoofdstuk wordt verder het belang en de variaties van de zogenoemde referentie frames in 3D beeldvorming voor craniosynostose gegeven. De behandelopties, de verschillende vormen van opvolg technieken en de variaties in de referentieframes maken het opvolgen van kinderen met craniosynostose lastig zoals verder uiteengezet in dit hoofdstuk. Het primaire doel van de thesis is dan ook het creëren van een nieuwe standaard methode in het objectief longitudinaal opvolgen van craniosynostose met stralings-vrije methoden.

In het **tweede hoofdstuk** introduceren we het zogenoemde Computed Cranial Focal Point (CCFP). Dit is een herkenningspunt welke, in tegenstelling tot andere herkenningspunten die zich op de huid van het hoofd of de schedel bevinden, voortkomt uit een berekening over het totale hoofd of schedeloppervlakte. Dit oriëntatiepunt is het gemiddelde snijpunt van alle normaalvectoren op het hoofd of de schedel. Er zijn om de methode te testen een aantal bolvormige 3D fantoom modellen gebruikt die kenmerken hadden van de meest voorkomende craniosynostose varianten. Deze tests lieten zien dat de methode betrouwbaar en robuust was bij vervormingen of ontbrekende data. Er was een afwijking te zien van de CCFP positie in de synthetische craniosynostose gevallen ten opzichte van de andere modellen. De theorie was dat deze afwijking gebruikt zou kunnen worden om eventueel in de toekomst craniosynostose objectief te kunnen diagnosticeren. Er is een onderzoek uitgevoerd onder een volwassen populatie om de positie van de CCFP te berekenen ten opzichte van de sella turcica in de schedel. De CCFP bleek zeer stabiel te zijn in deze populatie. Daarnaast was gezien dat er slechts een paar millimeter verschil was tussen een CCFP die berekend is gebruikmakende van de huid ten opzichte die van de schedel als er gebruik gemaakt wordt van 3D foto's of CT-scans. Hierdoor kan de CCFP zowel ingezet worden op de huid als de schedel als oriëntatiepunt. Het uitlijnen

van verschillende beeldmodaliteiten (zoals bijvoorbeeld CT-scans en 3D foto's) van eenzelfde individu creëerde een nagenoeg perfecte match. Kleine verschillen waren zichtbaar die ogenschijnlijk voortkwamen uit extra volume in 3D foto's door bijvoorbeeld groei, haar of een haarnetje. Samengevat geeft dit hoofdstuk de basis voor een nieuwe standaard methode in het objectief longitudinaal opvolgen van craniosynostose met stralings-vrije methoden door gebruik te maken van de CCFP.

Het matchen (over elkaar leggen van) weke delen uit scans is een van de primaire mogelijkheden met de CCFP. Het matchen van weke delen in deze thesis wordt gebruikt om verschillen tussen twee 3D hoofd vormen te bepalen over de tijd of vergeleken met een populatie. In eerdere studies was het echte effect van de aanwezigheid van scafocefalie of die van trigonocefalie tijdens het weke delen matchen met de CCFP methode nog niet onderzocht. In **hoofdstuk 3** worden de effecten bepaald in verschillende matching methoden met de CCFP. In deze methode is de CCFP-offset een belangrijk begrip. De CCFP-offset is de 3D positie van de CCFP ten opzichte van de sella turcica in de sella turcica-nasion (StN) oriëntatie. De gemiddelde populatie specifieke CCFP-offset was bepaald in 3D weke delen reconstructies van CT-scans voor zowel scafocefalie als trigonocefalie patiënten. Het gebruik van de oriëntatie methode met deze populatie specifieke CCFP(-offset) tussen een CT-scan en 3D foto zoals omschreven in **hoofdstuk 2** resulteerde in een goede match. Daarnaast was het gebruik van een generieke (referentie) CCFP-offset eveneens adequaat wanneer men zowel de CT-scan als de 3D foto oriënteerde middels de omschreven methode. Echter was hiermee de benaderde positie van de sella turcica niet meer accuraat in tegenstelling tot wanneer men de populatie specifieke CCFP-offset zou gebruiken. Afhankelijk van de beschikbaarheid van een dergelijke CCFP-offset en de noodzaak om de benaderde positie van de sella turcica te verkrijgen in 3D foto's kan er gekozen worden tussen welke oriëntatie methode er gebruikt wordt. Daarbij is het gebruik van een referentie CCFP-offset niet aan te raden in longitudinale follow-up gezien de CCFP-offset veranderingen over tijd of door invloed van behandelingen niet zeker is. Samengevat is in dit hoofdstuk is een deel van de onzekerheid de voorheen rondom de CCFP oriëntatie methode zat weggenomen voor scafocefalie en trigonocefalie.

De eerste klinische evaluatie van de data uit onze kliniek was die rondom het opvolgen na behandeling met endoscopisch geassisteerde craniosynostose

chirurgie. De stralings-vrije methode van **hoofdstuk 4** gebruikmakende van de CCFP was toegepast op kinderen die endoscopische trigonocefalie behandeling kregen met aanvullende helmtherapie. De 3D hoofd morfologie was geëvalueerd middels de groeikaarten. Hierin was te zien dat in deerste paar maanden na de chirurgie er een sterke groei was rondom in het gebied van de ingreep zelf. Echter was er aanvankelijk geen groei te zien op de locatie waar de aangedane schedelnaad was verwijderd. Deze volgde pas in een later stadium. Het breder worden van het hoofd gebeurde grofweg rond de leeftijd van 24 en 36 maanden na de ingreep. Er was echter nog geen referentie data beschikbaar van gezonde schedelgroei in 3D. Hierdoor was er noodzaak om de gezonde schedelgroei in 3D in kaart te brengen.

In het **vijfde hoofdstuk** is de normale groei van het hoofd in 3D bepaald met CT-scans voor de eerste vier levensjaren en met 3D foto's voor de eerste twee levensjaren. Hierin zijn volumes, breedte van hoofd, lengte van het hoofd, cephalic index, naadlengtes en 3D vorm parameters vastgelegd waar beschikbaar. De 3D foto's zijn geanalyseerd gebruikmakende van de CCFP oriëntatie workflow. De CT-scans zijn geanalyseerd gebruikmakende van de StN oriëntatie. De 3D groeikaarten lieten specifieke gebieden van het hoofd zien die verschillende groeipatronen lieten zien over de tijd. Als we enkel de volumes, hoofd breedte, hoofd lengte, enz. bekijken vallen deze specifieke gebieden niet op tijdens de analyse. Dit toont de waarde aan van de 3D groeikaarten wanneer we hoofdgroei en -verandering in de loop van de tijd analyseren. Dankzij **hoofdstuk 5** hebben we inzichten gekregen in de normale 3D groei en groei-veranderingen van het hoofd tot respectievelijk 2 en 4 jaar oud middels 3D foto's en CT-scans. Als resultaat hebben we een set van referentie 3D modellen verkregen die we kunnen gebruiken voor de vergelijking van gezonde kinderen in de loop van de tijd tegenover die met pathologie zoals craniosynostose.

Hoofdstuk 6 is een studie die de longitudinale 3D vorm ontwikkelingen van behandelde scafocefalie patiënten opvolgt. In deze studie gebruiken we wederom de CCFP oriëntatie methode op 3D foto's. Er worden twee groepen vergeleken: patiënten behandeld met de "Open cranial vault reconstruction" (OCVR) methode en die met de "Endoscopically assisted craniosynostosis surgery" (EACS). De 3D hoofd metingen en de groei/verschilkaarten worden als primaire uitkomstmaten gebruikt om de verschillen aan te tonen tussen beide groepen alsmede met gezonde controles. Daarnaast worden

chirurgische veiligheidsmaten bekeken tussen beide behandelgroepen. Deze maten zij de opnameduur, bloedverlies, operatietijden en transfusies. Veel van de 3D hoofd metingen waren in eerste instantie verschillend tussen de behandelingsgroepen. Deze verschillen verdwenen grotendeels in de loop van de tijd. Op 24 maanden oud waren de gemiddelde verschillen in 3D hoofdvormen tussen de twee behandelingsgroepen minder dan ±2 mm. Op de latere leeftijden waren er geen consistente statistisch significante verschillen voor de 3D hoofd metingen tussen zowel de behandelgroepen als de gezonde controles. De chirurgische veiligheidsmaten waren beter voor EACS ten opzichte van OCVR in vrijwel alle gemeten maten. Gezien de 3D uitkomsten en groei/verschilkaarten nagenoeg identiek waren tussen de behandelmethoden na verloop van tijd en dat EACS superieur was ten opzichte van OCVR rondom de chirurgische veiligheidsmaten is EACS de behandeloptie naar keuze in dit geval. Dankzij dit hoofdstuk zijn we eindelijk in staat om een vergelijking tussen twee behandelmogelijkheden en gezonden controles uit te voeren om zodoende de objectieve superioriteit van de ene behandeling over de andere vast te stellen.

Naast de conventionele 3D maten is het ook mogelijk om deep learning te gebruiken in de diagnosestelling van craniosynostose. In **hoofdstuk 7** verkennen we het gebruik van deep learning voor de craniosynostose diagnose met 3D foto's. Er is een set 3D foto's van de drie meest prominente vormen van craniosynostose verzameld. Dit betreft scafocefalie, trigonocefalie en plagiocefalie. Daarnaast is er een set van 3D foto's van gezonde controles verzameld random dezelfde leeftijd. Alle foto's zijn georiënteerd met de CCFP uitlijning methode. Een deep learning classificatie netwerk is gemaakt en toegepast op deze 3D foto's. Tijdens het testen was er slechts één 3D foto verkeerd geclassificeerd in de totale set. In dit hoofdstuk hebben we laten zien dat getrainde deep learning algoritmes toegepast op CCPF uitgelijnde 3D foto's accuraat de aanwezigheid van craniosynostose kunnen vaststellen en het betreffende subtype te kunnen bepalen. Dankzij dit hoofdstuk is er een zeer accurate diagnostiek methode middels 3D foto's en deep learning. Het opvolgen van craniosynostose na behadeling met deep learning lijkt door dit onderzoek ook tot de mogelijkheden te behoren.

De algemene discussie en de toekomstvisie zijn uiteengezet in **hoofdstuk 8**. Een groot deel van de algemene discussie is toegewijd aan de CCFP gezien dit een basis vormt in deze thesis. De kracht, beperkingen en alternatieve

gebruik van de CCFP worden hierin toegelicht. Er vind reflectie plaats over de studies betreffende patiënten en referenties. Hierbij is er specifiek gekeken nar de historie, methodologie en de uitkomsten van deze studies. De algemene beperkingen van de thesis en de toepassingen worden verder kort aangestipt. In de toekomstvisie laat verdere onderzoeksmogelijkheden rondom de CCFP en de berekening zien, met name voor bepaalde use cases. Binnen de toekomstvisie worden samenwerkingen, open data delen en methodologie delen als belangrijke punten aangestipt om zodoende de beste uitkomstmaten en behandelingsopties voor craniosynostose te komen. De potentie van kunstmatige intelligentie en met name deep learning binnen craniosynostose wordt verder uitgebreid behandeld. Als laatste is er een korte terugblik op de thesis en de behaalde doelen.

RESEARCH DATA MANAGEMENT

This thesis is based on the results of human studies, which were conducted in accordance with the principles of the Declaration of Helsinki. The medical and ethical review board Committee on Research Involving Human Subjects Region Arnhem Nijmegen, Nijmegen, the Netherlands has given approval to conduct these studies where applicable. Ethical approvals part of this thesis were registered under: CMO Arnhem – Nijmegen #2020-6128, CMO Arnhem – Nijmegen #2018-4935. Collected data for the most part has been irreversibly anonymized.

All study data is stored on the research server of the Radboudumc 3D Lab & Oral and Maxillofacial Surgery. The location is "*Not available in digital version.*" and access is regulated by an designated employee of the 3D Lab. Data is separated per chapter and a separate folder with the latest analysis tools is provided. These tools include the raw source code of the CranioView software (custom Unity based annotation program) as used in chapters 3-7 and the latest Matlab toolboxes from chapter 4, 6 and 7.

Only the original source data (e.g. dicoms & 3D Photos) as well as annotations are stored since the intermediate results and data often rely on custom and currently outdated tools. Providing the source data and latest tools as mentioned before should ensure the reproducibility of the study.

The data will be saved for 15 years after termination of the respective studies. Using these patient data in future research is only possible renewed approval from the medical ethical committee. The datasets analysed during these studies are available from the corresponding author on reasonable request and only with approval from the legal and ethics departments.

DANKWOORD

Not available in digital version.

Not available in digital version.

Not available in digital version.

Not available in digital version.

Not available in digital version.

Not available in digital version.

Not available in digital version.

Not available in digital version.

CURRICULUM VITAE

Guido de Jong was born on <*Not available in digital version*> in <*Not available in digital version*>. He attended the primary school <*Not available in digital version*>. On the secondary education he completed a dual profile of "Natuur & Techniek" and "Natuur & Gezondheid" at Nijmeegse Scholengemeenschap Groenewoud (Nijmegen, Gelderland, The Netherlands). He studied "Technical Medicine" at the University of Twente (Enschede, Overijssel, The Netherlands). During this study he had a broad variety of student jobs within programming, 3D technology and augmented reality. Furthermore he got into the board of the student consultancy agency "Unipartners". The final two years of the studies consisted of medical-technical internships which were attended at Radboudumc (Nijmegen, Gelderland, The Netherlands) and Meander Medisch Centrum (Amersfoort, Utrecht, The Netherlands). Within these last two years he became further interested in the field of 3D technology at the Radboudumc departments of Neurosurgery and the 3D-Lab. During the final year he became part-time research coordinator at the department of Neurosurgy while finishing the last internship in that same department. After graduating he expanded his function as research coordinator to a full-time basis. Next to the coordination task he started this PhD thesis graduation track at this department in 2017. In that same year he also became a regular member of the UMC-council. In 2018 he further expanded this seat to the daily board of the UMC-council. Guido transitioned to the 3D-Lab department in 2020 where he finalized this PhD thesis as it lies before you. After the completion of this thesis Guido will continue his work in the 3D-Lab on the subjects of Artificial Intelligence and 3D Technology in healthcare.

PUBLICATIONS

[1] M. L. Tolhuisen, G. A. De Jong, J. W. Meulstee, F. Van Der Heijden, and H. Delye, "A Method for the Creation of Normative Paediatric Skull Models : A Pilot Study," *Int. J. Eng. Sci. Innov. Technol.*, vol. 3, no. 6, pp. 1–7, 2014.

[2] G. A. de Jong, T. J. J. Maal, and H. Delye, "The computed cranial focal point," *J. Cranio-Maxillofacial Surg.*, vol. 43, no. 9, pp. 1737–1742, Nov. 2015, doi: 10.1016/j.jcms.2015.08.023.

[3] N. van der Stap *et al.*, "A Real-Time Target Tracking Algorithm for a Robotic Flexible Endoscopy Platform," in *Lecture Notes in Computer Science (including subseries Lecture Notes in Artificial Intelligence and Lecture Notes in Bioinformatics)*, vol. 8899, 2016, pp. 81–89.

[4] G. de Jong *et al.*, "Radiation-free 3D head shape and volume evaluation after endoscopically assisted strip craniectomy followed by helmet therapy for trigonocephaly," *J. Cranio-Maxillofacial Surg.*, vol. 45, no. 5, pp. 661–671, May 2017, doi: 10.1016/j.jcms.2017.02.007.

[5] J. W. Meulstee *et al.*, "A new method for three-dimensional evaluation of the cranial shape and the automatic identification of craniosynostosis using 3D stereophotogrammetry," *Int. J. Oral Maxillofac. Surg.*, vol. 46, no. 7, pp. 819–826, Jul. 2017, doi: 10.1016/j.ijom.2017.03.017.

[6] J. M. Janssen Daalen *et al.*, "Neurosurgery summer event for students by students: sharing interests," *Br. J. Neurosurg.*, vol. 33, no. 3, pp. 341–342, 2018, doi: 10.1080/02688697.2018.1540768.

[7] J. Martens, G. de Jong, M. Rovers, G. Westert, and R. Bartels, "Importance and Presence of High-Quality Evidence for Clinical Decisions in Neurosurgery: International Survey of Neurosurgeons," *Interact. J. Med. Res.*, vol. 7, no. 2, p. e16, 2018, doi: 10.2196/ijmr.9617.

[8] M. L. Tolhuisen, G. A. De Jong, R. J. M. Van Damme, F. Van Der Heijden, and H. H. K. Delye, "Cranial shape comparison for automated objective 3D craniosynostosis surgery planning," *Sci. Rep.*, vol. 8, no. 1, 2018, doi: 10.1038/s41598-018-21662-w.

[9] D. J. H. A. Henssen *et al.*, "Neuroanatomy Learning: Augmented Reality vs. Cross-Sections," *Anat. Sci. Educ.*, vol. 13, p. ase.1912, Jul. 2019, doi: 10.1002/ase.1912.

[10] G. A. de Jong and R. Aquarius, "Use of artificial neural networks to predict anterior communicating artery aneurysm rupture: possible methodological considerations," *Eur. Radiol.*, vol. 29, no. 5, pp. 2724–2726, 2019, doi: 10.1007/s00330-018-5794-3.

[11] D. J. H. A. Henssen *et al.*, "Systematic Review and Neural Network Analysis to Define Predictive Variables in Implantable Motor Cortex Stimulation to Treat Chronic Intractable Pain," *J. Pain*, vol. 20, no. 9, pp. 1015–1026, Sep. 2019, doi: 10.1016/j.jpain.2019.02.004.

[12] S. Vinayahalingam, T. Xi, S. Bergé, T. Maal, and G. de Jong, "Automated detection of third molars and mandibular nerve by deep learning," *Sci. Rep.*, vol. 9, no. 1, p. 9007, Dec. 2019, doi: 10.1038/s41598-019-45487-3.

[13] J. W. Meulstee, G. A. de Jong, W. A. Borstlap, G. Koerts, T. J. J. Maal, and H. Delye, "The normal evolution of the cranium in three dimensions," *Int. J. Oral Maxillofac. Surg.*, Nov. 2019, doi: 10.1016/j.ijom.2019.10.012.

[14] G. de Jong *et al.*, "Combining deep learning with 3D stereophotogrammetry for craniosynostosis diagnosis," *Sci. Rep.*, vol. 10, no. 1, p. 15346, Dec. 2020, doi: 10.1038/s41598-020-72143-y.

[15] L. B. Stam, R. Aquarius, G. A. de Jong, C. H. Slump, F. J. A. Meijer, and H. D. Boogaarts, "A review on imaging techniques and quantitative measurements for dynamic imaging of cerebral aneurysm pulsations," *Sci Rep*, vol. 11, no. 1, p. 2175, Dec. 2021, doi: 10.1038/s41598-021-81753-z.

[16] M. van Deursen, L. Reuvers, J. D. Duits, G. de Jong, M. van den Hurk, and D. Henssen, "Virtual reality and annotated radiological data as effective and motivating tools to help Social Sciences students learn neuroanatomy," *Sci Rep*, vol. 11, no. 1, p. 12843, Dec. 2021, doi: 10.1038/s41598-021-92109-y.

[17] K. A. Bölek, G. De Jong, and D. Henssen, "The effectiveness of the use of augmented reality in anatomy education: a systematic review and meta-analysis," *Sci Rep*, vol. 11, no. 1, p. 15292, Dec. 2021, doi: 10.1038/s41598-021-94721-4.

[18] G. de Jong *et al.*, "Prediction Models in Aneurysmal Subarachnoid Hemorrhage: Forecasting Clinical Outcome With Artificial Intelligence," *Neurosurgery*, vol. 88, no. 5, pp. E427–E434, Apr. 2021, doi: 10.1093/neuros/nyaa581.

[19] R. ter Horst *et al.*, "Three-dimensional virtual planning in mandibular advancement surgery: Soft tissue prediction based on deep learning," *J Cranio-Maxillofacial Surg*, 2021, doi: 10.1016/j.jcms.2021.04.001.

[20] K. A. Bölek, G. De Jong, C. E. E. M. Van der Zee, A. van Cappellen van Walsum, and D. J. H. A. Henssen, "Mixed-methods exploration of students' motivation in using augmented reality in neuroanatomy education with prosected specimens," *Anat Sci Educ*, p. ase.2116, Jul. 2021, doi: 10.1002/ase.2116.

(INTER)NATIONAL CONFERENCES PRESENTATIONS

- **Morphometric Meeting 2019**
  September 20th, London, United Kingdom
  Oral presentation: *Craniosynostosis and Deep Learning*
- **Nederlandse Vereniging voor Neurochirurige Wintermeeting 2019**
  October 31th – November 1st, Veenendaal, The Netherlands
  Oral presentation: *Automatische classificatie van craniosynostose door middle van 3D foto's en deep-learning*
- **3D Medical Conference & Expo 2019**
  January 30th – January 31th, Maastricht, The Netherlands
  Oral presentation: *GreyMapp – Augmented Reality (and more) for training purposes*
- **European Society for pediatric Neurosurgery Congress 2018**
  May 6th – May 9th, Bonn, Germany
  Oral presentation: *Radiation-free 3D head shape and volume evaluation after endoscopically assisted strip craniectomy followed by helmet therapy for scaphocephaly*
- **European Association of Neurosurgical Societies Congress 2017**
  October 1st – October 5th, Venice, Italy
  Oral presentation: *Artificial Neural Networks; the renewed future for outcome prediction in SAH disease models*
- **European Association of Neurosurgical Societies Congress 2017**
  October 1st – October 5th, Venice, Italy
  Oral presentation: *Radiation-free 3D head shape and volume evaluation after endoscopically assisted strip craniectomy followed by helmet therapy for scaphocephaly*
- **44th Annual Meeting of International Society for Pediatric Neurosurgery 2016**
  October 23th – October 27th, Kobe, Japan
  Poster presentation: *The Computed Cranial Focal Point*
- **European Society for pediatric Neurosurgery Congress 2016**
  May 8th – May 11th, Paris, France
  Oral presentation: *Radiation-free 3D head shape and volume evaluation after endoscopically assisted strip craniectomy followed by helmet therapy for scaphocephaly*

- **European Society for pediatric Neurosurgery Congress 2016**
  May 8th – May 11th, Paris, France
  Oral presentation: *The Computed Cranial Focal Point*
- **10th European Craniofacial Congress 2015**
  June 24th – June 27th, Götenborg, Sweden
  Oral presentation: *The Computed Cranial Focal Point*
- **European Association of Neurosurgical Societies Congress 2014**
  October 12th – October 17th, Prague, Czech Republic
  Poster presentation: *The Computed Cranial Focal Point*

SUPERVISED STUDENTS

- **Niels van Nistelrooij, Artificial Intelligence, Radboud University, March 2021, 6 Months**
  Learning from Unstructured Geometry: Quadric Error Metrics for Clinical Mesh Deep Learning
- **Sasha Teunissen, Technical Medicine, University of Twente, June 2021**
  Automatic Diameter Measurements Of The Aorta On Mri In Marfan Patients
- **Lotte Stam, Technical Medicine, University of Twente, March 2020, 10 Months**
  Verfijning van het ruptuur risico van aneurysmata op basis van pulsatiliteit met behulp van beeldvormende technieken
- **Lotte Ewals, Technical Medicine, University of Twente, March 2020, 3 Months**
  A method for three-dimensional quantitative evaluation of the effect of neurosurgery, either by the supraorbital or pterional approach, on the facial esthetics and functionality
- **Christijn Winkelmolen, Biomedical Engineering, Radboud University, January 2020, 5 Months**
  Automatic erosion detection in rheumatoid arthritis using artificial intelligence
- **Bram Knipscheer, Technical Medicine, University of Twente, December 2019, 3 Months**
  Computational Fluid Dynamics for Bifurcation Aneurysms with Flow Diverters
- **Ruby Egging, Technical Medicine, University of Twente, December 2019, 3 Months**
  Synthetic data augmentation using generative adversarial network for improved craniosynostosis classification
- **Freek Bielevelt, Technical Medicine, University of Twente, December 2019, 3 Months**
  Development of a (semi-)automatic method for preoperative planning of open vault reconstruction in craniosynostosis patients

- **Sifra Blok, Technical Medicine, University of Twente, September 2019, 3 Months**
  Creating a Deep Learning model to automatically segment the postoperative wound area and determine the ratio of redness in this area
- **Lotte Stam, Technical Medicine, University of Twente, June 2019, 3 Months**
  The use of a 4D CTA scan for quantifying wall movements in a cerebral aneurysm: a pilot study
- **Otto Muilwijk, Biomedical Sciences, Radboud University, April 2019, 6 Months**
  Automatic Segmentation of the Dense Artery Sign
- **Veerle Souverein, Biomedical Sciences, Radboud University, February 2019, 6 Months**
  The use of deep learning for the risk prediction of CPSP in stroke patients
- **Andrea Sterkenburg, Technical Medicine, University of Twente, December 2018, 3 Months**
  Generating unique fictive trigonocephaly data using a generative adversarial network
- **Renée Geraats, Technical Medicine, University of Twente, December 2018, 3 Months**
  Assessment of the Requirements for Robotic Spinal Screw Placement Using a Virtual Surgery Model
- **Elmar Bijlsma, Medicine, December 2018, 4 Months**
  Automatic, radiation-free detection of craniosynostosis using deep learning models
- **Nienke Wassenaar, Technical Medicine, University of Twente, December 2018, 3 Months**
  Assessment of the facial soft tissue asymmetry using three-dimensional images
- **Sisley Joosten, Biomedical Sciences, October 2018, 9 Months**
  Using artificial intelligence to distinguish an active postoperative wound infection
- **Myrte Wennen, Technical Medicine, University of Twente, September 2018, 3 Months**
  Early detection of Trigonocephaly in children using two-dimensional images as input for a convolutional neural network

- **Annapaula Coenen, Electrical Engineering, Fontys Hogeschool, September 2018, 4 Months**
  EVD Assistance
- **Maarten Huppelschoten, Technical Medicine, University of Twente, August 2018, 10 Months**
  Catch the A-train - Detection of A-trains in EMG during vestibular schwannoma resection making use of Neural Networks
- **Shankeeth Vinayahalingam, Medicine, University of Münster, March 2018, 6 Months**
  Automated detection of third molars and mandibular nerve by deep learning
- **Jens Mulder, Communicatie & Multimedia Design, Hogeschool Arnhem Nijmegen, February 2018, 4 Months**
  GreyMapp
- **Noes Bosch | Maartje Meijer | Robin Pampiermole, Medicine, Radboud University, November 2017, 4 months**
  Surgery for Scaphocephaly – Differences in the effect of endoscopic strip craniectomy and total cranial vault remodeling
- **Muhlise Canatan, Medicine, Radboud University, October 2017, 4 Months**
  The comparison of two surgical techniques in the treatment of scaphocephaly
- **Joacim Ingri, Electrical Engineering, Fontys Hogeschool, September 2017, 4 Months**
  E-EVD placement assistant - An accelerometer based neuronavigational system
- **Jenske Vermeulen, Technical medicine, University of Twente, December 2016, 6 Months**
  A reproducible automatic skull registration method: Identification of anatomical landmarks versus rigid ICP method
- **Dirk Loeffen, Medicine, Radboud University, June 2016, 6 Months**
  The introduction of a simple iPhone-app to assess the pupillary light reflex: a validation study

PROVIDED COURSES

- **3D Computer Vision for Medical Applications, University of Twente**

  2016-2020

BROK

BROK certificate date: 29th March 2019